JOURNAL OF
EMERGING
INVESTIGATORS

VOLUME 3, ISSUE 12 | DECEMBER 2020
emerginginvestigators.org

Paper ball physics

The correlation between crumpling and compression strength

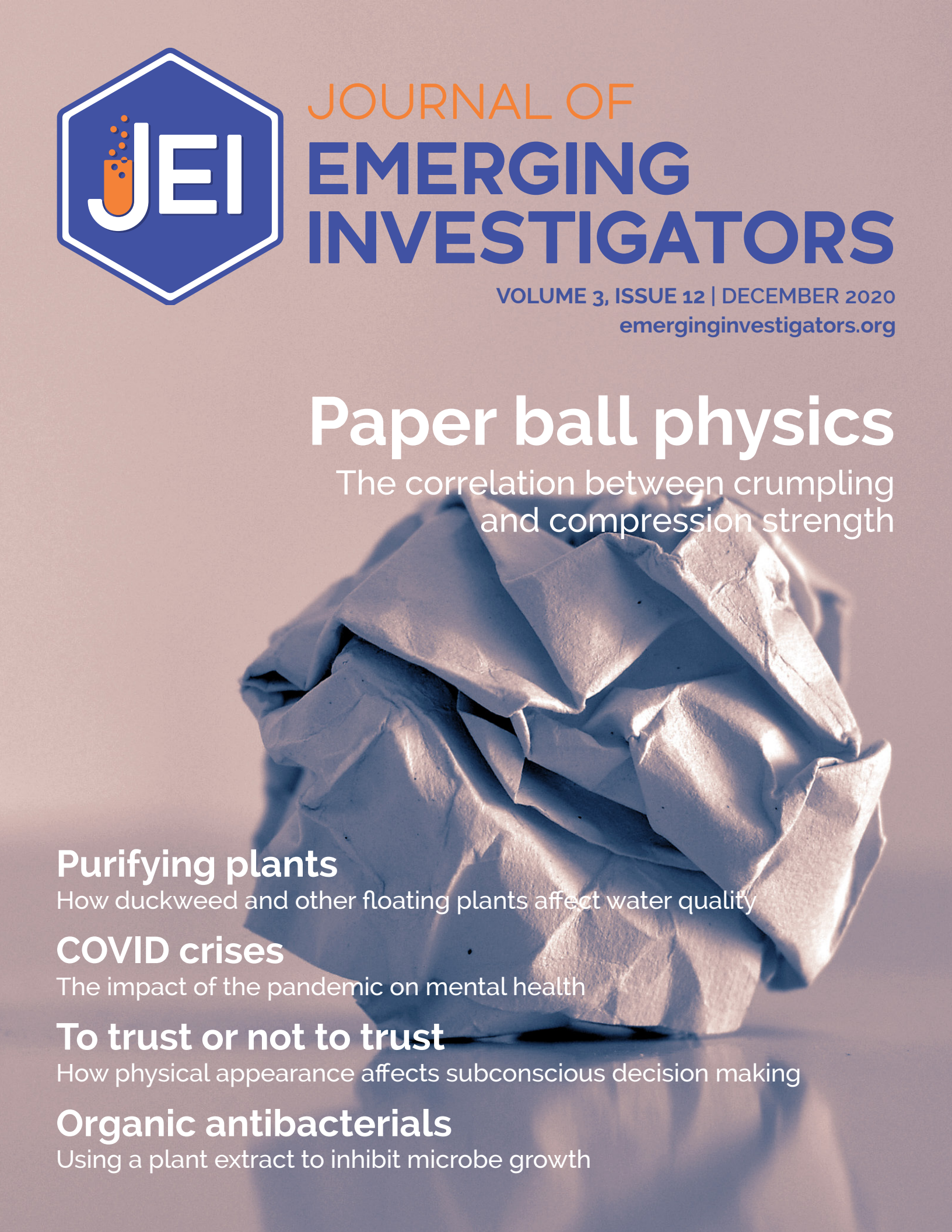

Purifying plants

How duckweed and other floating plants affect water quality

COVID crises

The impact of the pandemic on mental health

To trust or not to trust

How physical appearance affects subconscious decision making

Organic antibacterials

Using a plant extract to inhibit microbe growth

JOURNAL OF EMERGING INVESTIGATORS

The Journal of Emerging Investigators is an open-access journal that publishes original research in the biological and physical sciences that is written by middle and high school students. JEI provides students, under the guidance of a teacher or advisor, the opportunity to submit and gain feedback on original research and to publish their findings in a peer-reviewed scientific journal. Because grade-school students often lack access to formal research institutions, we expect that the work submitted by students may come from classroom-based projects, science fair projects, or other forms of mentor-supervised research.

JEI is a non-profit group run and operated by graduate students, postdoctoral fellows, and professors across the United States.

Contents

VOLUME 3, ISSUE 12 | DECEMBER 2020

OLED screens better exhibit the color black than LCD screens 5
Dylan Donahue and Deanna Donahue
Holliston High School, Holliston, Massachusetts

Physical appearance and its effect on trust 9
Abril Ledesma, Denisse Kraut, Rubén Quezada, Atzin Zayas, and María Elena Cano-Ruiz
Tecnológico de Monterrey High School, Cuernavaca, Mexico

The external presence of running water influences the root growth of pea plants (*Phaselous vulgaris*) 15
Jonathan Shu and Philip Allen
Interlake Senior High School, Bellevue, Washington

Integrated ocean cleanup system for sustainable and healthy aquatic ecosystems 21
Jomills Jose Anand, Srevin Saju, Shaji Sam T L
The New Indian School, Isa Town, Kingdom of Bahrain

Modeling the effects of acid rain on bacterial growth 26
Divyash Shah and Katherine McCormack
Tenafly Middle School, Tenafly, New Jersey

Luteolin's positive inhibition of melanoma cell lines 32
Wilson Su (1) and Feng Liu-Smith
University High School, Irvine, California

Strain-specific and photochemically-activated antimicrobial activity of berberine and two analogs 37
Stephanie Sun, Saira Hamid, Sarah Su, Andrew Su, Bhavesh Ashok, and Edward Njoo (6)
Mission San Jose High School, Fremont, CA; Los Altos High School, Los Altos, CA; Foothill High School, Pleasanton, CA; Amador Valley High School, Pleasanton, CA

Estimation of reproduction number of influenza in Greece using SIR model 44
Cleo M. Skarpeti and Michael G. Skarpetis
Hellenic-American Educational Foundation, Athens, Greece

The impact of effective density and compressive strength on the structure of crumpled paper balls 49
Hayley Chu and Rodolfo Fieller
Yew Chung International School of Shanghai Century Park, Shanghai, China

The impact of the COVID-19 pandemic on mental health of teens 55
Afaf Saqib Qureshi, Shamaila Fraz, and Kiran Saqib
Roots Ivy International School, Islamabad, Pakistan

The effect of floating plant on water purification: Comparison of the water purification capability of Water Hyacinth, Duckweed, and Azolla 61
Jiwoo Park and Jonathan Richard
American School of Bombay, Mumbai, India

A study to determine the anti-cancer and pro-apoptotic properties of *Amaranthus spinosus Linn*. extract, AS20 69
Ishir Sharma, Pooja Kasture, Ankita Umrao,, Jyothsna Rao, and Gururaj Rao
The International School Bangalore, Bangalore, KA, India

JOURNAL OF
EMERGING INVESTIGATORS

Article

OLED screens better exhibit the color black than LCD screens

Dylan Donahue, Deanna Donahue
Holliston High School, Holliston, Massachusetts

SUMMARY

We performed an experiment to determine the amount of light emitted from screens in order to assess the ability of organic light emitting diode screens (OLED) and liquid crystal display (LCD) screens to display the color black. These two competing screen types dominate the digital market, and the capability to exhibit black is one of many factors that should be considered when determining the better of the options. The better a screen can show black, the stronger the contrast of the screen appears to be. The mechanisms that create light within each suggest that OLED screens should be able to show the color black, while LCD screens may not. Therefore, we hypothesized that the light emitted from the LCD screen in this state would be significantly greater than in the OLED. We conducted thirty trials in an environment that eliminated all external light, allowing an accurate recording of emitted light. The results mostly supported our hypothesis: there was a significant increase in light emitted in the LCD screen compared to the OLED when both displayed identical black images at full brightness, though at minimum brightness the LCD performed with negligible difference than OLED.

INTRODUCTION

Our experiment investigated a key aspect of modern digital displays: the ability to show the color black. Almost everyone owns digital devices, making it invaluable to compare their performance. Companies continuously develop new and better screens, but a simple study into this aspect of competing types of displays can provide an insight into the current state of each. Through this, it may become easier to understand the future of these technologies and the potential for each to improve and grow. In showing a truer black, a screen appears more rich, real, and contrasted. Many users may notice this difference, which can serve as a selling point for a screen that displays it best. Less blue light emission would result in less eyestrain and circadian rhythm disruption when looking at a screen with a greater ability to show black (1).

In recent years, organic light emitting diode screens, commonly known as OLED screens, have been replacing liquid crystal displays, or LCDs, in many new gadgets and devices. Improved features such as a better electrical efficiency, a more environmentally sustainable production process, and the ability for incorporation into thinner displays make OLED screens an appealing alternative for use by competitive gadget makers (2,3). But LCDs generally remain cheaper while still performing well in many regards, creating a debate towards the future of digital displays.

These screens use entirely different mechanisms in order to show light and its vibrant colors. LCDs take advantage of a highly unique material: liquid crystals. These easily manipulated crystals exist in a state between a liquid and a solid (4). The addition or removal of heat causes bends and twists in their structure, causing polarization and filtration of certain light (4,5). So, LCD screens do not produce any light themselves. Instead, they rely on a backlight, usually a light emitting diode (LED) source, to create a uniform white light. Transistors push the crystal structures to excited and unexcited states, thus resulting in an instantaneous shifting and filtration (4). Because they do not produce light themselves, the color black is created by the filtration of all light. After first discovering the crystals in 1888, researchers are making vast improvements to their color capabilities primarily by finding new ways to stretch the crystals, creating greater polarization and filtration (6).

OLED screens, conversely, produce their own light. In these displays, multilayer polymers exist in an electric field. Influx of voltage moves electrons differently depending on intended color, and they eventually rejoin and jump across energy levels (2). The combination of polymers that produce blue, green and red light create a spectrum of colors within their devices (2). Given this ability, they should not produce any light when showing the color black, as the light simply turns off. These displays are far newer than LCDs, as the first came into the market in the 1990s. The primary improvements that were made to OLED technology allowed it to be used in far larger devices than it originally could be (7). Though minor adjustments have been made, its color capability has remained fairly constant since its creation.

The absence of light filtering in OLED displays should give them a distinct advantage towards exhibiting black. This is because, although close, no light filter is perfect. Some light, however minimal, will escape through any given filter. To evaluate this, we used a photometer device that measures light intensity to compare emission values for LCD and OLED screens when projecting the same black image. The data that was collected during this study supported our hypothesis that the amount of light emitted from a bright LCD screen when showing black is significantly greater than light emitted from a bright OLED screen, as there was a 3300 % increase in emitted light from OLED to LCD. However, under the dimmest settings of the screens, the gap was decreased and became negligible. This ability of an OLED screen to show a better black than LCD allows it to be a better competitor for personal devices as the sharper contrast and less blue light emission produce a more elegant and less straining experience.

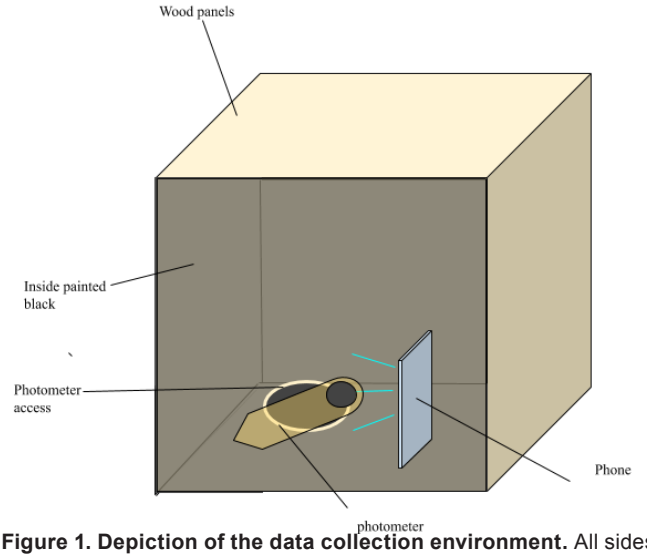

Figure 1. Depiction of the data collection environment. All sides were surrounded by black-painted walls, with only a small opening to allow for photometer access during collection.

RESULTS

In this experiment, we assessed the ability to produce the color black within an external-light controlled system. A photometer measures light intensity by reading adjusted electrical properties due to different light intensities (8). Because the color black is actually the absence of light, a photometer that informs of the intensity or presence of light was helpful and necessary in assessing the quality of black. We used a photometer and placed it directly in front of an OLED screen, LCD screen, or no screen. These screens were measured while bright, dimmed, and turned off, and were replaced by the next screen once 30 data points had been collected. In order to eliminate as much environmental light as possible, we did this in an enclosed box of plywood with black painted walls. We cut out a hole for photometer access and ensured that the roof could be moved to adjust the system (**Figure 1**).

We conducted 30 trials, each with three controls and four experimental data sets. The first control recorded a value of light with no screen present, while the second and third measured OLED and LCD screens turned off, respectively. These accounted for both errors in the measuring device and for environment light that could have reflected off of the screen. Because that light was not emitted from the screens, it was irrelevant to the data being collected. By recording values for these controls, we established a likely non-zero value to represent "no light emitted", giving a better standard to compare the experimental values against.

We took measurements for each phone screen at both the brightest and dimmest settings that the phones allowed, thus producing the four experimental groups. The conditions for each trial were essentially identical, and each displayed similar results: the light emitted from the LCD screen was significantly more than that of the OLED screen. In fact, the average value across all trials for the bright LCD screen was roughly 24 times as large as in the bright OLED (**Table 1**). Also, given the resolution of the device, resulting in a zeroth order uncertainty of ±0.005 lux, and a one-way ANOVA comparison, we concluded that the difference in values between both the dim and bright OLED screen, and either the LED or OLED screen turned off compared to any control condition, was negligible (**Table 1**). There were few outliers, and though they were not ignored when running the ANOVA test, they clearly did not impact the results greatly (**Figure 2**).

DISCUSSION

Most of the trials that we completed suggest a significantly larger amount of light being emitted from LCD screens showing the color black, supporting our hypothesis. The average of 0.68 ± 0.132 lux emitted for bright LCD screens is quite significant, and the *p*-value suggests that it is extremely unlikely that this data was statistically equivalent to that of the control groups; light was surely emitted under this condition. Seemingly, the light-filtering crystals within LCD screens were limited in their ability, and some light from the LED backlight escaped through under those circumstances. The OLED screen did not appear to emit any light, as the difference in means across this data set and the "no screen" control was insignificant. This was also true for both "turned off" control groups. Given the nature of OLED screens, this makes sense, as they have the ability to turn off individual pixels. However, the dimmed LCD screen boasted similar results to the OLED, turned off screens, and no screen. Though, based upon our hypothesis, we did not directly expect this, it does make sense. As proven by the bright LCD screen data, light-filtering is not perfect. But, techniques have improved, and given this outcome, it is clear that they are still very competitive when showing black. Dimming this screen reduced the amount of light emitted by the backlight, thus allowing the liquid crystals to filter less light. The LCD screen that we used must have been able to filter enough light in the dimmed setting to leave only a negligible amount to escape and be emitted. Therefore, in such a dimmed setting, LCD screens seem to be competitive with OLED screens. Using the dimmest setting of a display is not ideal though, as contrast is sacrificed. The OLED screen

	Recorded Amount of Light Emitted						
	No Screen	**OLED (Bright)**	**LCD (Bright)**	**OLED (Dim)**	**LCD (Dim)**	**OLED (Off)**	**LCD (Off)**
Mean Value	0.01 ± 0.013	0.02 ± 0.048	0.68 ± 0.134	0.00 ± 0.000	0.01 ± 0.008	0.00 ± 0.008	0.00 ± 0.005
High Value	0.06	0.26	1.27	0.00	0.03	0.03	0.01
Low Value	0.00	0.00	0.51	0.00	0.00	0.00	0.00
P-value	N/A	0.214695	<0.00001	N/A	1	0.19018	0.189065

Table 1. Amount of Light Emitted from OLED and LCD Screens Under Various Conditions - The amount of light, in lux, emitted from OLED and LCD screens. This was measured by a photometer in a dark and otherwise light controlled environment. The mean for each data set was calculated with a standard deviation, and a one-way ANOVA test was conducted comparing each experimental group to the controls. A significance level of 0.05 was utilized, suggesting that all data sets except for the Bright LCD were found to have statistically insignificant difference in means when compared to the 'no screen" control. The test could not be completed for the dimmed OLED screen as it had no variation in values.

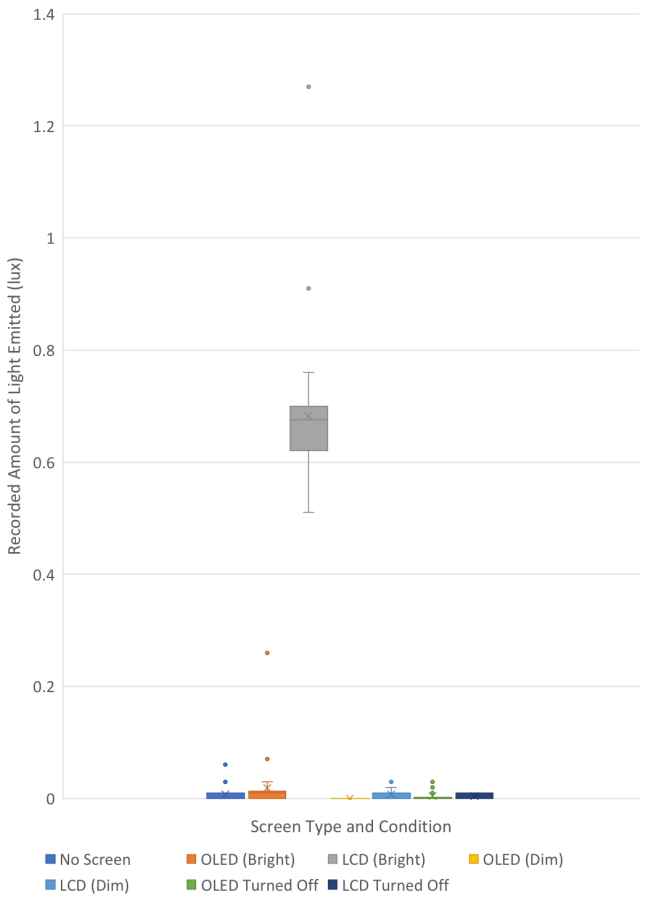

Figure 2. Comparison of light emitted. The boxes represent where the majority of the data lies, while the bars extend to show outliers present for each. Because they were so infrequent, these outliers were disregarded when making qualitative conclusions from this data, and instead attributed to error. The bright LCD screen emits much more light than any other data set.

would have its pixels turned off whether dim or bright, which explains how both the OLED dimmed and OLED bright data sets produced similar results.

Although the trends are very clear, and the similarly valued data sets do not represent significantly different measures, the values recorded are not identical for each trial despite the exact same image being shown for each. A few elements could have contributed to this. The first of these is environment light. Obviously, any light that was recorded that was not emitted from the screens hurts the reliability of data. If it entered the system, the photometer may have sensed and recorded it. However, this is unlikely, as the many measures to prevent environment light from entering the system limited the effect that it could have. Likewise, any effect it managed to have would be fairly consistent for all trials and situations, as we accounted for through our controls. The recording device could have also led to error, as we did not conduct any tests to ensure that our photometer was either reliable nor consistent. Nonetheless, its ability to get fairly similar results for 30 trials suggest that this did not occur. There were few outliers, and though they were not ignored when running the ANOVA test, they clearly did not impact the results greatly (**Figure 2**).

Understanding this, we determined that although limited by light-filtering capacity, LCD screens are still capable and competitive in showing the color black. An average of 0.73 ± 0.132 lux represents a measure of light that is still very small. For reference, most LED light bulbs claim to emit hundreds or even thousands of lumens (1 lux = 1 lumen/m2). Also, when dimmed, the limits of light-filtering seemed to become unnoticeable. Even though our data was reliable enough to conclude that LCDs generally show more light than OLEDs when attempting to exhibit black, it was not a great enough difference to warrant LCD technology a failure in this regard.

Of course, the ability to show one color is not the only determining factor in which screen is better. Further studies that examine the color saturation, vibrancy, precision and ability to adjust quickly, among others, would offer a more complete understanding of their performance overall. These could be conducted under fairly similar conditions, with different tools being used to record these other measures. Studies like these would provide a basis to determine which screen, as they exist today, has a better display for the user. Continuing to monitor these factors can help determine which, if either, are likely to be the better option to invest resources into advancing. Also, these technologies are implemented in a wide variety of places. Though in our everyday lives, they are most often seen in our phones, TVs, watches, etc. they are also used in a wide variety of machines and devices. One study published in the National Library of Medicine compared OLEDs and LCDs in order to determine which would be a better replacement for Cathode-Ray tubes in electroretinograms, which are devices that can analyze cone and rod responses within human eyes. Though it too found OLED performed better for a number of reasons, particularly its fuse threshold, showing black was not a relevant nor important metric of performance in this study (9). Although it is very relevant in deciding which screen is more attractive and vivid to a phone or TV user, this may not be an important measure for other implementations of this technology.

METHODS

The screens used to collect this data were from an IPhone 8, which has an LCD display, and an IPhone X, which has an OLED. They were released at the same time in 2017, and thus represent an equal and recent point in time in the development of each screen. The data collection system was made of ¾ inch plywood, cut into six one-foot long pieces. Each piece was carefully fitted together to create a completely closed box. Because they were cut and fit perfectly, no agent was needed to hold the pieces together. Prior to this, a hole that is large enough to fit the BTMeter BT-881E photometer was drilled into one of the six panels, and the inside of each panel was coated in two layers of Stuart Semple's Black 2.0 paint. As an extra precaution, single sheets of paper were also painted in two coats of this paint and placed to cover each corner of the box in case inconspicuous gaps in the wood were present. The lights in the room were turned off during data collection, and for each trial the photometer was placed through the hole, thus being directly in front of the display, and removed after roughly five seconds of recording a value. The top panel was slid to create an opening, and the display was switched to record the next data point. After replacing the screen, the panel was slid back into its original position. This process was

repeated for all seven situations, thirty times each. When turned on, the same stock photo of the color black was shown on each screen. iPhones have a setting in which the screen brightness automatically adjusts, and so this setting was turned off and the brightness was manually adjusted to both minimum and maximum levels at the appropriate times. After completion, the data was inputted into Microsoft Excel where graphs, data tables, and ANOVA *p*-value statistical tests comparing experimental groups to the controls were completed.

ACKNOWLEDGEMENTS

I would like to thank Mr. Galster, my classmates, scientific reviewers and the Journal of Emerging Investigators for their support and guidance throughout this process.

Received:
Accepted:
Published:

REFERENCES

1. David Ramsey, MD. "Will Blue Light from Electronic Devices Increase My Risk of Macular Degeneration and Blindness?" *Harvard Health Blog,* Harvard Health Publishing, 1 May 2019, www.health.harvard.edu/blog/will-blue-light-from-electronic-devices-increase-my-risk-of-macular-degeneration-and-blindness-2019040816365.
2.Patel, Bhrijesh N, and Mrugesh M Prajapati. "OLED: A Modern Digital Display" *International Journal of Scientific and Research Publications,* vol. 4, no. 6, June 2014.
3. Luo, Zhenyue, and Shin-Tson Wu. "OLED Versus LCD: Who Wins*?" Optics Innovations*, Optics and Photonics News, Feb. 2015, lcd.creol.ucf.edu/Publications/2015/19-21-OptInnov-Feb15.pdf.
4. Williams, Marshall. "LCD Displays." *MSU Engineering*, Michigan State University, www.egr.msu.edu/classes/ece480/capstone/spring15/group03/docs/ECE480ApplicationNote.pdf.
5.*"*Light Filtration" *Molecular Expressions: Science, Optics, and You: Light and Color*, Florida State University, 13 Nov. 2015, micro.magnet.fsu.edu/optics/lightandcolor/filter.html.
6. Kawamoto, Hirohisa. "The History of Liquid-Crystal Displays." *Proceedings of the IEEE,* vol. 90, no. 4, Apr. 2002, pp. 460-500.
7."OLED Timeline", *Michigan State University,* msu.edu/~dunnjam7/timeline.html.
8. Measuring Light Levels / Photometry." *Castle Group Ltd,* 29 June 2017, www.castlegroup.co.uk/guidance/light-measurements/photometry-and-light-measurement/.
9. Matsumoto CS;Shinoda K;Matsumoto H;Seki K;Nagasaka E;Iwata T;Mizota A; "What monitor can replace the cathode-ray tube for visual stimulation to elicit multifocal electroretinograms?" *Journal of Vision,* U.S. National Library of Medicine, pubmed.ncbi.nlm.nih.gov/25096155/.

JOURNAL OF
EMERGING INVESTIGATORS

Article

Physical appearance and its effect on trust

Abril Ledesma, Denisse Kraut, Rubén Quezada, Atzin Zayas, María Elena Cano-Ruiz
Tecnológico de Monterrey High School, Cuernavaca, Mexico

SUMMARY

The first assessment of another person's trustworthiness may depend on several factors, such as previous experiences, education, cultural context, and prejudices, but also on the physical attributes and appearance of the person. We hypothesized that different physical traits would affect teenagers' initial trust of an unknown person and that they would give greater trust to women and people of similar ethnicity. To test this hypothesis, we developed a survey to determine the sets of physical characteristics that affect a person's trustworthiness, including gender, skin color/ethnicity, and facial expressions by asking teenagers to select pictures of young adults presented in pairs based on their physical appearance. For this, 52 teenage volunteers answered this survey in which each of the questions displayed two computer-generated images of people that represented hypothetical Uber drivers of the same age with different physical characteristics. The participants selected the person they preferred to have as an Uber driver based only on the images shown. Results indicated that female participants preferred women drivers, but male participants had no preference for the driver´s gender. Mexican drivers were selected less than white or black drivers, and participants trusted a smiling expression over neutral expressions. We concluded that gender and expression were the main physical traits associated with how trustworthy an individual looks, and ethnicity was also important.

INTRODUCTION

Trusting others is essential for adequate social development, and many factors influence how people judge each other´s trustworthiness. Trustworthy is defined as "deserving of trust, or able to be depended on" (1), and trust is defined as "to that someone is good and honest and will not harm you, or that something is safe and reliable" (1). Aspects such as emotional expressions, gender, and expected characteristics affect our perception of trustworthiness and when a person does not know someone, first impressions become important and can be triggered by initial physical appearance (2-6).

Social and psychological investigations have indicated the importance of physical appearance in social perception; humans have evolved rapid, intuitive, and unreflective mechanisms for evaluating the interpersonal danger potential of other humans based solely on the physical attributes of their conspecifics (2). When referring to physical appearance, previous research has focused on facial characteristics using images of faces (not even including hair, neck, and ears) for testing trustworthiness based on physical appearance (3). People tend to form judgments about how attractive, likable, or even trustworthy others could be as a way to plan their behavior, yet there is not a concise understanding of what the specific characteristics are that make someone look trustworthy.

Whenever something is typical it "shows all the characteristics that would be usually expected from a particular group of things" (1). This virtue leads to a psychological effect, known as typicality, where "people are quicker to make category judgments about typical members of a category than they are to make such judgments about atypical members" (7). Some research suggests that typical faces influence trustworthiness since these faces were judged as safer and more trustworthy (4). In a study where a computer modified a typical face into more extreme appearance trustworthiness decreased as the distance of computer-generated faces from the typical face increased; the more atypical the faces, the more untrustworthy they were perceived to be (8). As such, the face is an important determinant of perceived trustworthiness; as a face becomes more attractive or more unattractive, the trustworthiness decreases (3). This may be because typical faces are perceived as more familiar. Familiarity is referred to a feeling of recognition in the memory, not specifically recalled but remembered (1), which makes familiar features more likable and judged as safe (4, 9-10). The high level of perceived trustworthiness of the typical face likely arises from the inherent preference for typicality, which can be mediated by familiarity (3). It is important to remark that every nation has its typical face that derives from both the ideal face of the nation and the most consensually familiar face in a population (11). Individuals show greater trust in those belonging to groups that they favor but do not necessarily favor the group or ethnicity to which they belong (12).

Emotional expressions affect judgments of trustworthiness as well (2). Subtle happy expressions, such as smiling, increase the likelihood of a trustworthy judgment (3). People inferred that smiling individuals are extraverted, kind, and open to experience (10). In contrast, subtle anger cues and

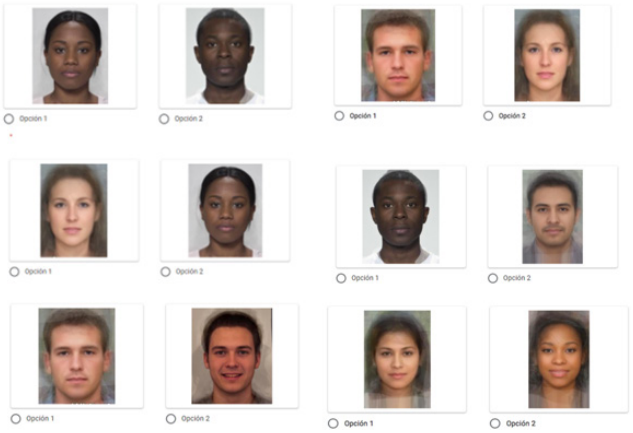

Figure 1. Examples of computer-generated images of hypothetical Uber drivers used in the survey. 1st row: gender preferences - pairs 1 (black female - black male) and 2 (white male - white female); 2nd row: skin color/ethnicity preferences - pairs 3 (white female - black female) and 4 (black male- Mexican male); 3rd row: facial expression preferences - pairs 5 (white neutral male – white smiling male) and 6 (Mexican neutral female – black smiling female).

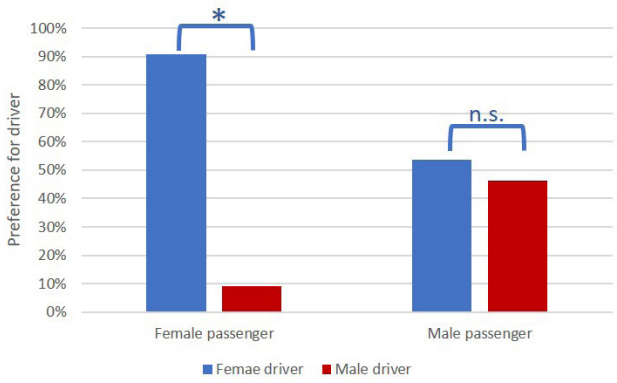

Figure 2. Preference for a female or male driver according to the gender of the passenger. There was a statistical dependence between the gender of the driver and the gender of the passenger (Chi-squared test, df_1=1, df_2=1, N=52, *p-value < 0.005) with female passengers preferring female drivers over male drivers but no preference for male passengers.

emotionally neutral faces are perceived as untrustworthy (3).

In addition to familiarity and emotional expressions, gender may also influence trustworthiness. Women or faces with feminine cues evoke more trust than men and masculine cues, especially for women (5). Gender plays a role in trust behavior: men are on average more trusting and women more trustworthy (13). This also occurs in adolescents; boys are more trusting than girls, but no perceived gender difference in trustworthiness for adolescents has been observed (6).

This study investigated three components of trustworthiness in Mexican teens: gender, skin color/ethnicity (used as a surrogate for familiarity), and facial expression, using computer-generated faces with different traits. We hypothesized that the physical appearance of an individual will affect whether others trust them and that feminine and Mexican traits will be preferred by Mexican teenagers.

RESULTS

Our study included 52 teenage volunteers (27 females, 25 males) with an average age of 17 years (**Table 1**). All participants were Mexican from an urban area attending the same private high school. The survey displayed a total of 35 questions and was administered in two parts. The first part contained 13 questions, and the second contained the remaining questions four months later. The survey was carried out in two parts since in the first survey the interactions between facial expression with gender and ethnicity were not addressed. Each question in both surveys showed two images of people who represented hypothetical Uber drivers with different gender, skin color/ethnicity, and/or facial expression (**Figure 1**). We obtained the images of hypothetical Uber drivers through Face Research (14), an online software that generates images of the average faces of men and women, and we used these generated average faces (not real people's faces) to represent different physical traits of young people in their twenties. The participants were asked, based only on the images shown, to choose the person in the pair presented they preferred as a hypothetical Uber driver. In total, each participant made 34 selections plus a final open question indicating motives for their selections.

Table 2 shows the main motives indicated by participants for Uber driver selection. There are important differences between motives for female and male teenagers (referred to as passengers henceforth). Gender and trust for selecting a driver are more important for female passengers than for male passengers, and quality of the image, which participants associated with professionalism and service quality, was more important for male passengers. Although the images of Uber drivers were computer-generated, a few images seemed less sharp than others, resulting in a confounding factor associated by passengers with professionalism.

A difference in the preference for the gender of Uber drivers depending on the gender of the passenger was evident. This preference was statistically significant (Chi-squared test, df_1=1, df_2=1, N=52, p-value < 0.005), indicating

Table 1. Demographic data of participants

Gender	Sample size	Mean age (years)	Standard deviation (years)
Female	27	17.4	1.1
Male	25	17.9	1.3
Total	52	17.7	1.2

Table 2. Motives for selecting hypothetical Uber Driver according to passenger's gender

Motives	Female passengers	Male passengers
Gender	26%	4%
Trust	33%	15%
Kindness/smile	26%	37%
Quality image/professionalism	7%	26%
Other	4%	11%

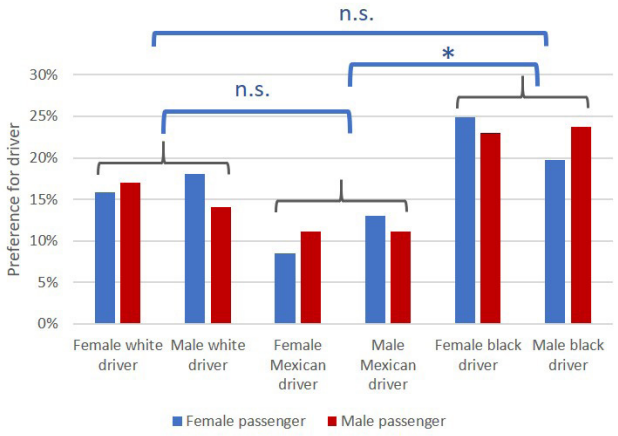

Figure 3. Preference of passengers for different ethnicity of drivers. There was a statistical difference due to skin color/ethnicity with male and female passengers selecting more black drivers over Mexican drivers (Chi-squared test, df=2, N=52, *p-value < 0.046).

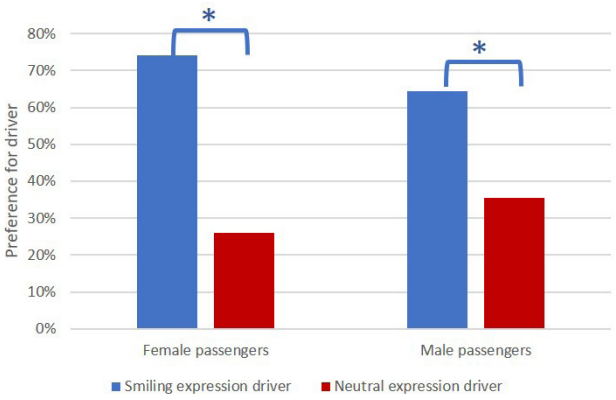

Figure 4. Preference of passengers for smiling vs. neutral facial expressions of drivers of the same gender and skin color/ethnicity. There was a statistically significant difference (Chi-squared test, df=1. N=52, *p-value < 0.006) by male and female passengers.

that female passengers prefer having female drivers, whereas male passengers did not have a preference for drivers based on gender (**Figure 2**). In most cases, female passengers preferred female drivers, whereas male passengers had no preference, independent of skin color/ethnicity.

For skin color/ethnicity preferences of the drivers, no statistical differences were found (Chi-squared test, df_1=1, df_2=2, N=52, p-value > 0.099) that indicated a skin color/ethnicity preference was affected by the gender of the passengers. But there was a statistical difference (Chi-squared test, df=2, N=52, p-value < 0.046) in hypothetical Uber drivers´ selection due to their ethnicity. Black drivers were selected preferably over white or Mexican drivers within the same gender and Mexican drivers were the least favored (**Figure 3**).

We also analyzed the influence of facial expressions on preference for hypothetical Uber drivers and found no differences in hypothetical Uber driver selection due to passenger´s gender (Chi-squared test, df_1=1, df_2=1, N=52, p-value > 0.094) and passengers preferred drivers with smiling expressions over neutral expressions when controlling for skin color/ethnicity and gender (Chi-squared test, df=1, N=52, p-value=0.006) (**Figure 4**). When the gender of the driver was controlled but skin color/ethnicity was not, both female passengers (Chi-squared test, df=1. N=27, p-value=0.021) and male passengers (Chi-squared test, df=1. N=25, p-value=0.045) still preferred smiling female drivers over neutral expression female drivers (**Figure 5).** Male passengers also selected more smiling male drivers (Chi-squared test, df=1. N=25, p-value=0.045), but there was no statistical difference for female passengers in their selection of male drivers (Chi-squared test, df=1. N=27, p-value=0.248) because of their facial expression **(Figure 6**).

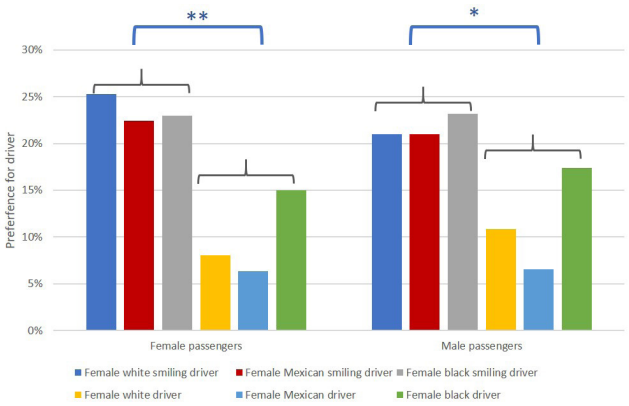

Figure 5. Preferences of passengers for smiling vs. neutral facial expressions for female drivers with different skin color/ethnicity. There was a statistically significant difference for smiling over neutral expressions by female passengers (Chi-squared test, df=1. N=27, **p-value = 0.021) and male passengers (Chi-squared test, df=1. N=25, *p-value = 0.045).

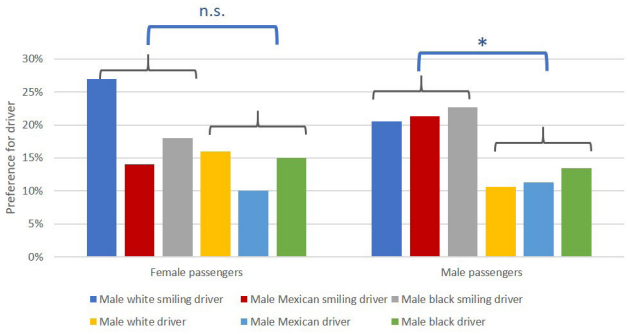

Figure 6. Preference of passengers for smiling vs. neutral facial expressions for male drivers with different skin color/ethnicity. There was a statistically significant difference for smiling over neutral expressions by male passengers (Chi-squared test, df=1. N=25, *p-value = 0.045), but not for female passengers (Chi-squared test, df=1. N=27, p-value = 0.248).

When facial expression of the drivers was tested without controlling for skin color/ethnicity and gender, female passengers preferred female drivers independent of the facial expression (75% of the time), while male passengers did not show any evident preference, showing in almost all cases 50/50 chances for selecting between the pair presented. An exception for male passenger selection happened when a Mexican driver was present; regardless of their gender or facial expression, male passengers favored the other driver (Chi-squared test, df=1, N=25, *p*-value = 0.033).

DISCUSSION

The applied surveys comparing two hypothetical Uber drivers with different physical traits (**Figure 1**) found differences in passengers' preference due to drivers' gender, skin color/ethnicity, and facial expression. The main reasons stated by participants for driver selections (**Table 2**) showed the differences between male and female teenagers when considering taking an Uber service. While females are more worried about security, reflected in gender and trust, males are more concerned about the quality of the service.

For gender influence, female passengers indicated more trust in female drivers than male drivers (**Figure 2**), whereas men did not consider gender as an important factor for selecting the driver. These results support previous investigations that expressed that women's faces are more trustable (3, 5). Our results agree with this statement in that female drivers were significantly preferred over male drivers by female passengers (**Figure 2**). Sociocultural and evolutionary perspectives have been used to explain this (5). Interpersonal, facilitative, and friendly behavior has been associated with female gender roles socially, whereas instrumental, more outcome-based roles have been associated with males, therefore associating female roles as more altruistic and thus more trustworthy (6, 15). From the evolutionary perspective, females (especially mammals) spend more time raising offspring and need to be more selective when choosing a partner, therefore women tend to be more careful in whom they trust (6). However, because females are more selective in their partners, males need to evolve more competitively and engage in risky behavior making them less trustworthy (16), but generally more trusting of others to have a better chance to establish relationships and cooperation within a group (6, 16). It is also important to consider the social context of Mexico, where ten women are murdered every day, and the rate of female homicides has doubled in the last five years (17). Most of these crimes are perpetrated by men, and it is commonly known that a modus operandi of some of these murders is through kidnapping and abusing the victim while they are traveling via ride services such as Uber. This is probably less concerning for male passengers, who are less likely to be victims of this type of crime, therefore explaining why men show no preferences concerning driver gender. For female teenagers answering the survey, this factor may increase the fear towards male drivers, leading to increased trust in female drivers.

When it comes to ethnicity, we discovered two interesting results. First, we expected that participants would choose Mexican drivers more than black or white drivers by identification with the Mexican faces since passengers were Mexican, but this was not the case. Second, black faces seemed to be preferred over the other choices. Familiar faces tend to be affable and judged as safe (4, 10). In this case, the most familiar face was believed to be the Mexican drivers; however, participants did not choose a face of their ethnicity, and black faces seem to be preferred (**Figure 3**). This difference in preference for black drivers over white and Mexican drivers, regardless of the passengers' gender, should be considered with caution. One explanation is that the survey was answered by teenagers with a mean age of 17.7 years old, who belong to the "gen Z" or "centennials" generation and are more used to seeing different ethnicity representations in social media. Being in touch with other cultures has made the younger generations much more tolerant of diversity compared to older generations (18-19). In Mexico, skin color varies from white to dark brown, but very few people are considered black, and in the area where this survey took place, black people are very unusual. Another possible explanation is that volunteers from the high school where this survey took place also have been educated in a multicultural environment that aims to form global citizens, this education develops a tolerant vision through classes like history and civics and international exchanges aimed for students to learn and respect different cultures and ethnicities, which could, in turn, explain that participants did not want to be perceived as racially prejudiced. Still, this is a theoretical scenario that needs to be challenged with real-life experiments. Most intriguing was the result that Mexican drives of both genders were selected less over white or black drivers. This can be explained by a cultural construct in Mexico, known as "malinchism". Malinchism is defined as an attraction for foreign values and aversion to your own culture (20). The term comes from the historic figure, "La Malinche," an indigenous woman advisor and lover of Spanish conqueror Hernán Cortés, who stood with the Spanish conquistadors assisting them to defeat the Aztec empire. This result, where Mexican participants frequently rejected Mexican drivers, is an example of internalized racism that has a powerful influence on thoughts and actions but is unconscious (21). Although Mexicans do not recognize themselves as racists, this internal racism against indigenous people exists and is very common (22). Still, the sample size was small (52 participants), and the participants all came from an urban private high school from the middle-upper class economic background, which does not represent the heterogeneity of the Mexican population.

Concerning facial expression, smiling drivers were selected moreover drivers with neutral expressions (**Figure 4**) when controlling for gender and skin color/ethnicity. This finding could support the idea that smiling is important

for building social trust (23), which is also associated with kindness (**Table 2**). It is worth mentioning that people make judgments based on facial expressions since emotional expressions are a common way to know people's behavioral intentions. Typically, people with happy expressions are perceived as approachable, while individuals who show an angry expression are seen as people who should be avoided (2). When gender was controlled but not skin color/ethnicity, both male and female participants preferred, in general, smiling expressions over neutral expressions of the drivers (**Figures 5** and **6**), which is also seen in the motives indicated for selecting drivers (**Table 2**), where a smile is associated with kindness. However, for female passengers there was no statistical difference in preference of smiling male drivers over neutral expression male drivers (**Figure 6**) which can be a result of the small sample size. When facial expression was tested but with no control of gender or skin color/ethnicity, female teenagers still preferred female drivers regardless of their facial expression, confirming they trust more women, but males show no preferences, except where the "malinchism" effect was present and teenage males preferred other drivers instead of Mexican drivers, independent of facial expression.

There are certain patterns when it comes to physical characteristics that make someone trustworthy. In this study, gender, ethnicity, and facial expression were determinants of trustworthiness for Mexican teenagers. The use of experiments and participants with a wide age range and socioeconomic background is recommended to improve this study. A social experiment were passengers, before selecting their Uber driver, can see the pictures of two or more drivers and then make their selection using only the pictures of drivers will give us more insight into how physical appearance affects trust in others. Doing social experiments is important since surveys are not always good representations of real conditions and can influence real behavior.

METHODS

We designed a survey in Google Forms. The survey was anonymous and only personal questions of gender and age were asked. We asked 52 high school teenage volunteers (27 females, 25 males) with ages ranging from 16 to 20 years old to participate in answering the survey in a private environment.

The survey had a total of 35 questions: 13 questions were administered first, and four months later, the rest of the questions were answered by the same volunteers. Each question displayed two images of people who represented hypothetical Uber drivers (**Figure 1**), except for the last question which was an open question asking participants to explain their motives for selecting the drivers. The images of the people were created through Face Research online software (14) that generates images of average faces of men and women with different physical traits (but are not faces of real people). The images were selected for the survey to display different physical characteristics, such as gender (male or female), skin color/ethnicity (white, Mexican, or black), and facial expression (neutral or smile), but looked the same age (in their twenties). For gender preferences, four questions (three on the first survey and one on the second survey) were used with different gender but controlling for ethnicity and facial expression (neutral) for each pair. For skin color/ethnicity preferences, six questions (all six on the first survey) were used varying ethnicity but controlling gender and facial expression (neutral) in each pair. Finally, for facial expression discrimination, a total of 24 questions were used (4 on the first survey, the rest on the second survey), and some were controlled for gender or skin color/ethnicity but not all. Participants were forced to discriminate four times for gender preferences, six times for skin color/ethnicity preferences, six times for facial expression preferences balancing for gender and skin color/ethnicity, twelve times for facial expression preferences balancing for gender but not skin color/ethnicity, and finally six times for facial expression preferences not balancing gender or skin color/ethnicity. Participants were asked, based only on the image shown, to choose the person that they want to have as a driver for each pair shown. Questions were randomly arranged according to preference trait: gender, ethnicity, or physical expression, but were presented in the survey in the same order for each participant. Last, an open question asked participants to indicate their motives for selecting the different hypothetical drivers. Participants did not know the images were computer generated and believed they belonged to real Uber drivers.

The data were analyzed using the chi-square test of independence and chi-square test of goodness of fit using a significance level of 0.05, and the chi-square test function from Microsoft Office Excel, 2020. Chi-square tests of independence were used for each question to test if the passenger´s gender was related to Uber driver selection according to the three variables tested: gender, ethnicity, and facial expression of the driver. When no statistical differences in Uber driver selection were found due to passenger´s gender, chi-square tests of goodness of fit were done pooling the questions that tested the variable of the Uber driver being evaluated: ethnicity or facial expression, and dividing the counts in each category by the number of questions used so that proportions of selections were compared keeping participants as the independent variable, with N=52 for each chi-squared goodness of fit test.

ACKNOWLEDGMENTS

The authors would like to thank the students of our high school that participated in answering this survey.

Received: May 19, 2020
Accepted: October 8, 2020
Published: November 9, 2020

REFERENCES

1. Cambridge Dictionary. "Trustworthy." *Cambridge Dictionary*, 2020, dictionary.cambridge.org/dictionary/english/trustworthy.
2. Oosterhof, N. N., and A. Todorov. "The Functional Basis of Face Evaluation." *Proceedings of the National Academy of Sciences*, vol. 105, no. 32, 2008, pp. 11087–11092., doi:10.1073/pnas.0805664105.
3. Sofer, Carmel, *et al*. "What Is Typical Is Good." *Psychological Science*, vol. 26, no. 1, 2014, pp. 39–47., doi:10.1177/0956797614554955.
4. Zebrowitz, Leslie A., *et al*. "The Contribution of Face Familiarity to Ingroup Favoritism and Stereotyping." *Social Cognition*, vol. 25, no. 2, 2007, pp. 306–338., doi:10.1521/soco.2007.25.2.306.
5. Mattarozzi, Katia, *et al*. "Effects of Gender and Personality on First Impression." *Plos One*, vol. 10, no. 9, 2015, doi:10.1371/journal.pone.0135529.
6. Derks, Jeffrey, *et al*. "Adolescent Trust and Trustworthiness: Role of Gender and Social Value Orientation." *Journal of Adolescence*, vol. 37, no. 8, 2014, pp. 1379–1386., doi:10.1016/j.adolescence.2014.09.014.
7. APA Dictionary of Psychology. "Familiarity". *American Psychological Association*, 2020.
8. Todorov, Alexander, *et al*. "Social Attributions from Faces: Determinants, Consequences, Accuracy, and Functional Significance." *Annual Review of Psychology*, vol. 66, 2015, pp. 519–545., doi:10.1146/annurev-psych-113011-143831.
9. Bartlett, James C., *et al*. "Typicality and Familiarity of Faces." *Memory & Cognition*, vol. 12, no. 3, 1984, pp. 219–228., doi:10.3758/bf03197669.
10. Halberstadt, Jamin and Gillian Rhodes. "It's Not Just Average Faces That Are Attractive: Computer-Manipulated Averageness Makes Birds, Fish, and Automobiles Attractive." *Psychonomic Bulletin & Review*, vol. 10, no. 1, 2003, pp. 149–156., doi:10.3758/bf03196479.
11. Galton, Francis. "Inquiries into Human Faculty and Its Development." 1919, doi:10.1037/10913-000.
12. Stanley, D. A., *et al*. "Implicit Race Attitudes Predict Trustworthiness Judgments and Economic Trust Decisions." *Proceedings of the National Academy of Sciences*, vol. 108, no. 19, 2011, pp. 7710–7715., doi:10.1073/pnas.1014345108.
13. Ben-Ner, Avner, and Freyr Halldorsson. "Trusting and Trustworthiness: What Are They, How to Measure Them, and What Affects Them." *Journal of Economic Psychology*, vol. 31, no. 1, 2010, pp. 64–79., doi:10.1016/j.joep.2009.10.001.
14. DeBruine, Lisa and Ben Jones. "Face Research: Experiments about face and voice perception", *Face Research*, www.faceresearch.org.
15. Eckes, Thomas, and Hanns Martin Trautner. *The Developmental Social Psychology of Gender*. Lawrence Erlbaum Associates, 2000.
16. Balliet, Daniel, *et al*. "Sex Differences in Cooperation: A Meta-Analytic Review of Social Dilemmas." *Psychological Bulletin*, vol. 137, no. 6, 2011, pp. 881–909., doi:10.1037/a0025354.
17. Sandin, Linnea. "Femicides in Mexico: Impunity and Protests." *Center for Strategic and International Studies*, 19 Mar. 2020, www.csis.org/analysis/femicides-mexico-impunity-and-protests.
18. Llaneras, Kiko, *et al*. "La Generación Que Desbanca a Los 'Millennials'." *El País*, 20 Aug. 2018, elpais.com/internacional/2018/08/19/actualidad/1534683555_936952.html.
19. Rothman, Darla. "A Tsunami of learners called Generation Z."*www. mdle. net/JoumaFA_Tsunami_of_Learners_Called_Generation_Z. pdf*, 2016.
20. Dantas Alexis Toríbio, and Maria Teresa Toribio Brittes Lemos. *América: visões e versões, Identidades Em Confronto*. 7 Letras, 2010.
21. Leff, Jacqueline Fortes De. "Racism in Mexico: Cultural Roots and Clinical Interventions1." *Family Process*, vol. 41, no. 4, 2002, pp. 619–623., doi:10.1111/j.1545-5300.2002.00619.x.
22. Moreno Figueroa, Monica G. "Naming Ourselves: Recognising Racism and Mestizaje in Mexico". *Contesting Recognition. Identity Studies in the Social Sciences*. Edited by J. McLaughlin *et al*., Palgrave Macmillan, London, 2011, pp. 123-125., doi.org/10.1057/9780230348905_7
23. Centorrino, Samuele, *et al*. "Honest Signaling in Trust Interactions: Smiles Rated as Genuine Induce Trust and Signal Higher Earning Opportunities." *Evolution and Human Behavior*, vol. 36, no. 1, 2015, pp. 8–16., doi:10.1016/j.evolhumbehav.2014.08.001.

JOURNAL OF
EMERGING INVESTIGATORS

Article

The external presence of running water influences the root growth of pea plants (*Phaselous vulgaris*)

Jonathan Shu, Philip Allen
Interlake Senior High School, Bellevue, Washington

SUMMARY

Each year, invasive tree roots cause large amounts of damage to underground pipes. While this is usually due to leaks and cracks, tree roots can also invade pipes that are structurally sound. We are interested in investigating whether plant roots have an affinity towards flowing water, measured through mass, even when the running water is not in direct contact with soil. We tested this by creating a choice chamber with water running under one end and no stimulus on the other end. We grew the plants in their chambers until their stems reached 10 inches before removing the plants to measure the mass of the roots growing towards either side of the choice chamber. Data from other scientists as well as a previously conducted experiment seemed to show that flowing water attracted plant roots. Therefore, we hypothesized that there would be greater root mass on the side of the chamber exposed to flowing water. Overall, the masses of the roots growing towards flowing water were greater than the masses of the roots growing towards the end with no stimulus, showing that plant roots did have an affinity towards flowing water. The remarkable sensitivities of plants to sound are still being discovered, but the delicacy already shown by experiments such as ours leaves concerns regarding a new facet of the impact of sound pollution on our ecosystems.

INTRODUCTION

Tree roots are notorious for growing towards and clogging sewer pipes, causing serious amounts of damage each year (1). This issue is usually treated through heavy use of strong herbicides. What makes this notable is that the direction of root growth does not seem random, but instead very intentional (1).

Plants have long been known to show clear responses to environmental stimuli, known as tropisms. These tropisms, such as gravitropism and phototropism, are what cause roots to follow the force of gravity, as well as leaves and stalks to bend towards the light (2). The growth hormone auxin primarily controls these responses (2). Contrary to the typical notion of plants as stationary and unresponsive, plants have developed surprisingly sensitive reactions to external influences. In addition to these well-known tropisms, there is also growing evidence showing that plants are sensitive towards more minor stimuli like sound vibrations (3).

A previous study looked the response of plants towards external sources of water, finding that roots grew towards flowing water rather than stagnant water despite neither water source directly contacting the soil (4). In a preliminary experiment, we replicated this study's setup, and similarly found that roots were longer and more numerous towards the water flowing outside the soil. Root responses to water are often due to hydrotropism, which is thought to be linked to membrane proteins as well as water uptake through the root. As water potential decreases, it affects the activity of proteins in the plasma membrane such as aquaporins, in turn affecting the ease in which water could travel through the root, known as hydraulic conductivity (5). This conductivity could change root direction through cell elongation or through changing concentrations of abscisic acid, a growth inhibitor. There is a "set point" at which plasma membrane protein behavior changes could cause a signal cascade resulting in directional changes (5). However, hydrotropism requires direct contact between the root and water. The fact that plant root growth was still concentrated towards flowing water in the study and our preliminary experiment even without direct contact raises the possibility of lesser-known mechanisms, such as sound vibrations.

We therefore hypothesized that the roots of the garden bean (*Phaselous vulgaris*) would show increased growth in the direction of externally flowing water, possibly responding to sound to compensate for the lack of contact. Through these studies, we were able to show that plants have evolved remarkably accurate responses to stimuli.

RESULTS

In our preliminary experiment, we measured the length of the longest root growing down either side of the chamber, as well as the number of roots longer than two thirds the length of an arm of the chamber (3.33 inches). We found some signs of a relationship between flowing water and greater root growth. In six of nine trials, we saw a greater percentage of roots longer than 3.33 inches growing towards the flowing water. However, these percentages of increase varied widely, from 50% to 100% (Figure 1). Additionally, one trial had a majority of growth towards the stagnant water. However, both flow and stagnant control chambers experienced equal growth on either side, suggesting an influence of flowing water.

The data was similar in regard to the length of the longest

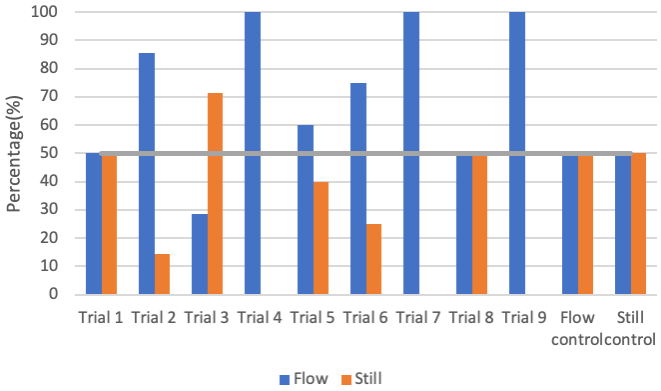

Figure 1: The percentage of roots longer than 3.33 inches growing down either side of each chamber. This graph shows the number of roots that grew to at least two-thirds the length of the choice chamber; the data is represented as a percentage of the total amount of roots longer than 3.33 inches. There is a horizontal line marking 50 percent, the height of the bar if growth was even This graph shows a general trend of more numerous roots towards flowing water, as well as even growth in the control chambers.

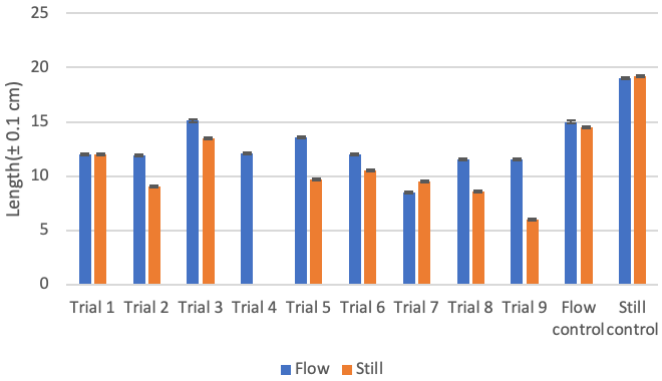

Figure 2: The maximum lengths of roots growing down either side of each chamber. The graph shows the longest root growing down either end of each trial with error bars of 0.1 cm to account for measurement error. This graph shows greater maximum root length towards flowing water, as well as even growth in the control chambers.

root growing down either end of the chamber. Seven of nine trials saw a longer maximum root length growing towards flowing water. As with the previous data, there was much variance between trials. Some trials experiencing complete one-sided growth towards flowing water while others were even or saw more growth towards stagnant water. The maximum length of the roots down either end of both control tubes was even, showing differences of 0.5 centimeters or less (Figure 2). Viewing both forms of measurement as a whole, we came to a tentative conclusion that flowing water will attract roots over stagnant water.

In our final experiment, we measured the mass of the roots growing down either side of the chamber. We found that the roots growing down the ends exposed to flowing water were on average 0.35 grams heavier than ends exposed to no water, making the roots exposed to flowing water about 51% heavier than those exposed to no stimulus (Figure 3).

We used the Wilcoxon signed-rank test on our raw data to determine if there was a statistical correlation that could further strengthen our conclusions. The null hypothesis was that the medians of the "flow" and "still" data groups were equal, while the alternative hypothesis was that the two medians differed. Since the sample size was smaller, we used the W value to evaluate the hypothesis. The critical value for W ($p<0.05$) at a sample size of 10 is 10; the W value of our data set was zero. The Wilcoxon signed-rank test therefore showed that our results were statistically significant.

In addition, each individual trial saw a greater percentage of total root mass growing towards the running water (Figure 4). In the control tubes, plants grew exposed to the same conditions (flowing water or no water) on both ends of the choice chamber, there was little change in growth. Instead, both sides saw an even distribution of root mass with each end of the chamber containing 49-51% of the total root mass (Figure 4). There appeared to be no specific side that the roots favored in the control tubes, showing that the experiment experienced minimal effects from influences like gravitropism. An additional observation was that there was only root branching on the roots exposed to flowing water (Figure 5). Overall, the resulting data and statistical analysis shows a correlation between greater root growth and the presence of flowing water.

DISCUSSION

The data collected supports the hypothesis of greater growth in the direction of the flowing water. There was an evident trend of greater root mass down the end of the chamber exposed to flowing water. This larger mass signifies greater growth and implies that plants are "attracted" to running water, concentrating their growth in that direction. The observation that only roots growing towards flowing water showed branching further supports this. Root branching facilitates water uptake and nutrient extraction (6), suggesting that roots on the "flow" side of the chamber were more developed and used. In both control scenarios, the plants showed little change in growth, growing down both ends without distinction. This shows that specifically changing the stimulus did, in fact, result in a change in growth. These results are supported by the findings of our preliminary experiment, which saw longer and more numerous root growth towards externally flowing water rather than stagnant water. This distinction between flowing water and stagnant water justifies the hypothesis of sound detection, rather than simply the presence of water. The results of our experiment were also consistent with that of the study done by M. Gagliano, where seedling roots showed a greater proportion of growth towards flowing water enclosed in a pipe as opposed to stagnant water (4).

Throughout these experiments, we identified several sources of error including a potential lack of variable control. Other influences, such as gravitropism or hydrotropism, will overpower a plant's response to external flowing water.

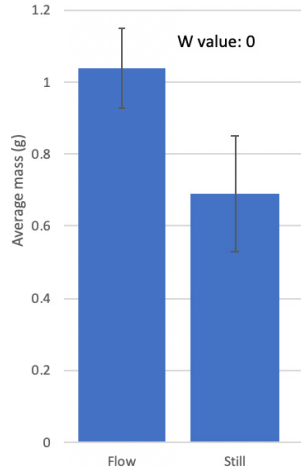

Figure 3: The average mass of roots growing down either side of each chamber. This graph shows the average mass of the roots growing down either side of the chambers of each trial, with error bars representing one standard deviation. This graph also shows the W value of zero obtained from the Wilcoxon signed-rank test.

Failing to control for these aspects in an early test trial resulted in roots that followed the tilt of the chamber, away from the running water. Rerunning the trial with a leveled tube saw growth in the opposite direction, towards flowing water. Despite this, we believe it is unlikely our experiments were impacted by other tropisms, as the soil was level and evenly moistened. There also could have been error in measuring the differences in root growth, as root activity involves many factors. In our preliminary experiments, this source of error was especially prevalent as we came to see that root length or number did not accurately represent root growth some of the time. We attempted to correct for this error in the final experiment, and measuring mass seemed to be a comprehensive and effective method. We identified a related, more potent source of error in maintaining root configuration while removing the plants from their choice chambers. Once the roots lost the support of the surrounding soil, some of the original directionality and positioning was inevitably lost, which could have led to inaccurate masses on either side.

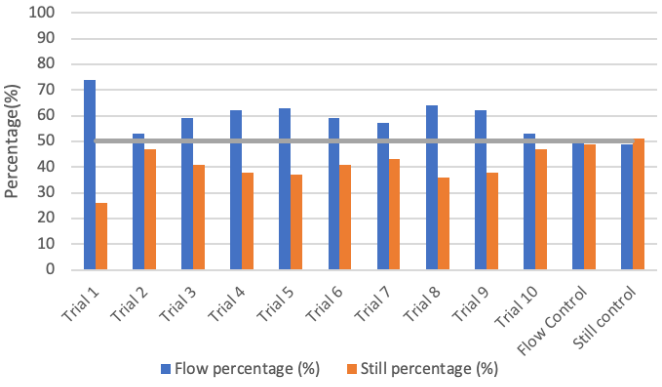

Figure 4: The percentage of root mass of each trial growing down either side of each chamber. The graph shows the root mass growing towards either end of the chamber as a percentage of the total root mass. There is a horizontal line marking 50 percent, the height of the bar if growth was even. This graph shows a greater percentage of mass growing towards flowing water for each trial, as well as the minimal difference in mass distribution when there was no difference in stimuli.

This issue could be resolved in the future by using clear tubing wrapped in black cloth. The cloth would protect the roots from the influence of light during growth and be removed at the end of the experiment. We could then examine the original configuration of the root system with greater ease. This would also give more certainty in the various mass measurements.

While our conclusion satisfies the initial research question, it does not provide full insight into how or why plants are able to target flowing water. Our preliminary experiment seemingly suggests the movement of water specifically influences growth. However, our final experiment only tested flowing water against no stimulus, making it difficult to conclusively support this claim. In the future, it would be interesting to bring the ideas of our preliminary experiment to our final experiment's setup and methods, explicitly testing stagnant water against flowing water. And further extensions could include the use recordings of running water as opposed to real water or soundproofed choice chambers to truly determine if sound is the primary influence.

But from the study done by M. Gagliano, the main theory appears to be that plants use vibrations to help detect the movement of water. Sound waves originate from vibrating objects and are transmitted by the oscillation of particles in a medium. Plants have been shown to change their behavior when exposed to multiple different types of vibrations (5). Certain frequencies influence germination, elongation, and cell cycling (7-9). This shows that vibrations can influence growth and directionality. In wheat and rice, exposure to vibrations increases overall yield, nutrient content, and resistance against pests (10). Plants have also been shown to produce glucosinolate and anthocyanin, defensive components, when exposed to frequencies mimicking feeding (11). These effects heavily imply that vibrations cause chemical changes which regulate growth. More specifically, streamside trees have been found to grow their roots into deeper layers of soil rather than shallower streams (12). Deeper layers of soil provide a steadier source of water than shallow streams, and differences in vibration could explain how roots are able to direct themselves past the closest source of water and instead choose the most effective.

The current concept of the influence of sound vibrations on a plant cell is a combination of research and hypothesis. It appears that sound vibrations increase the membrane tension of the plasma membrane of cells through microfilament rearrangement (3). The changes in the plasma membrane caused by these vibrations allow for the movement of a "messenger" through stretch-activated channels, most likely the calcium ion Ca2+. Through either Ca2+ sensors or calcium dependent protein kinases, the generated Ca2+ "message" is passed through proteins or transcription factors, eventually resulting in gene expression (3). Cells exposed to vibrations also synthesize more proline and reactive oxygen species (ROS), auxin and ethylene, and ATP. Proline and ROS increase activation of Ca2+ and K+ channels, further increasing gene expression, while auxin

and ethylene may target specific response genes (3). This aspect is of particular interest as ethylene and auxin are both known to regulate plant growth. Auxin is found in shoot and root tips and promotes stem and root growth as well as controls orientation. ATP production increases in order to support these processes (3). This general pathway of sound-induced gene regulation is most likely how the plant roots in our experiments differentiated the source of flowing water.

We can therefore see that the behavior of tree roots is most likely intentional. With the most supported hypothesis being that plants can detect vibrations, this could solve the issue of root invasion of sewer pipes. Rather than the typical treatment of harsh chemicals, actions like soundproofing could present an eco-friendly solution.

As plants have evolved to be so tuned in to their environment, it is inevitable that human development will affect them. Besides the obvious concerns of deforestation and degradation of soil quality, growing knowledge of the sensitivity of plants raises other concerns as well. Plants make up 80% of Earth's biomass, yet they are often overlooked because they operate at a different pace than other organisms (13). However, time lapse videos of plants have shown them competing for territory and nutrients and even communicating through various signals (14). The effects of noise pollution is well documented in animals, but its effects on plants remain unknown. If plants can detect vibrations as small as chewing caterpillars, noise pollution could prove to have larger consequences than expected, blocking off sonic information channels (11). It is therefore important to further understand how plants respond to external stimuli. If plants are truly able to distinguish between vibrations with as much subtlety as current data suggests, this leaves unknown concerns for the impact of sound pollution on plant behavior. Neglecting such a large part of our ecosystem could therefore prove detrimental in the future.

Figure 5: Root branching example. This image shows the secondary branching of roots growing towards the left side of the image, which was the side exposed to flowing water. This branching is not present on the side exposed to no stimulus.

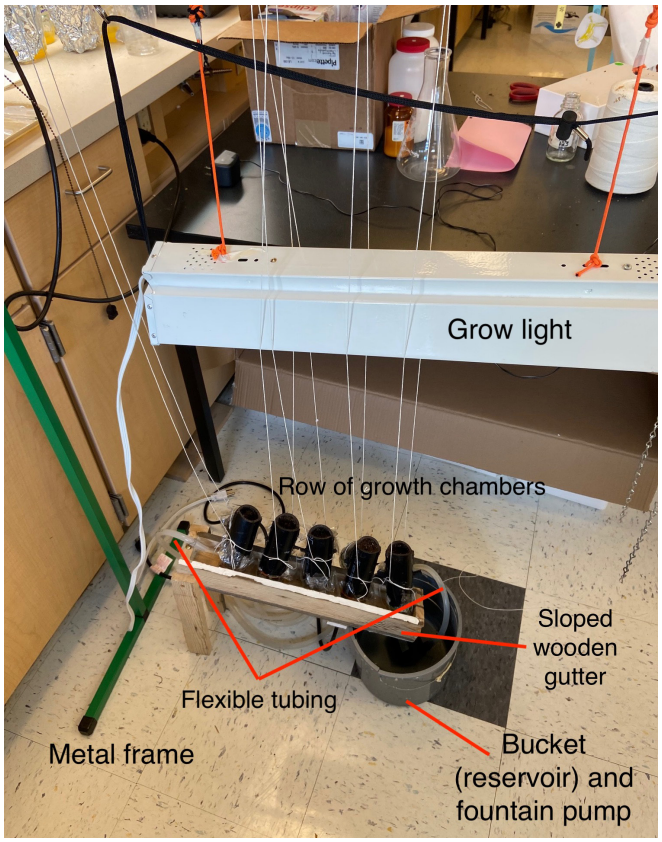

Figure 6: Experimental setup. This labeled image shows the entire setup of the experiment. It shows how each component was hung from the metal frame, as well as the setup of the gutter system to ensure that a consistent water flow was delivered to one end of each choice chamber.

MATERIALS AND METHODS

To test the question of whether plants could detect the external presence of running water, a double ended choice chamber was created to grow each plant in. Each chamber had one end suspended above a gutter with water flowing through it, while the other end was exposed to no sound. To analyze root growth, plants were removed from their chambers and the roots were grouped into those that had grown down the end exposed to flowing water and the end exposed to no sound. Root growth was quantified through mass, with groups being weighed individually. The results were standardized by converting the values into percentages of the total root mass of the plant. A greater percentage of total mass was taken as a sign of increased growth.

The manipulated variable was the presence of running water. The responding variable was the amount of root growth, measured by mass. As controls, two chambers were grown: one where both ends were exposed to running water and one where neither end was exposed to running water. This allowed for a better determination of whether changing the plants' exposure to flowing water was the specific factor that influenced growth. The controlled variables were the type of plant grown, orientation and build of each chamber, and general growing environment (such as light and temperature). Different species of plants have different affinities for water and could therefore react differently in this experiment. These variables were managed by growing the same species of bean throughout each trial under an overhead grow light, which kept the light source consistent. The plants were also grown indoors at a stable temperature of around 18˚C. Each chamber was leveled to ensure that stronger influences on growth, such as gravitropism, had a minimal effect on the root directionality. When building the chambers, the separation angle between the two prongs was kept as consistent as possible. This standardized the degree of separation between the paths the roots could take, improving clarity of results. Keeping these variables consistent increased certainty that the presence of running water was the main condition changing the directionality of root growth.

To create the chambers, PVC pipes were cut into 10 five-inch segments. Angled portions were then cut off each segment. Pairs of segments were joined with PVC cement, creating five chambers with an inverted "Y" shape, before the cement was left to harden. Potting soil was then placed in a bucket and mixed with water until it was moist to the touch. The two open ends at the bottom of each choice chamber were wrapped with plastic wrap, and each chamber was filled with soil. Five seeds were germinated between damp paper towels within a sealed bag. Once each seed had germinated, they were removed from the bag and each was placed within its own choice chamber.

In the preliminary experiment, one end of each of the five choice chambers was placed in a tray filled with water. Flexible tubing was connected to a fountain pump and wrapped around the other end of each chamber. Supports were added under the ends of each chamber to ensure they were all level. The pump was then switched on and each plant was allowed to grow until its stem had reached 10 inches. At that point, each plant was removed, and the longest root on either side of the chamber was measured. The number of roots that had grown longer than 3.33 inches (two thirds the length of each arm of the chamber) was measured as well.

In this experiment, a cord was used to hang a grow light from a metal frame. The gutter system was set up underneath. One end of the gutter was elevated, using blocks as support. The lower end of the gutter was placed on top of a bucket filled with water containing the fountain pump, which served as the reservoir. Flexible tubing was connected to the fountain pump, and the other end of the tubing was secured to the elevated end of the gutter. Four plastic dividers were placed within the gutter to differentiate spaces for each chamber to occupy, and small pebbles were added throughout to create more disturbances and vibrations in the water (Figure 6). Using string, each chamber was hung from the metal frame with one end placed in the gutter above the running water (Figure 7). After the plants had grown to around 10 inches, a hose was used to flush the soil out. Roots that had grown in the same direction were grouped together and massed. After recording this data, the chambers were refilled, five new seeds were germinated, and the process was repeated.

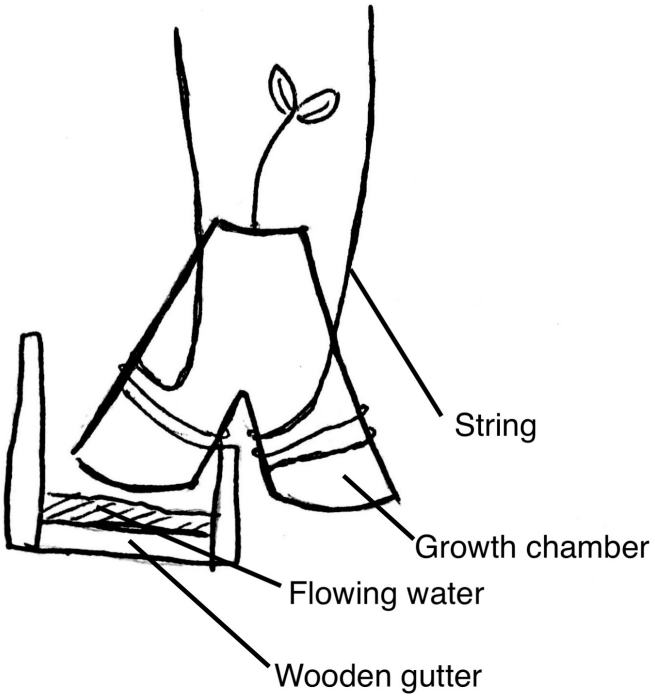

Figure 7: Cross sectional gutter diagram. This labeled drawing shows a cross sectional view of the wooden gutter, giving a closer view of the placement of each choice chamber.

For the control tube with no stimulus, the chamber was hung underneath the grow light in a similar fashion as mentioned above, but the gutter system was not placed beneath the tube. For the control tube with running water, the chamber was hung underneath the grow light and the gutter was aligned to expose both ends of the chamber to running water. Both ends of the gutter level were kept level to ensure that both ends of the chamber were the same distance away from the running water. The fountain pump maintained the movement of water through the system. The same standards of growth and methods of data collection were used for both control tubes as well.

REFERENCES

1. M.A., Pohls, O. "Study of Root Invasion of Sewer Pipes and Potential Ameliorative Techniques." Acta Horticulturae, vol. 643, 2004, pp.113-121, doi: 10.17660/

ActaHortic.2004.643.13.
2. Biggs, Alton. "Plant Structure and Function." Glencoe Biology, 1st, McGraw-Hill, 2009, pp. 648, 651.
3. Mishra, Ratnesh C., et al. “Plant acoustics: in the search of a sound mechanism for sound signaling in plants.” Journal of Experimental Botany, vol. 67, no. 15, 2016, pp. 4483-4494, doi: 10.1093/jxb/erw235.
4. Gagliano, Monica, et al. “Tuned in: plant roots use sound to locate water.” Oecologia, vol. 184, no. 1, 2017, pp: 151-160, doi: 10.1007/s00442-017-3862-z.
5. Dietrich, Daniela. “Hydrotropism: how roots search for water.” Journal of Experimental Botany, vol. 69, no.11, 2018, pp. 2759-2771, doi: 10.1093/jxb/ery034.
6. Atkinson, Jonathan A., et al. “Branching Out in Roots: Uncovering Form, Function, and Regulation.” Plant Physiology, vol. 166, no. 2, 2014, pp. 538-550, doi: 10.1104/pp.114.24542.
7. Gagliano, Monica. “Green symphonies: a call for studies on acoustic communication in plants.” Behavioral Ecology, vol. 24, no. 4, 2013, pp. 789-796, doi: 10.1093/beheco/ars2006.
8. Chowdhury, Emran K., et al. “Update on the effects of sound wave on plants.” Research in Plant Disease, vol. 20, no. 1, 2014, pp. 1-7, doi: 10.5423/RPD.2014.20.1.001.
9. da Silva, Jaime A.T., et al. “Sonication and ultrasound: impact on plant growth and development.” Plant cell Tissue and Organ Culture, vol. 117, no. 2, 2014, pp. 131-143, doi: 10.1007/s11240-014-0429-0.
10. Hassanien, Reda H.E., et al. “Advances in effects of sound waves on plants.” Journal of Integrative Agriculture, vol. 13, no. 2, 2014, pp. 335-348, doi: 10.1016/S2095-3119(13)60492-X.
11. Appel, Heidi M., et al. “Plants respond to leaf vibrations caused by insect herbivore chewing.” Oecologia, vol. 175, no. 4, 2014, pp. 1257-1266, doi: 10.1007/s00442-014-2995-6.
12. Dawson, Todd E., et al. “Streamside trees that do not use stream water.” Nature, vol. 350, 1991, pp. 335-337, doi:10.1038/350335a0.
13. Thompson, Andrea. "Plants Are the World's Dominant Life-Form." Scientific American, Springer Nature, 1 Aug. 2018, www.scientificamerican.com/article/plants-are-the-worlds-dominant-life-form/.
14. Gowan, Jessi. "How Much Can Plants Hear?" Permaculture Research Institute, 28 Aug. 2017, www.permaculturenews.org/2017/08/28/much-can-plants-hear/.

Article submitted: May 6, 2020
Article accepted: June 14, 2020
Article published: November 10, 2020

JOURNAL OF
EMERGING INVESTIGATORS

Article

Integrated Ocean Cleanup System for Sustainable and Healthy Aquatic Ecosystems

Jomills Jose Anand[1], Srevin Saju[1], Shaji Sam T L[1]`
[1]The New Indian School, Isa Town, Kingdom of Bahrain

SUMMARY

In an attempt to find a natural alternative to the commercially used oil-spill adsorbents, we investigated natural adsorbents such as sugarcane, cotton, charcoal, and clay. It has been observed that, up to a certain limit, these materials can be used to clean up oil spills. In addition, particular combinations of these materials could perhaps increase the efficiency of the cleanup. Subsequently, we carefully tested the adsorbing efficiency of each natural adsorbent with oils of different viscosities. By prototyping with a small-scale model, we found that some materials adsorbed oil more than the others, with bentonite and activated charcoal having the highest capacity of up to 100% oil-water mixture adsorption in the first two passes and nearly 90% adsorption in the third pass. Creating different layers of different materials helped to better filtrate the oil-water mixture. Upon testing with seawater, the prototype that we developed was able to adsorb three passes of a mixture of equivalent volume with nearly 100% efficiency. This means that the natural adsorbents tested have comparable efficiency to commercially used nonwoven polypropylene, while being non-toxic to aquatic life and easier to dispose of. Here we describe in detail our studies and prototyping of an effective oil cleanup system.

INTRODUCTION

From their rich biodiversity to their biophysical and chemical buffer systems, aquatic ecosystems play a tremendous role in the biosphere. They comprise the hydrosphere, which houses marine flora and fauna, regulates the water cycle, and provides various resources for civilization. It's therefore essential to maintain a clean and healthy hydrosphere, as these ecosystems provide over half of the breathable oxygen present in air and consists of over 97% of the world's water. These ecosystems also provide nutrition to humans and animals and play a major role in the world's economy from transportation to marine-based investments.

However, the ocean has been contaminated with various kinds of plastics and large patches of oil that mainly collect at five points in the ocean, called the Great Garbage Patches (1). Some of these contaminants, however, do not get collected and are found floating on the ocean and seasides, killing numerous aquatic flora and fauna (2). The floating ocean debris has severely decreased the albatross population and killed over 100,000 marine animals each year (3). Oceanic wastes have been alarming to humans, and the seafood industry is inhibited by the harmful chemicals enclosed in the food chain. Modern non-governmental organizations have taken technological initiatives by using polymer sheets and ocean booms to attract plastic pieces together and destroy them (2). However, recent efforts are focusing on modern and eco-friendly means of ocean cleanup, which are sustainable and have the lowest carbon footprint (4).

With the rising need to clean up the polluted ocean, various methods have incorporated traditional and contemporary technologies. Several popular methods of cleaning up oil spills exist today (5). In-situ burning involves the controlled burning of the oil at the surface of oceans until there is very little or no spilled oil remaining. However, this method isn't always successful, and the fumes released could cause environmental pollution. Another method, natural degradation, also known as bioremediation, comprises the use of certain microorganisms that breaks down these complex oil molecules into non-toxic substances. A physical method is oil collection, which involves using booms to trap the spilled oil over the surface and collecting the oil in a vessel.

One of the most efficient methods of cleaning oil spills is adsorption (5). Adsorbents are materials that trap oil on their surface. For oil adsorption, nonwoven polypropylene has been used repeatedly due to its high water-adsorption capacity and low density. Due to its low cost, polypropylene has been used to clean oil spills around the globe. However, polypropylene disposal became a great issue for the environment as it is either burnt or left in the oceans afterwards (6).

In the wake of this issue, we decided to use natural materials to create a highly efficient ocean cleaner. We hypothesized that in opposition to the commercially used nonwoven polypropylene, a material with high oil affinity and natural origin is likely to have a lesser environmental impact and be sufficiently efficient in terms of the oil it adsorbs. In this paper we describe the efficiency of several adsorbent materials which could potentially be used as viable alternatives for present commercial adsorbents.

RESULTS

In a preliminary test with organic adsorbent materials such as cotton, coconut husk, and jute, the oil adsorbed appeared to be minimal [data not shown]. However, the few inorganic adsorbents that were tested exhibited significantly higher adsorption properties, thus we proceeded to test them with different oils.

We calculated the efficiency of each inorganic material in adsorbing kerosene, petrol, diesel, and engine oil as the ratio

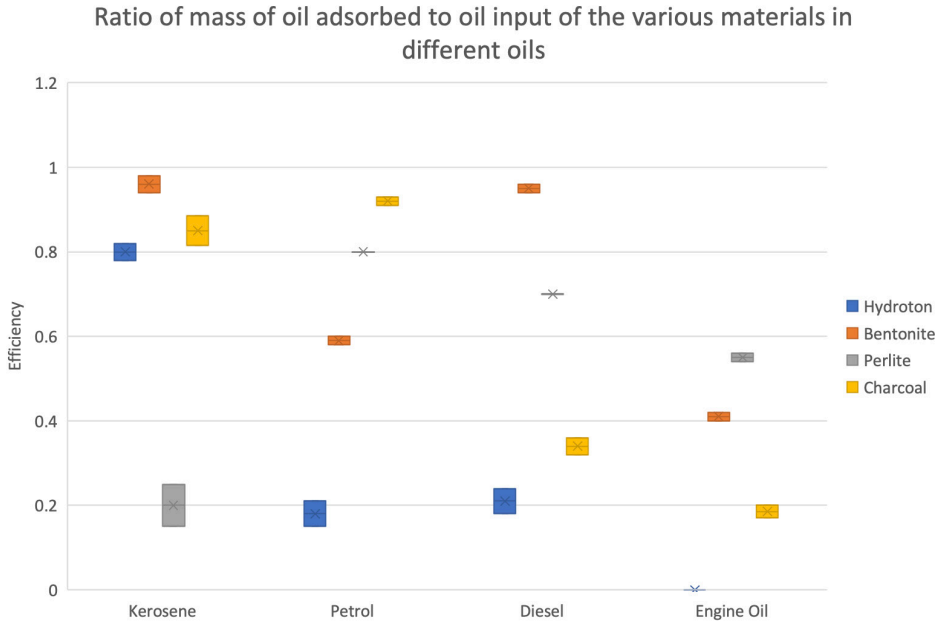

Figure 1. Efficiency of the various components of our prototype in oils of varying viscosities. The graph displays the percentage of oil-adsorbed to oil-input when bentonite, perlite, hydroton, and activated charcoal are introduced with four oils kerosene, engine oil, diesel, and petrol. The data from this figure was used to determine the order of materials incorporated into the prototype. On average, bentonite and activated charcoal displayed high oil-adsorption capacities overall.

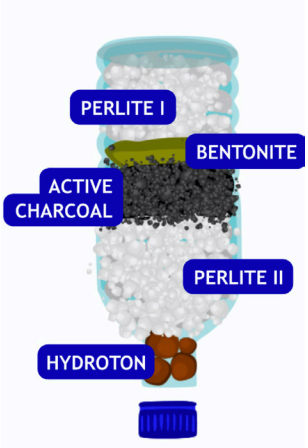

Figure 2. Prototype design. The prototype consisted of perlite, bentonite, activated charcoal, and hydroton layered in the order perlite-bentonite-activated charcoal-perlite-hydroton in the ratio 3:1:2:3:2. Results from Figure 1 and economic feasibility of each material were used to determine order and ratio.

of oil-adsorbed to oil-input (**Figure 1**). Bentonite on average showed the highest oil adsorption efficiency, while hydroton exhibited the least. Additionally, perlite served as a midline. Hence with all this data, we constructed a prototype composed of perlite-bentonite-activated charcoal-perlite-hydroton in the ratio 3:1:2:3:2 (**Figure 2**). The order of materials was decided based on their adsorption, placing the higher adsorbing materials towards the middle. The ratio composition was based on the economic feasibility of each material. For further experiments, the oil was an equal mixture of the three oils kerosene, petrol, and diesel since engine oil is much denser and viscous in comparison to crude oil (7).

As part of the oil-water emulsion test, we passed the equivalent weight (33 g) of oil-seawater emulsion through the apparatus. The first two passes were completely adsorbed by the apparatus. During the third pass, the apparatus collected 25 g of water, which was determined to be pure enough for household use. We inferred that the water adsorption capacity may have reached the maximum limit, meaning that the apparatus had successfully taken up 99 g of oil-water emulsion, but upon reaching the limit of adsorption, released 25 g of water as residue. For confirmation, we added 33 g of water once again to the apparatus following the end of the third pass, after removing the leftover residue from the conical flask. This experiment released 20 g of water into the conical flask, with infinitesimal but observable traces of oil.

To confirm the potential absence of oil in the filtrate from the third pass, we conducted a flame test. A filter paper dipped into the oil-seawater emulsion caught on fire almost immediately once introduced into a flame. The flame test with newspaper dipped in the filtrate from the third pass, however, did not catch fire, likely due to the considerably less or negligible amount of oil.

We conducted a Baeyer's reagent test, which is an experiment used to test the presence of oil in a solution. When testing the oil-seawater emulsion with Baeyer's reagent, we obtained a brown precipitate and clear purple supernatant. Hence, the presence of oil was confirmed by brown precipitate and the purple supernatant indicated clear water. With the filtrate-Baeyer's reagent mixture, the test

Media	Refractive Index
Pure distilled water	1.333
Seawater	1.349
Filtrate produced in the experiment	1.35
Crude oil	1.46

Table 1. Mean refractive index of the various tested media. This table displays the average of the calculated values of refractive indices we have measured in the refracting index test. The refractive index was calculated by passing a laser beam through a hollow rectangular prism containing the media and measuring the change in position of an object when placed in front of the prism.

NON-WOVEN PROPYLENE	RESEARCH PROTOTYPE
(C3H6)n Polypropylene	69% Perlite 13% Charcoal 7% Bentonite 11% Hydroton
Non-biodegradable	Highly biodegradable
Disposable / One-time use	Can be used as fuel
Artificial / man-made product	Natural / eco-friendly product
Can adsorb up to 15 times its weight theoretically. (9)	Experimentally could adsorb up to 3 times its weight before releasing some of the adsorbed water.
Hydrophobic and oleophilic	More oleophilic and less hydrophilic. Adsorbs both water and oil. Releases water, as the prototype has more affinity towards oil.
Harms aquatic ecosystem and harmful when consumed by animals.	Not harmful to animals, if large-scale model is implemented.

Table 2. Comparison between commercially used adsorbents to the prototype we constructed. We have used the data collected from our experiments as well as references from other research to compare our small-scale prototype and non-woven polypropylene.

produced a purple colored clear solution, with no precipitate. Typically, a brown precipitate is formed even when there are trace quantities of oil, and hence this experiment indicates that the presence of oil in the solution is <5%, making it safe for domestic usage (8).

Next, we performed an acrolein test, which tests for the presence of oil in a solution. In this test, when we added potassium bisulfate to the oil-seawater emulsion and heated the mixture, a potent smell was released. On the other hand, when only a mixture of seawater and potassium bisulfate was heated, the residue was odorless. When we performed the experiment on oil alone, it released a potent smell. When the filtered water from the third pass was tested with potassium bisulfate, the residue, again was odorless.

Lastly, we conducted a Refractive Index Experiment (**Table 1**). This provides a quantitative analysis which further supports the results of the qualitative experiments performed earlier.

DISCUSSION

Dense oils include grease, diesel, and petrol variants (5). Heavier oil particles are separated by oil booms having larger molecular surfaces. As each adsorbent material has a certain inherent adsorption capacity, we had to carefully select materials in order to maintain the efficiency and integrity of our apparatus.

Dense oil layers are selectively adsorbed by coconut husk, a natural oil-adsorbing material. Coconut husks have both oil- and water-adsorbing capacity; however, adsorbed water evaporates in the atmosphere relatively quicker than oil. Thinner oils pass through the husk layer to the internal layers. However, due to its poor capability in the preliminary test, coconut husk was not considered as an addendum to the prototype. In addition, the last layer of the prototype featured common clinical filter paper, to contain the internal layers of components.

Perlite is a natural metamorphic-igneous rock, which is similar in its properties to the commonly found pumice. Perlite is an amorphous volcanic glass that has a relatively high water content, typically formed by the hydration of obsidian. It occurs naturally and has the unusual property of greatly expanding when heated sufficiently. It is an industrial mineral and a commercial product useful for its low density after processing (6).

Activated carbon, carbon, and its derivatives are powerful absorbents of oil spills. In comparison to the commercially used polystyrene sheets are less powerful than carbon, charcoal, and ash as organic absorbent. Activated charcoal, adsorbs the oil molecules, and being oleophilic in nature, water-suspended charcoal particles attach itself to the oil molecules, making filtration easier. Moreover, perlite adsorbs the activated carbon particles, increasing its net efficiency. Activated charcoal has a high bonding area of 2,000 m^2 per gram, which attracts organic molecules to itself making it an excellent adsorbent (6).

Bentonite is an absorbed aluminum phyllosilicate clay, which is known for its natural healing properties. Bentonite particles are the finest among the ones present in the prototype, but they are very porous with a large surface area. This increased surface area contributes to larger oil

adsorption. Since the density of oil is less than water, it adsorbs the oil molecules more than water. Research has shown that bentonite clay can adsorb up to 100% oil in relative quantity, in barely the first pass itself, while other materials can achieve 100% only after many passes (6).

The refractive index of the filtrate from the third pass lies very close to that of seawater, and there is a tremendous displacement from the refractive index of crude oil (**Table 1**). This again shows that the filtrate contains negligible amounts of oil.

Our prototype was made of 100% natural materials potentially lessening harm to the aquatic organisms and marine biome (10, 11). These natural adsorbents are very efficient in combating oil spills. In addition, our prototype is also more oleophilic as compared to commercial adsorbents. The materials used in our prototype are highly biodegradable and can be used as fuel once served its purpose (**Table 2**). Based on tests and research of various sorbents on various oils, we decided to form a layer-by-layer filtration unit. The ease to build and cost-effectiveness makes it an even advantageous alternative to models used commercially. We could use an integrated system that could be used as a microcontroller or mini-CPU for propelling the rover. Solar power could be used to fuel this mechatronic and thereby makes it an eco-friendly module.

Here we've proposed a new model of a sustainable ocean cleanup module that can be used for cleaning up oil spills in oceans. It incorporates completely natural components such as bentonite, activated charcoal, perlite, and hydroton arranged in layers within a prototype (**Figure 2**), and these components adsorb the oil-seawater emulsion with an adsorption capacity of up to 100% in the first two passes of water, and with nearly 90% adsorption rate in the third pass. The model proposed was tested in terms of efficiency and a set of experiments were performed to describe the purity of the seawater that was released from the third pass thereby demonstrating its efficiency. Further developments and ideas were also proposed to further advance the project.

If our model was implemented on a large scale, there could be an immediate response system to an oil spill; the once spilled oil that was deemed unusable could be reused as a source of fuel, and it would make the vast deep blue ocean into a sustainable marine biome.

MATERIALS AND METHODS

A number of natural materials including cotton, coconut husk, jute, activated charcoal, bentonite, hay, vegetable fibers, sand, hydroton, and perlite were tested for oil adsorption by passing oil equivalent to the weight of the adsorbent used. This experiment was performed twice.

After the finalization of the adsorbents, testing was conducted to furnish a rough analysis of the volume of each adsorbent that needs to be used in the prototype. Four types of oils were used, namely kerosene, petrol, diesel, and engine oil. The test consisted of passing equivalent mass of each oil through each of the adsorbents and finding the ratio of oil adsorbed to oil input. This test was performed twice.

For the oil-water emulsion test, a mixture of oil and seawater was passed through the prototype shown in Figure 2. The oil used was a combination of diesel, petrol, and kerosene. To begin with the experimentation, 33 g (equivalent weight of the apparatus), where 30 g was seawater and 3g was oil (about 9.1% of the emulsion was oleic), was added to the laboratory prototype. This was recorded as Pass I. A second pass of the same 33 g of the oil-water emulsion was added into the prototype from the end of the first pass. The third pass was tested with 33 g of the oil-water emulsion, added to the prototype from the end of the second pass. This whole experiment was carried out twice, with two nearly identical prototypes, and the average data was reported.

In the flame test, a sheet of newspaper was dipped into both the oil-seawater mixture and the filtrate received after Pass III, and then burnt. We also performed the Baeyer's reagent test with the oil-seawater mixture as well as the filtrate. We added Baeyer's reagent equivalent to the volume of the sample used. In the presence of unsaturated compounds, the color of the solution turns to brown, and finally disappears, otherwise remains purple, in accordance with the color of potassium permanganate ($KMnO_4$). Next, we performed the acrolein test. According to this experiment, a solution to which potassium hydrogen sulfate is added, releases an irritating odor when heated in the presence of organic compounds. We performed this test by adding potassium hydrogen sulfate equivalent to volume of the sample used to oil-seawater emulsion, seawater, oil, and the filtrate from Pass III. The final test for confirmation is to check the refractive indices (12) of the filtrate, oil, and seawater. We did this by passing a laser beam through a hollow rectangular prism containing the filtrate and oil-water emulsion and measuring the change in position of an object when placed in front of the prism. The flame test and acrolein test were performed only once, however, the Baeyer's reagent test and the refractive index test was conducted thrice; the refractive index test was precise up to 0.01 and the average data was reported.

ACKNOWLEDGEMENTS

First of all, we would like to thank God Almighty, for giving us a splendid chance to undertake this research. We thank our respected Chairman Dr. Jaan M.T. Thottumalil, the Director Dr. V. Gopalan, and the Principal Mr. Gopinath Menon of The New Indian School, Bahrain, for guiding us and giving us the full support for the successful presentation of the research project. We also thank Mrs. Nithyasree, Mrs. Lesheeja Shaji, along with other science teachers for directing us. We thank Mrs. Asha, Lab Assistant, who has actively supported our successful experiments in the Chemistry lab and spent time with us to find accurate results. They helped us to immerse in this vast field of environmental science and engineering and to understand the significance of methods to control oil spills and plastic management. We also thank our dear parents and

all our dear friends for supporting us.

Received: January 20, 2020
Accepted: November 04, 2020
Published: November 12, 2020

REFERENCES

1. Welch, Jeff. "OIL SPILL INTELLIGENCE REPORT INTERNATIONAL OIL SPILL DATABASE: RECENT TRENDS". *International Oil Spill Conference Proceedings*, vol 1995, no. 1, 1995, pp. 1006-1009. International Oil Spill Conference, doi:10.7901/2169-3358-1995-1-1006.
2. Fingas, Mervin F., and Carl E. Brown. "Review Of Oil Spill Remote Sensing". *Spill Science & Technology Bulletin*, vol 4, no. 4, 1997, pp. 199-208, doi:10.1016/s1353-2561(98)00023-1.
3. Magazine, Hakai. "The Oil Spill Cleanup Illusion". *Hakai Magazine*, 2016. Accessed 9 Nov 2019.
4. Siswoyo, Eko, and Shunitz Tanaka. "Development Of Eco-Adsorbent Based On Solid Waste Of Paper Industry To Adsorb Cadmium Ion In Water". *Journal Of Clean Energy Technologies*, 2013, pp. 198-201, doi:10.7763/jocet.2013.v1.45.
5. Behnood, Reza *et al*. "Oil Spill Sorption Using Raw And Acetylated Sugarcane Bagasse". *Journal Of Central South University*, vol 23, no. 7, 2016, pp. 1618-1625, doi:10.1007/s11771-016-3216-8.
6. Lee, Young-Hee *et al*. Effect Of Blend Ratio Of PP/Kapok Blend Nonwoven Fabrics On Oil Sorption Capacity. *Environmental Technology,* vol. 34, no. 24, 2013, pp. 3169-75, doi: 10.1080/09593330.2013.808242.
7. Akhavan, B., Jarvis, K. and Majewski, P. “Hydrophobic Plasma Polymer Coated Silica Particles for Petroleum Hydrocarbon Removal”. *ACS Applied Materials & Interfaces*, vol. 5, no. 17, 2013, pp.8563-8571.
8. Centers for Disease Control and Prevention. "Light Crude Oil and Your Health". *Agency for Toxic Substances and Disease Registry*. Accessed 9 Nov 2019.
9. Spill Solutions Canada. “The Science of Sorbents and How They Actually Work?” *Sorbents Explained*, 2019. Accessed 9 Nov 2019.
10. Maxim, L., Niebo, R. and McConnell, E., “Perlite toxicology and epidemiology – a review”. *Inhalation Toxicology*, vol. 26, no. 5, 2014, pp.259-270.
11. Moosavi M. “Bentonite Clay as a Natural Remedy: A Brief Review”. *Iran. J. Public Health*., vol. 46, 2017, pp. 1176–1183.
12. Gholami, Amin *et al*. "Prediction Of Crude Oil Refractive Index Through Optimized Support Vector Regression: A Competition Between Optimization Techniques". *Journal Of Petroleum Exploration And Production Technology*, vol 7, no. 1, 2016, pp. 195-204, doi:10.1007/s13202-016-0229-7.
13. History.com Editors. “Exxon Valdez Oil Spill.” History.com, *A&E Television Networks*, 9 Mar. 2018. Accessed 9 Nov 2019.

JOURNAL OF
EMERGING INVESTIGATORS

Article

Modeling the effects of acid rain on bacterial growth

Divyash Shah, Katherine McCormack
Tenafly Middle School, Tenafly New Jersey

SUMMARY

Acid rain has caused devastating decreases in ecosystems across the globe. This problem has been escalating due to the burning of fossil fuels. To mimic the effect of acid rain on the environment, we analyzed the growth of gram-negative (*Escherichia coli*) and gram-positive (*Staphylococcus epidermidis*) bacteria in agar solutions with different pH levels. We tested the hypothesis that agar with higher concentrations of vinegar would inhibit growth of gram-negative and gram-positive bacteria. We used agar with no bacteria as the negative control to ensure that there was no contamination of the agar from the environment. After 7 days at 25°C, we measured the size and number of the bacterial colonies. Our results showed that there was growth of both bacteria in each of the different agar concentrations, while the control agar exhibited no growth. The growth of the *Escherichia coli* (*E. coli*) colony was much greater than from the Staphylococcus epidermidis (*S. epidermidis*) colony at 3 different concentrations of vinegar: 6.25% Vinegar, 12.5% Vinegar, and 25% Vinegar. 6.25% Vinegar models current conditions in lakes while 25% represents future models at the rate we are going. While both bacteria grew in all solutions, there was clear evidence that more growth was visible in the agar with less vinegar. Also, measurement of the growth of each bacterium with daily check-ups over the week-long study showed the bacteria grew quicker in the agar with no vinegar. These results show that in a given acidic environment there was a significant decrease in bacterial growth with an increase in vinegar concentration in the agar, suggesting that bacterial growth is impacted by the pH of the environment. Therefore, increased levels of acid rain could potentially harm the ecosystem by altering bacterial growth.

INTRODUCTION

Humanity's footprint on the world has caused the influx of gases in our atmosphere. Gases, like sulfur dioxide (SO_2) and nitrogen oxides (NO_x), enter the atmosphere, where they mix with water (H_2O) deposits and form acidic liquids (1). During precipitation, these acidic liquids can cause damage to populations of species as well as their environments. Acid rain is often forgotten as a damaging consequence of the burning of fossil fuels (2).

The potential dangers of acid rain include damaging vegetation, destroying aquatic food chains, and polluting lakes and rivers, among many other bodies of water (1). Acid rain, also known as acid deposition, refers to any source of precipitation that includes acid, mostly SO_2 and NO_x, that falls to the ground in either wet or dry deposits. The United States Environmental Protection Agency declares that the primary causes of acid rain include the burning of fossil fuels, emissions from automobiles and other vehicles, and byproducts from labor industries, including manufacturing and oil refineries (3). Though human involvement is the key reason for increased acid rain in the 21st century, there have been natural causes for the release of SO_2 and NO_x, including volcanic explosions, lightning, and decaying biological life (4). The combination of man-made and natural releases of these gases causes a disastrous impact. Natural water has a pH of 6.5 – 7.0, while acidic rain has a pH of 4.4, well below the normal levels for our biosphere or the animals in it (5).

The consequences of acid rain include major damage to both water and land ecosystems on the surface of the earth (3). When these dissolved gases fall to the ground, the acidic components can seep into the soil and hurt vegetation (1). Moreover, the acidic components of this rain can remove aluminum and calcium from the roots of plants, which can prevent them from absorbing water, with the potential to cause premature death in these plants (1). Their impact is just as severe on animals and microbes. Many animals, such as birds, are not adapted to acidic environments and thus cannot consume water from bodies of water which have a low pH level (1). Similarly, animals that are part of the aquatic food chain may die, impacting the ecosystem.

The impact to the ecosystem is taken a step further when studying microbes. Microbes, also known as microorganisms, make up a large part of the world biome. Their role is pertinent in ecosystems, nutrient cycles, and the environment (6). Microbes have a major role as decomposers, especially in fresh-water ecosystems, because they consume dead bodies of plants, animals, and other microbes (7). After consuming these organisms, they convert the decaying matter into much needed nutrients for the ecosystem, such as nitrate, phosphate, and sulfate (6). They also continue to be important in life cycles, such as the carbon and nitrogen cycles (8). Without microbial decomposers, minerals, and nutrients critical to plant and animal growth would not be made available to support other levels of the fresh-water food

chain (7).

Thus, microbes are important, especially in fresh-water ecosystems, which are key in the survival of many animals, as well as in creating products needed for the world biome to survive (9). In freshwater ecosystems, there is a unique composition of microorganisms. Fresh-water microbes span a wide range, which includes both anaerobes and aerobes (7). As well as depending on the make-up of the aquatic ecosystems, a wide variety of protists, proteobacteria, actinobacteria, Bacteroides, and cyanobacteria can be found (7). These microbes assist in performing photosynthesis and maintaining ecosystem health. The fish and other larger species that are the consumers in this food chain are directly affected by nutrient cycling and other work performed by microbes (6, 10).

The established make-up of freshwater microbes makes their response to acid rain especially important. These microbes have been shown to be clearly affected by acid rain in the natural environment, but there are few studies quantifying their response. Certain bacteria, called acidophiles, prefer a lower pH environment, but as most bacteria are not classified in this subtype, the effects of acid rain and low pH level remain unknown. A previous study found a link between lower pH and decreased biological diversity in Adirondack lakes (11). The Adirondack lakes have been forced to adapt to increased acidification, and studies like these are crucial to see how lowering pH levels in the environment may affect microbes (11). This study shows that although major microbe species did not seem to be affected significantly, there needs to be further research of the effect of pH on microbe species. Further studies tested pH levels on soil microbes and showed that lowering the pH level resulted in less microbe survival (12).

Lastly, acid rain has potential disturbances to human health (4). SO_2 can create a low ozone level, which is a pollutant damaging to the respiratory system of humans, especially young children and the elderly (4). All these consequences of acid rain can endanger all aspects of the Earth, from humans to the tiny microbes that create the base of all life on this planet.

The nature of the issue leads us to the hypothesis that agar made with a liquid that is acidic would inhibit bacterial growth compared to agar made with regular water (pH = 6.5) as shown in past studies. An acidic environment was created with vinegar; one concentration of vinegar shows current pH conditions of lakes and an increased concentration of vinegar models future pH level of lakes if we continue at the current rate. Two commonly studied bacteria, gram-negative *Escherichia coli* (*E. coli*) and gram-positive *Staphylococcus epidermidis* (*S. epidermidis*), were tested. Our results show that the data supported the initial hypothesis. It was clear that regardless of the bacterial strain, a more acidic agar environment both inhibited overall growth and decreased the rate of growth of the bacteria.

RESULTS

The dangers of acid rain were modeled in this study using the acidic agar created with a mix of water and distilled white vinegar. Different concentrations of acidic agar were created and treated with two different bacteria, gram-negative E. *coli* and gram-positive *S. epidermidis* (**Table 1**). *E. coli* is gram-negative, while *S. epidermidis* is gram-positive, which gives an opportunity to see the difference in growth based on bacterial strain. Gram-positive indicates bacteria that have peptidoglycan in the cell wall of the cell while gram-negative bacteria lack this material. Both types of bacteria are present in aquatic ecosystems and thus having two strains of bacteria with these two bacterial stains allows us to see the effects of vinegar based on bacterial stain. White vinegar is made from acetic acid, which is similar in pH to the sulfurous acid present in acid rain, and at different concentrations this helps accurately model the pH of the freshwater biome when exposed to acid rain. The different concentrations of acidic agar created a spectrum of pH levels. The regular agar solution had a pH of 6.5, agar with 6.25% vinegar had a pH of 5, agar with 12.5% vinegar had a pH of 4.5, and agar with 25% vinegar had a pH of 3.

Bacteria were left to grow for a week in an incubation container at a constant temperature of 25°C. During the week-long period, *E. coli* and *S. epidermidis* exhibited similar growth in colony count based on the concentration of vinegar (**Figures 1-2**). After the week of growth, the areas of *E. coli* and *S. epidermidis* were measured. The growth in the petri dish with no vinegar exhibited many more colonies throughout the week-long period, regardless of the strain of bacteria. For gram-negative *E. coli*, there were 6.67 times as many colonies in the agar plate with no vinegar compared to the agar plate with 25% vinegar, which exhibited only 3 colonies after 7 days (**Figure 1**). For gram-positive *S. epidermidis*, there were 10 times as many colonies in the agar plate with no vinegar compared to the agar plate with 25% vinegar, which exhibited only 1 colony after 7 days (**Figure 2**). On average, the total area (mm2) of *E. coli* colonies was much larger than that of *S. epidermidis* regardless of vinegar concentration (**Figure 3**). Similarly, the total area of growth was much larger in the agar plates with smaller vinegar concentrations

Table 1. The conditions of the different plates that were grown during this study to model the different effects of acid rain on the two bacteria used.

Variables	Group 1	Group 2	Group 3	Group 4	Group 5
Type of Bacteria	**No bacteria (Control)**	**G- E.Coli**	**G- E.Coli**	**G- E.Coli**	**G- E. Coli**
Concentration of solution mixed with agar	Regular Water	Regular water	25% Vinegar with 75% Water	12.5% Vinegar with 87.5% Water	6.25% Vinegar with 93.75% Water
Variables	Group 1	Group 6	Group 7	Group 8	Group 9
Type of Bacteria	**No bacteria (Control)**	**G+ Staph epidermidis**	**G+ Staph epidermidis**	**G+ Staph epidermidis**	**G+ Staph epidermidis**
Concentration of solution mixed with agar	Regular Water	Regular water	25% Vinegar with 75% Water	12.5% Vinegar with 87.5% Water	6.25% Vinegar with 93.75% Water

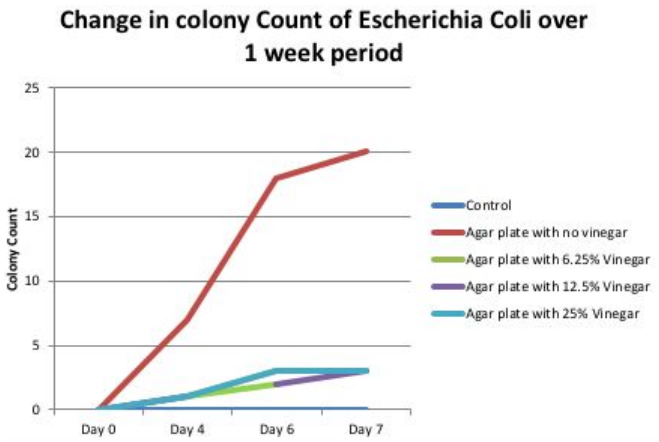

Figure 1 The growth in the number of gram-negative *E. coli* colonies over a one-week period. Each line represents a different concentration of vinegar in the agar in which the bacteria was grown. (Red: 0% Vinegar, Green: 6.25% Vinegar, Purple: 12.5% Vinegar, Light Blue: 25% Vinegar) The rate of colony count in the petri dish with 6.25% vinegar concentration is identical to the rate of growth of the 12.5% concentration, shown by the overlapping lines.

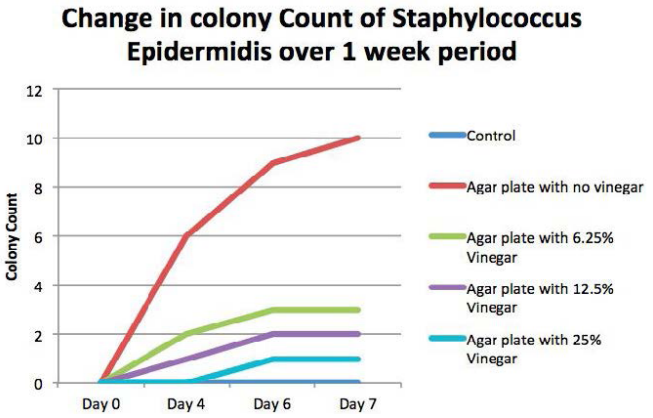

Figure 2. The growth in the number of gram-positive *S. epidermidis* colonies over a one-week period. (Red: 0% Vinegar, Green: 6.25% Vinegar, Purple: 12.5% Vinegar, Light Blue: 25% Vinegar) Growth in the petri dish with 25% vinegar concentration doesn't start until after day 4. Growth in 6.25% vinegar, 12.5% vinegar, and 25% Vinegar doesn't change from day 6 to day 7 unlike in the petri dish with no vinegar.

(**Figure 3**). For *E. coli*, there was an 89% decrease in total area from the agar with no vinegar to the agar with 25% vinegar (**Figure 3**). For *S. epidermidis*, there was a 99% decrease in total area from the agar with no vinegar to the agar with 25% vinegar (**Figure 3**). This decrease showed the clear effect that large vinegar concentrations have on bacterial growth. There was also a 48.4% decrease in *E. coli* and a 63.7% decrease in *S. epidermidis* from the agar with 6.25% vinegar to the agar with 25% vinegar (**Figure 3**). This data revealed how the pH values, which attempted to model current freshwater ecosystem levels, play a role in the decrease of bacterial growth, showing the severe effects as the concentration of vinegar increases. Individual colony size was examined and compared using a logarithmic scale with maximum, minimum, and mode intervals (**Figure 4**). Looking at *E. coli*, there was much overlap between the individual colony data, showing that colony size on average was similar in these gram-negative bacteria across different vinegar concentrations. However, in *S. epidermidis*, the data exhibited less overlap, indicating a difference in the individual size of the colonies in these gram-positive bacteria across the different vinegar concentrations. This indicated that vinegar concentration may not necessarily interfere with the size of individual bacterial colonies (**Figure 4**), as the average size of the colonies did not change significantly between concentrations, but it influenced the general number of bacteria colony growth.

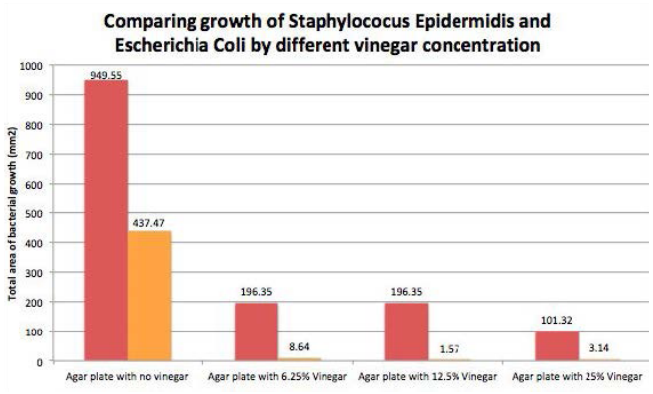

Figure 3. Comparing total bacteria growth of *E. coli* and *S. epidermidis* side-by-side based on plating conditions. (Red: *E. coli*, Orange: *S. epidermidis*) Vinegar concentration has a negative growth effect on both gram-positive and gram-negative bacteria however vinegar inhibits more growth in gram-negative bacteria.

DISCUSSION

To better understand the effect of acid rain, a two-part study was conducted to understand how acidic deposits caused by acid rain affected two bacterial strains. In this study, gram-negative *E. coli* and gram-positive *S. epidermidis* were grown in acidic agar conditions to model the effects of acid rain on the growth of bacteria.

Tests on both bacteria showed that the increase in vinegar drastically hurt the number of colonies as well as the total bacterial growth of all the colonies. The gram-negative and gram-positive bacteria grew slower in the agar prepared with vinegar versus the agar prepared without vinegar (**Figure 4**). In gram-negative *E. coli*, the bacteria grew larger with declining vinegar concentration in the agar. The total area of growth in both gram-negative and gram-positive bacteria was significantly larger in the agar plate with no vinegar (**Figure 3**). The data supported the initial hypothesis, as an increase in acid in an environment appeared to hurt the growth of bacteria in that environment. These results indicate that bacteria that are the foundation of aquatic food chains would suffer in the presence of acid rain, which could lead to a non-stable food chain in areas with higher acid concentrations.

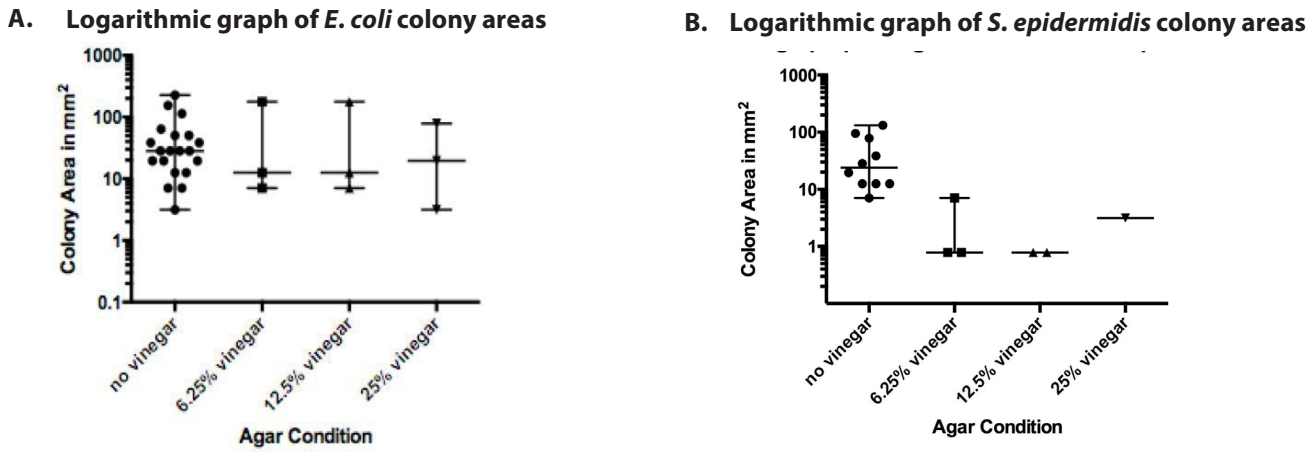

Figure 4. Logarithmic graph of individual colonies divided by vinegar concentrations. A: Individual colonies of *E. coli*. **B:** Individual colonies of *S. epidermidis*. Vinegar concentration does not appear to affect size of individual bacteria colonies but does appear to affect the number of colonies in both *E. coli* and *S. epidermidis*. Colonies were counted and measured after one week of incubated growth. Colony area is in mm^2.

This was observed via the growth curves that show the difference in growth between acidic agar and agar with no vinegar (**Figures 1-2**).

Acidic agar had notably fewer colonies compared to the control plates. This showed that the agar with vinegar is inhibiting the growth of the bacterial colonies, showing the potential destabilization of the food chain in acidic environments. An unstable food chain could lead to the elimination of many plants and animals. As well, the inhibition of growth by decreasing pH may affect nutrient cycles, as microbes play a role in the carbon, nitrogen, and phosphorus cycles, which help with photosynthesis, production of macromolecules, and productivity of the food web, respectively (6). Thus, the decrease in pH levels caused by acid rain can raise major concerns for ecosystems across the world. The pH levels of the different agar conditions accurately modeled live stream pH levels (3). The 6.25% vinegar concentration shows the pH of current streams after precipitation of acid rain. Similarly, the pH of 25% vinegar is what is expected in upcoming years if active effort is not taken to lower acid rain and subsequently increase the pH of freshwater streams.

We additionally showed that acidic vinegar affected both gram-positive and gram-negative bacteria. *E. coli* and *S. epidermidis* both showed <3 total colonies in the agar with 12.5% vinegar and even less in the agar with 25% vinegar (**Figure 4**). As the pH of agar with 6.25% vinegar models the pH of current acid rain deposits, the significant decrease in total area of bacterial growth between agar with 6.25% vinegar and 0% vinegar supports the fact that acidic conditions could be detrimental to bacterial survival (**Figure 3**). If a pH as low as 3 is reached in freshwater ecosystems, this may pose a threat to the survival of these crucial microbes, as both colony count and total area of growth is significantly decreased at this pH level.

Bacterial growth was represented by either colony count or colony size. Bacteria were equally distributed among all the petri dishes, thus colony count indicated sole areas where bacteria were able to sustain and grow. As colony count decreased with increased vinegar concentration, it seems to reveal that lower pH levels severely decrease the ability of bacteria to grow (**Figures 1-2**). Colony size, on the other hand, focuses on bacteria's growth rate and how much the bacteria can reproduce in the 7-day growth period. Colony size appeared to remain similar regardless of vinegar concentration (**Figure 4**) in *E. coli* colonies. However there appears to be a slight difference in colony size based on vinegar concentration in petri dishes with *S. epidermidis.*

It is also possible that bacterial growth could have been inhibited by factors other than the vinegar. To measure daily growth, the bacteria needed to be removed from the incubation container, and this may have caused disturbances in the growth. Possible unequal swabbing between the different petri dishes could have given disproportional initial bacteria, leading to diverse differences in the results. *E. coli* and *S. epidermidis* only account for two strains of bacteria that make up the large, diverse microorganisms on this planet and even though *E. coli* and *S. epidermidis* are not commonly found in the freshwater ecosystem, they are considered model organisms which allow them to shed light on how both bacterial strains perform under different pH conditions. Thus, these bacteria give us prime examples to model aquatic microorganisms, however it is possible that other bacteria may respond differently and that other strains may have adapted to the acidic water.

E. coli and *S. epidermis* represent all prokaryotes that may make up an ecosystem, not just a few. They are both prototrophic microorganisms, meaning they do not require a special medium with supplements to grow as they are able to synthesize their own organic material. In addition, *E. coli* and *S. epidermis* are also classified as autotrophic and heterotrophic respectively (14-15). Autotrophs and

heterotrophs are crucial in both decomposition and the nutrient cycles in freshwater ecosystems. Freshwater systems contain both types of prokaryotes (16). Though *E. coli* and *S. epidermis* are not commonly found in freshwater ecosystem, they are considered model organisms which allow them to shed light on how both bacterial strains perform under different pH conditions.

Results again provide great hope into truly understanding the depths of how microbes are affected by both pH and acid rain. This first study provides a basis for further research where bacteria and acid that more closely model nature can be tested and compared to this study in which model organisms were used. Further research can help verify the conclusions revealed in this study. To further support our conclusions, multiple data samples should be tested, and these tests should be repeated to ensure that the data is scientifically accurate. The data presented in this study revealed that we still need to address the problem facing microorganisms in aquatic environments. To model current findings, we can refer to the results from agar with 6.25% vinegar. If the world does not change and aim to reduce acid rain levels, as well as pH levels, the severe decrease in bacterial colonies and growth shown by the agar with 25% vinegar will be our new normal, causing many issues to the global environment.

METHODS

The bacteria were grown in different conditions to model the effects of acid rain on microorganism growth. To collect the data, different agar solutions were prepared with varying pH levels. Nine different groups were established with one petri dish per group. The entire experiment was performed in a Biosafety Level 1 laboratory. Dehydrated media nutrient agar was ordered via Carolina Biological Company.

Normal agar was made of 1.6 g of agar powder dissolved in 75 mL of water by boiling. Three other conditions were created to model the continual increase in acid rain in aquatic environments. Acidic solutions were modeled using a white distilled vinegar solution. The distilled vinegar had a pH of 2.4 and needed to be diluted to model pH levels of aquatic ecosystems in the world.

Current freshwater pH conditions were mimicked with a 6.25% concentration of vinegar (4.6875 mL of vinegar in 70.3 mL of water); this solution had a pH of 5. To model near future water conditions, with increasing acid rain occurrence, 12.5% vinegar (9.375 mL of vinegar) was mixed with 65.625 mL of water; this solution had a pH of 4.5. Lastly, to model potential conditions in the next decades, 25% vinegar (18.75 mL of vinegar) was mixed with 56.25 mL of water; this solution had a pH of 3. pH was measured using Litmus paper and cross-checked with a standard lab colorimeter. After measuring pH, these solutions were mixed with the dissolved agar in standard glass beakers and brought to a boil in a microwave. Each of these three acidic agar solutions were split evenly into two petri dishes creating a total of six petri dishes with acidic conditions and nine totals, including the three with standard agar.

Two different bacteria strains, *E. coli* and *S. epidermidis*, were tested. *E. coli* and *S. epidermidis* are the most accessible microorganisms available to test, as they qualify under Biosafety Level 1.

The bacteria were ordered dehydrated through Carolina Biological Company (*Staphylococcus epidermidis*- Item # 155556A, *Escherichia coli*- Item # 155065A). While the agar solidified, bacteria were rehydrated using a provided medium and incubated at room temperature for 30 minutes. When the agar was at the right solid consistency, sterile inoculating loops were dipped in the respective bacteria and used to apply an even coating of each bacteria on the given petri dish. The use of the inoculating loop with the same number of bacteria was used to ensure even distribution of bacteria in each petri dish, preventing another defining variable. Inoculating loops were placed in a biohazard bag after one-time use. One petri dish was swabbed with an unexposed inoculating loop to establish a control.

After dish preparation, nine petri dishes with nine unique conditions were created to measure. The variables for this project were the concentration of vinegar in the agar solution and the bacterial strain of the bacteria. All nine petri dishes were sealed with tape and labeled appropriately. After this, they were placed in an incubation container and left at 25°C for seven days. Bacteria were measured on four days: day 0, day 4, day 6, and day 7, and the number of colonies were counted, and their growth was compared from the previous day of measurement. Besides this measurement, the bacteria were kept undisturbed for the week-long growth period.

After one week of growth, the bacteria colonies were counted, the size of the colonies was measured, and then the petri dishes were appropriately disposed of. The size of the colonies as seen in **Figures 3-4** was measured by outlining each colony on the petri dish and using a ruler and protractor to estimate the size of each colony.

Figures showing data of the bacteria growth over the week as well as comparisons of gram-negative *E. coli* and gram-positive *S. epidermidis* were created with Prism 6 program. **Figure 3** represents the $\log_{10}$ size of individual bacteria colonies. The box plots represent maximum and minimum size with the middle line representing the mode size of colonies.

ACKNOWLEDGMENTS

I would like to thank my parents, my brother, my grandparents, and my aunts who reviewed my work as well as Ms. McCormack, the teacher that inspired me to conduct this project and to the Journal of Emerging Investigators for considering my journal article and giving me the chance to publish my project.

Received: July 20, 2020
Accepted: November 8, 2020
Published: November 17, 2020

REFERENCES

1. Nunez, Christina. "Acid Rain facts and information." *National Geographic*, 28 Feb. 2019 https://www.nationalgeographic.com/environment/global-warming/acid-rain/.
2. Madaan, Sonia. "Primary Causes of Acid Rain." *Earth Eclipse*, 17 Apr. 2016, www.eartheclipse.com/environment/primary-causes-of-acid-rain.html.
3. "What Is Acid Rain?" *EPA*, Environmental Protection Agency, 18 Apr. 2019, www.epa.gov/acidrain/what-acid-rain.
4. Boumis, Robert. "Negative Health Effects of Acid Rain on Humans." *Sciencing*, 19 June 2019, https://sciencing.com/negative-health-effects-acid-rain-humans-24007.html.
5. Abrahamsen, G., Hovland, J., and Hagvar, S., Effects of artificial acid rain and liming on soil organisms and the decomposition of organic matter, in: Effects of Acid Precipitation on Terrestrial Ecosystems, pp. 341–362. Eds T. C. Hutchinson and M. Havas. Plenum Press, New York 1980.
6. *Acid Rain*. http://nadp.slh.wisc.edu/educ/acidrain.aspx. Accessed 7 Mar. 2020.
7. Chapter 5 ~ Flows and Cycles of Nutrients. (2020, August 21). Retrieved August 21, 2020, from https://ecampusontario.pressbooks.pub/environmentalscience/chapter/chapter-5-flows-and-cycles-of-nutrients/.
8. Robinson, R., & Clark, N. (n.d.). Microbes in Lakes and Streams - river, important, system, plants, source, oxygen, human. Retrieved August 20, 2020, from http://www.waterencyclopedia.com/La-Mi/Microbes-in-Lakes-and-Streams.html#:~:text=Leaves%20and%20branches%20that%20fall,available%20for%20other%20aquatic%20creatures.
9. UNC Institute for the Environment. (n.d.). Investigating Freshwater Microbes and Their Role in the Carbon Cycle. Retrieved August 20, 2020, from https://ie.unc.edu/files/2014/12/Freshwater-microbes-lessons-FINAL.pdf.
10. Dodds, W., & Whiles, M. (n.d.). Freshwater Ecosystem - an overview | ScienceDirect Topics. Retrieved August 21, 2020, from https://www.sciencedirect.com/topics/earth-and-planetary-sciences/freshwater-ecosystem.
11. Society, N. (2019, August 2). Freshwater Ecosystem. Retrieved August 21, 2020, from http://www.nationalgeographic.org/article/freshwater-ecosystem/.
12. Rensselaer Polytechnic Institute (RPI)Database Shows Effects of Acid Rain on Microorganisms in Adirondack Lakes. (n.d.). Retrieved August 20, 2020, from https://news.rpi.edu/luwakkey/2461.
13. Xu HQ, Zhang JE, Ouyang Y, *et al*. Effects of simulated acid rain on microbial characteristics in a lateritic red soil. *Environ Sci Pollut Res Int*. 2015;22(22):18260-18266. doi:10.1007/s11356-015-5066-6.
14. Blount Z. D. (2015). The unexhausted potential of E. coli. *eLife*, *4*, e05826. https://doi.org/10.7554/eLife.05826.
15. Animals of Freshwater. (2015, April 5). Retrieved September 9, 2020, from https://askabiologist.asu.edu/animals-freshwater.
16. Lab-Evolved E. coli Consume Carbon Dioxide. (n.d.). Retrieved September 9, 2020, from https://www.the-scientist.com/news-opinion/lab-evolved-e--coli-makes-energy-solely-from-carbon-dioxide-66788.
17. Staphylococcus Aureus: Structure and Function. (n.d.). Retrieved September 9, 2020, from https://www.ukessays.com/essays/biology/identification-of-staphylococcus-aureus-from-bacterial-genus-biology-essay.php.
18. "How to Grow Bacteria: Lesson, Science Projects, Video." *Home Science Tools*, 12 Feb. 2019, learning-center.homesciencetools.com/article/bacteria-experiment-guide/.3.
19. Francis, A.J. Acid rain effects on soil and aquatic microbial processes. *Experientia* 42, 455–465 (1986). https://doi.org/10.1007/BF01946683.
20. Liang, X., Liao, C., Thompson, M. L., Soupir, M. L., Jarboe, L. R., & Dixon, P. M. (2016). *E. coli* Surface Properties Differ between Stream Water and Sediment Environments. *Frontiers in microbiology*, *7*, 1732. https://doi.org/10.3389/fmicb.2016.01732.
21. Pandey, P. (2012). *Modeling In- Stream Escherichia coli Concentrations*. Iowa State University. Retrieved from https://lib.dr.iastate.edu/cgi/viewcontent.cgi?referer=https://www.google.com/&httpsredir=1&article=3862&context=etd.

JOURNAL OF
EMERGING INVESTIGATORS

Article

Luteolin's positive inhibition of melanoma cell lines.

Wilson Su[1], Feng Liu-Smith[2]
[1]University High School, 4771 Campus Dr, Irvine, California, United States of America
[2]University of California, Irvine Department of Medicine 256A Irvine Hall, Irvine, California, United States of America

SUMMARY

If not treated early, melanoma, a form of skin cancer, can lead to death in patients. Currently the few treatments for melanoma include surgical removal, chemotherapy, or immunotherapy without any treatment based on natural small molecules currently available. Luteolin (3′,4′,5,7-tetrahydroxyflavone) is a flavonoid that occurs in fruits, vegetables, and herbs. Research suggests that luteolin is effective against various forms of cancer by triggering apoptosis pathways. In addition, luteolin was consistently shown to have marginal cytotoxicity against normal cells. Thus, luteolin is currently being researched as a possible anticancer agent. This experiment was performed using an MTT (3-(4,5-dimethylthiazol-2-yl)-2,5-diphenyltetrazolium bromide) assay to test cellular cell viability. Each sample was administered varying doses of luteolin by 2-fold serial dilution. These samples were later administered an MTT solution and scanned using an absorbance microplate reader to measure cell viability.The results of our study demonstrate that increased luteolin dosage limited melanoma cell survival rate by as much as 98% *in vitro*. Although promising, further research is needed to accept luteolin as a clinical drug. This experiment analyzes the effects of luteolin on the cell viability of malignant melanoma cells using an in vitro experiment to research alternative melanoma treatments and hopefully to help further cancer research as a whole.

INTRODUCTION

Historically, almost 34% percent of medicines found between 1981 and 2010 are either natural compounds themselves or are derivatives of natural compounds (1). Luteolin, or 3′,4′,5,7-tetrahydroxyflavone, is a flavonoid that commonly occurs in many different types of fruits, vegetables, and medicinal herbs (2). In plants, Luteolin is used as a protection against microorganisms, infection, and UV radiation (3). Plants rich in luteolin have been used in traditional Chinese medicine to reduce inflammation, treat disease, and battle cancer (3). With the lower risk of breast, colon, and prostate cancer with populations in Asia compared to the West, researchers have raised the question of whether luteolin has anticancer effects (4).

In 2019, advanced stages of melanoma caused around 7000 deaths in the United States alone (5). Melanoma is caused by mostly UV radiation damage to melanocytes, skin cells that produce the skin pigment melanin (6). Some potential indicators of melanoma include moles that have asymmetrical shape, uneven borders, different colors, large size, and the tendency to change size, shape, or color over time (6). The severity of melanoma depends upon its stage, which are ranked 0 to IV. While Stage 0 to Stage I are not dangerous, Stage II can easily spread to important tissues such as the lymph nodes (7). Stage III tumors have spread to the local lymph nodes and Stage IV melanomas have advanced to major organs such as the brain, heart, and liver (7). The last two stages both cause deaths due to organ failure, with Stage IV melanomas being terminal for most patients (7). Although early stage melanomas can be easily removed with surgery, late stage melanomas are more difficult to treat (7). Immunotherapy, radiation therapy, and chemotherapy may not always work and can leave many side effects (8). Since early stages are not commonly detected and late stages can result in many complications, it is thus useful to find alternative methods of combating melanoma (8).

Recent evidence has established a positive effect of luteolin against various forms of cancer (9). Luteolin may primarily have its antioncogenic effect due to its ability to block cell-survival pathways and instead trigger apoptosis by primarily suppressing MMP-2, and MMP-9 proteins (1). In research performed by Mano Horinaka et al, luteolin was shown to have marginal cytotoxicity against normal cells even at high doses (9). Additionally, long term exposure did not show any apparent toxicity in rats (30 mg/kg, p.o. for 20 days) (4). Both research indicates that high dosages of luteolin have little effect in healthy cells for both *in vitro* and *in vivo*. A combination of its proven effects against several forms of cancer, low toxicity in healthy cells, and prevalence in history allows for this compound to be a prime candidate for testing for alternative forms of melanoma treatment.

The goal of this research is to establish the relationship between luteolin and melanoma cell death to develop an alternative drug candidate to melanoma by treating melanoma cells under *in vitro* conditions with luteolin. Though healthy cells have a high tolerance to luteolin, at high enough doses it can still be toxic to some degree. Therefore, it is desirable to find the highest dose that effectively inhibit cancer cells while remaining nontoxic to normal cells.

RESULTS

To evaluate luteolin's effect on melanoma cells, cells were

a

Dosage (µM)	Col 1 0 µM	Col 2 0.0313 µM	Col 3 0.0625 µM	Col 4 0.125 µM	Col 5 0.25 µM	Col 6 0.5 µM	Col 7 1 µM	Col 8 2 µM	Col 9 4 µM	Col 10 8 µM	Col 11 16 µM	Col 12 32 µM
570nm	1.4235	1.2783	1.2296	1.2736	1.3163	1.1313	1.1331	1.131	0.9461	0.4469	0.14378	0.0562
650nm	0.1629	0.1558	0.1532	0.1534	0.1592	0.1398	0.1415	0.1456	0.12445	0.0758	0.049	0.0403
Absolute Difference	1.2605	1.1224	1.0763	1.1202	1.157	0.9914	0.9915	0.9855	0.8216	0.3711	0.0946	0.01586

b

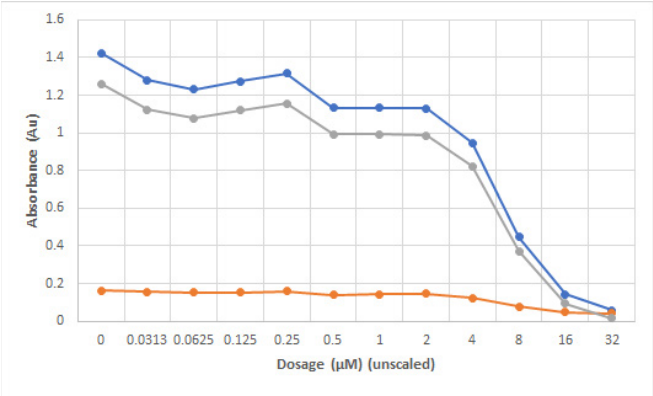

Figure 1: Higher dosage results in lower absorbances. (a) Absorbance of each wavelength (n=4). (b) Data points indicate the mean absorbances of each dosage.

a

Dosage (µM)	Col 1 0 µM	Col 2 0.0313 µM	Col 3 0.0625 µM	Col 4 0.125 µM	Col 5 0.25µM	Col 6 0.5µM	Col 7 1µM	Col 8 2µM	Col 9 4µM	Col 10 8µM	Col 11 16µM	Col 12 32µM
Trial 1	88.41	86.28	90.15	87.36	93.37	83.82	77.23	73.30	66.74	25.35	5.88	0.83
Trial 2	98.26	81.70	81.06	74.46	84.42	79.56	81.75	77.61	63.50	36.10	9.42	1.98
Trial 3	102.58	89.01	91.797	99.56	99.86	86.91	85.46	91.69	73.29	29.50	8.39	0.95
Trial 4	110.79	82.48	78.548	94.11	89.51	64.32	70.20	70.11	57.22	26.82	6.33	1.28
Average	100.00	89.05	85.389	88.87	91.79	78.65	78.66	78.18	65.19	29.44	7.51	1.26

b

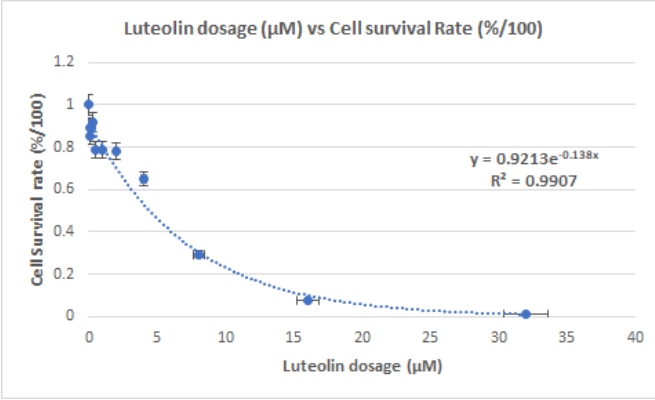

Figure 2: Luteolin inhibits melanoma cell survival rates in a dose dependent manner. (a) Survival rate of cells relative to the control. (b) Data points indicated the mean survival rate for each dose. The survival rate decreased exponentially as dosage increased, with the highest tested dosage of 32 µM resulting in only about 1% of cells surviving.

administered dosages varying from 0–32 µM. These dosages were chosen because it was outside of the toxicity which would otherwise affect normal cells and these dosages have been shown to result in a range of responses from almost no termination to complete termination of melanoma cells (4)(14). These cells were then evaluated using spectrophotometry of an MTT Assay. MTT is a dye that when in contact with NAD(P)H oxido-reductases enzymes in cells reduces into a formazan which gives off a purple hue. When cells do not metabolize NAD(P)H, such as when they are undergoing apoptosis, MTT is not reduced and solution remains clear. Therefore, a sample with higher cell viability will have a greater absorbance of a longer wavelength compared to a sample with a low cell viability, which will have more light pass through instead of being absorbed (**Figure 1**).

After each trial was analyzed using spectrophotometry, the reference absorbance was subtracted by the foreground to avoid any skewed data due to the environment (**Figure 1**). Then using the average control as a baseline for 100% survival rate, a dilution curve was calculated to test the dose-dependent effect of luteolin on cell survival (**Figure 2b**).

The overall trend showed the percentage of survival

Dosage (µM)	***0***	***0.0313***	***0.0625***	***0.125***	***0.25***	***0.5***	***1***	***2***	***4***	***8***	***16***	***32***
Absorbance deviation	0.0842	0.1052	0.0704	0.1003	0.0608	0.0904	0.0623	0.0852	0.0608	0.0423	0.0177	0.0047
Survival Rate Deviation	6.678	4.183	5.583	7.959	5.826	7.169	4.940	6.758	4.825	3.358	1.400	0.371
Survival Rate Percent Deviation %	6.678	4.697	6.538	8.956	5.257	9.114	6.281	8.645	7.404	9.405	9.658	10.449
Final Average Percent Deviation	7.757											

Table 1: Absorbance deviation, survival rate deviation, and the mean percentage deviation of the survival rate.

Levine's Test (homogenity of variance)				
Total Degree of Freedom	**Sum of Squares**	**Mean Square**	**F-Statistic**	**P-value**
47	0.08676	0.001845	1.18969	0.330119
ANOVA Summary				
Total Degree of Freedom	**Sum of Squares**	**Mean Square**	**F-Statistic**	**P-value**
47	5.1897	0.005	89.987	0.01

Table 2: Dosage is statistically significant to cell survival rate. The Levine's Test (left) tested for eligibility of the data for a one-way ANOVA (right). The one-way ANOVA returned the p-value, or the statistical significance, of the data. The low p-value indicates a high statistical significance of the data.

exponentially decreased as the dosage increased, with the full dose bringing an average 98% termination rate (**Figure 2a**). This shows that as the dosage increases the survival rate exponentially decreases, which means that luteolin similarly induces apoptosis in malignant melanoma cells.

The overall percentage deviation was relatively low with average percent deviation of 7.757% amongst all samples (**Table 1**) and a R^2 of 0.99 (**Figure 2b**). This suggests the experiment is very consistent and can be replicated in similar laboratory settings. The data also fits well with the line of best fit, meaning that the data was not heavily skewed by outliers. After performing a Levine's test on the data, we got a p-value of 0.33, and since that value is higher than 0.05, it was eligible for a one-way ANOVA. This gave us a p-value of 0.01 (**Table 2**). Therefore, luteolin is shown to significantly affect melanoma's survival rate.

DISCUSSION

This research's purpose was to demonstrate the effects of luteolin, a chemical compound commonly found in fruits and vegetables, on the cell viability of cancerous melanoma cells in hopes of contributing towards the use of luteolin in the treatment of disease. The overall trend showed the percentage of survival exponentially decreased as the dosage increased, with the highest dose bringing an average 98% elimination rate (**Figure 2a**). With a significant statistical significance and This further supports our hypothesis that luteolin can be used to effectively reduce the cell viability of melanoma cells. Thus, luteolin may be a viable drug candidate for the treatment of melanoma.

Although the overall trend showed a decrease in cell viability as the dosage increased, 0.125 μM and 0.25 μM instead seemed to have a slight increase in cell proliferation from lower doses (**Figure 2a**). Due to the high statistical significance of the data, it may be likely that simply at lower doses, luteolin has a relatively similar effect. The effectiveness of a drug generally is similar in low doses but as the dosage increases its effectives increases dramatically, until it plateaus past a certain point. This can be seen in **Figure 2b**, where the cell elimination rate dramatically increases at dosages greater than 2 μM (**Figure 2b**). It is entirely possible that a difference of dosage at 0.0625 μM or 0.125 μM has little effect on the elimination rate, which will cause these results to display about the same cell proliferation, if not a bit higher even for a higher dose. Still, we cannot rule out the possibility of an error due to serial dilution. Serial dilution was chosen in that it is flexible, quick, and can give an even range of values. One weakness of serial dilution is that it may be prone to error propagation at low doses. This may result in some of the doses being a bit lower than the expected, hence the slight increase in cell propagation.

In future experiments, there are some practices that can be done to improve this experiment's accuracy. One alternative method to serial dilution is to create multiple existing stock concentrations instead of having one stock concentration to perform serial dilution across. This allows for the concentrations to have fewer errors, but at the cost of having less variability, less ease of use, and uneven spacing. Additionally, it is labor and resource intensive to create enough stock concentrations to have enough conclusive data, but the option was available to us it would be the ideal method. The 4 trials do help to reduce inconsistencies, but more trials should be done in the future to mitigate the effect of random errors and bias on the overall data. Though it was established that luteolin has little effect on healthy cells, the dosages tested in this experiment should be tested on healthy cells *in vitro* to be certain. Other chemical compounds that have similar properties need to be studied in case they have similar properties for manufacturing additional medical treatments.

After this experiment, there is still much more testing before luteolin can be considered an official treatment, however. Preclinical studies such as *in vivo* experiments in animals are already being done to determine toxicity and optimal dosage (9). This is even before considering clinical studies with real patients, which may take upward 10 years before luteolin can be approved as an optimal drug. It may

take decades before luteolin can be available to the public. Ultimately, as research is still being performed on luteolin, this experiment has identified an effective dosage for melanoma cells, contributing towards the use of luteolin as a new treatment for disease.

MATERIALS AND METHODS

Setup

To test for cell viability among the melanoma cell lines, the independent variable was the dosage of luteolin (micromolars) applied to the samples and the dependent variable was the cell survival rate. This experiment was done by using an MTT assay, an investigative procedure to determine cellular cell viability by using the dye (3-(4,5-dimethylthiazol-2-yl)-2,5-diphenyltetrazolium bromide), or MTT.

All cell cultures came from the same SK-mel-28 cell line (vendor: ATCC, catalog number: ATCC® HTB-72™), maintained at a temperature of 37°C inside of a 5% CO2 incubator, and were treated with the same amount of medium and growth factor. The medium used, Eagle's minimum essential medium (EMEM) (vendor: Lonza, catalog number: 12-611F), was supplemented with 5% FBS and 5% NBS (fetal bovine serum, newborn bovine serum) and 1% Penicillin/ Streptomycin antibiotics. No other growth factors were used. The passage number was estimated to be 50. Cells are expected to grow to about 60-70% confluence level, with the control not exceeding 90%. To avoid contamination, all experimentation was performed in a BSL2 biosafety hood that was cleaned regularly with UV light. All laboratory equipment was properly cleaned or disposed of to mitigate any contamination (with approved IBC protocol, UCI 2013-1458).

Cell Culture

Cells were detached using 1 ml 0.25% trypsin (vendor: Lonza, catalog number:17-161E),. After leaving the sample in the CO2 incubator for 5 minutes, 4 ml of EMEM added to the dish. Approximately 5000 cells were seeded into each well of a 96-well plate, about 100 µl in each well for this experiment, which was then placed back into the incubator. After waiting 24 hours, the cell medium was disposed of and 500 µl of EMEM was added to all the wells except for the 12th column, which had 1000 µl medium. 2 µl of 16 mM luteolin was added to the 12th column of the cell culture and a 2-fold serial dilution was performed across the plate. The cells were not disturbed as they remain adhered to the plate. The first column, the control, was not diluted. The culture was then placed in the incubator for 72 hours.

MTT Assay

After 72 hours, the MTT was prepared by mixing 0.5g of solid powdered MTT with 10ml of PBS to create a liquid solution, and 100 µl was placed inside each well for 1 hour. Then 100 µl DMSO is used to dissolve the MTT. The data was analyzed using a Synergy HTX, multimode reader (BioTek) to find the cell viability in each well. The experiment was repeated 4 times in total, using a different well plate each time.

Statistical Analysis

When analyzing an MTT assay, the Synergy multimode reader will give two tables of data, one absorbance of 570 nanometers, and another of reference wavelength of 650 nanometers. 650nm must be subtracted by 570nm to get the actual absorbance by the samples (**Figure 1a**).

The cell survival rate is calculated by dividing the mean control absorbance difference with every cell well then finding the mean survival rate for said dosage by dividing the sum of all the trials for said dosage by the number of total trials. (**Figure 2a**).

Deviations are calculated by finding the absolute difference from the mean. The survival percentage deviation is the survival deviation divided by the corresponding average

$$Survival\ rate = \frac{\sum \frac{Experimental}{Mean\ Control}}{Number\ of\ trials}$$

of that dosage and the final average percentage deviation is the average of all percentage deviations (**Table 1**).

The data ran through Levine's test (homogeneity of variance test) to find if the data was eligible for a one-way ANOVA. After checking if the p-value was over 0.05, the data was put through a one-way ANOVA with the null hypothesis being the dosage having no effect of cell survival. A p-value was calculated from the result, which was used to find statistical significance. A p-value of under 0.05 was listed as statistically significant while a p-value over 0.05 was listed as not significant **(Table 2**).

Received: Jun 26, 2020
Accepted: Jun 30, 2020
Published: November 17, 2020

REFERENCES

1. Yao, Xin et al. "Luteolin inhibits proliferation and induces apoptosis of human melanoma cells in vivo and in vitro by suppressing MMP-2 and MMP-9 through the PI3K/AKT pathway." Food & function, vol. 10, no.2, 2019, pp.703-712. doi:10.1039/c8fo02013b
2. Imran, Muhammad et al. "Luteolin, a flavonoid, as an anticancer agent: A review." Biomedicine & pharmacotherapy, vol. 112, no.108612, April 2019, pp.131-134.doi:10.1016/j.biopha.2019.108612
3. Pu, Yansong et al. "Luteolin exerts an anticancer effect on gastric cancer cells through multiple signaling pathways and regulating miRNAs." Journal of Cancer, vol. 9, no.20, 8 Sep. 2018, pp.3669-3675. doi:10.7150/jca.27183
4. Lin, Yong et al. "Luteolin, a flavonoid with potential for cancer prevention and therapy." Current cancer drug targets, vol. 8, no.7 , Nov 2008, pp.634-646. doi:10.2174/156800908786241050

5. Leonardi, Giulia C et al. “Cutaneous melanoma: From pathogenesis to therapy (Review).” International journal of oncology, vol. 52, no.4, 2018, pp.1071-1080. doi:10.3892/ijo.2018.4287
6. Rastrelli, Marco et al. “Melanoma: epidemiology, risk factors, pathogenesis, diagnosis and classification.” In vivo (Athens, Greece), vol. 28, no.6, 2014, pp.1005-1011.
7. Davis, Lauren E et al. “Current state of melanoma diagnosis and treatment.” Cancer biology & therapy, vol. 20, no.11, 2019, pp.1366-1379. doi:10.1080/15384047.2019.1640032
8. Domingues, Beatriz et al. “Melanoma treatment in review.” ImmunoTargets and therapy, vol. 7, no.7 Jun. 2018, pp.35-49. doi:10.2147/ITT.S134842
9. Horinaka M, Yoshida T, Shiraishi T, et al. Luteolin induces apoptosis via death receptor 5 upregulation in human malignant tumor cells. Oncogene. vol 24, no.48, 2005;pp.7180-7189. doi:10.1038/sj.onc.1208874
10. Seelinger, Günter et al. “Anti-carcinogenic effects of the flavonoid luteolin.” Molecules (Basel, Switzerland), vol. 13, no.10, 22 Oct. 2008, pp.2628-2651. doi:10.3390/molecules13102628
11. Luo, Yuanyuan et al. “Luteolin: A Flavonoid that Has Multiple Cardio-Protective Effects and Its Molecular Mechanisms.” Frontiers in pharmacology, vol. 8, no.6, 6 Oct. 2017, pp.692-701. doi:10.3389/fphar.2017.00692
12. Aziz, Nur et al. “Anti-inflammatory effects of luteolin: A review of in vitro, in vivo, and in silico studies.” Journal of ethnopharmacology, vol. 225, 2018, pp.342-358. doi:10.1016/j.jep.2018.05.019
13. Kwon, Youngjoo. “Luteolin as a potential preventive and therapeutic candidate for Alzheimer's disease.” Experimental gerontology vol. 95, 2017, pp.39-43. doi:10.1016/j.exger.2017.05.014
14. Liu-Smith, Feng, and Frank L Meyskens. “Molecular mechanisms of flavonoids in melanin synthesis and the potential for the prevention and treatment of melanoma.” Molecular nutrition & food research vol. 60, no.6, 2016,1264-74. doi:10.1002/mnfr.201500822

ACKNOWLEDGEMENTS

In the successful completion of this project, we would like to thank Researcher Jun Xie for assisting with the research and Mr. Tim Smay for encouraging me to write this paper. Without them, this report would not have been possible.

JOURNAL OF
EMERGING INVESTIGATORS

Article

Strain-specific and photochemically-activated antimicrobial activity of berberine and two analogs

Stephanie Sun[1], Saira Hamid[2], Sarah Su[3], Andrew Su[4], Bhavesh Ashok[5], Edward Njoo[6]

[1] Basis Independent Silicon Valley, San Jose, CA
[2] Mission San Jose High School, Fremont, CA
[3] Los Altos High School, Los Altos, CA
[4] Foothill High School, Pleasanton, CA
[5] Amador Valley High School, Pleasanton, CA
[6] Department of Chemistry, Biochemistry, & Physical Science, Aspiring Scholars Directed Research Program, Fremont, CA

SUMMARY

Berberine, a natural product alkaloid, and its analogs have been reported to have a wide range of medicinal properties, including antibacterial activity. Berberine has been shown to be a photosensitizer - photochemical excitation at the correct wavelengths generate highly reactive singlet oxygen species in situ, and this has biomedical applications in photodynamic therapy. Here, we explore the antibacterial effects of berberine and two semisynthetic berberine analogs, dihydroberberine and 8-methyl-7,8-dihydroberberine, as a result of photoirradiation across three strains of bacteria. Through two antibiotic susceptibility assays, the Kirby Bauer assay and an infused agar assay, it was determined that the antibacterial activities of berberine and two semisynthetic analogs were more potent upon photoirradiation. An understanding of the photosensitizing ability of berberine may inform the design of future compounds towards the photodynamic therapy of bacterial infections.

INTRODUCTION

Widespread use of antibiotics has resulted in the emergence of strains of antibiotic resistant bacteria, which continues to present an ever-growing problem in medicine, particularly in hospital settings. Every year, tens of thousands of Americans die from infection from antibiotic resistant bacteria (1). Therefore, the development and discovery of novel antibacterial agents has been and continues to be an area of great scientific and biomedical importance.

Berberine, a naturally occurring alkaloid, is extracted from the plants in the genus Berberis, and has been documented to have a wide range of biological activities, including anticancer, antitumor, and antimicrobial activities (2-4). The use of berberine-containing extracts as a medicinal agent dates back to 3000 BCE, where it was first reported to be used in ancient Chinese medicine (5). Berberine has also been shown to be a photosensitized DNA intercalating agent. Berberine intercalates with DNA to form a berberine DNA complex (6). Upon photoirradiation of this complex, a highly reactive singlet oxygen species is generated (7). Singlet oxygen then oxidizes guanines within DNA, resulting in DNA damage and the inhibition of DNA replication, which has applications in the photodynamic treatment of cancers (8). We believe that berberine may inhibit bacterial growth through a similar mechanism of action.

Compounds with photosensitizing ability and singlet oxygen have been previously studied for antimicrobial and anticancer photodynamic therapies (9). A study on the kinetics of singlet oxygen production and decay in Escherichia coli upon photoirradiation with photosensitizers representative of three different structural classes found that the photochemical properties of photosensitizers and their abilities to be taken up by bacterial cells differ throughout different classes of compounds (10). On cancer, it has been previously reported that berberine, upon photoirradiation, induced anticancer effects on renal carcinoma cells (11).

Previously, we reported the dose dependency and strain specific antimicrobial activity of berberine compared to five broad spectrum antibiotics representative of different structural classes (12). We found that berberine is less potent than the broad-spectrum antibiotics screened (ampicillin, enrofloxacin, kanamycin, nalidixic acid, and sulfanilamide), but seemed to exhibit strain specificity.

Semisynthetic analogs of berberine have been previously demonstrated to have more potent antimicrobial activity in-vitro and in-vivo compared to berberine (13-15). Grignard additions with alkyl chains and phenyl substituents have demonstrated more potent antimycobacterial effects against tuberculosis (16). 8-alkyl-12-bromo derivatives of berberine have been previously synthesized through Grignard addition followed by radical bromination, and it was found that these compounds have more potent antimicrobial activity (17). However, it has been previously reported that a borohydride reduction of berberine to dihydroberberine resulted in decreased antimicrobial activity (18).

Here, we report photoirradiation-dependent, comparative antimicrobial activity of berberine and two chemically synthesized analogs. Two separate experiments were conducted to study this: a Kirby Bauer assay based on our previous methodology, which is a disc diffusion assay, and an agar infusion assay, in which the agar was infused with the compound solution and inhibition was quantified by

Table 1: Bacterial strains studied and some of their characteristics

Bacterial Strain	Related Diseases	Characteristics
Bacillus cereus	Food poisoning, diarrhea (20)	Can produce ATP in the absence of oxygen - Facultative anaerobic (21)
Neisseria sicca	Pneumonia, meningitis, endocarditis (22)	Oxidase-positive (aerobic)- uses oxygen as an electron acceptor in the electron transport chain (23)
Staphylococcus epidermidis	Hospital acquired infections - nosocomial infections (24)	Forms biofilm - protects the bacteria from immune response and antibacterial agents (25)

means of cell density (12). We were interested in two carbon 8 analogs of the berberine: dihydroberberine and 8-methyl-7,8-dihydroberberine.

We are interested in the effects of photoirradiation on the antimicrobial inhibitory activity of berberine and two analogs on the growth of three bacterial strains: *Bacillus cereus* (gram-positive), *Neisseria sicca* (gram-negative), and *Staphylococcus epidermidis* (gram-negative) (**Table 1**). The selection of gram-positive and gram-negative bacterial strains allows us to understand the strain-specific antimicrobial activity of berberine and its analogs (19). Strains belonging to the three species have been found to be pathogenic. Based on prior literature, we hypothesize that dihydroberberine will have less potent antimicrobial activity than berberine, and 8-methyl-7,8-dihydroberberine will be more potent. Moreover, we hypothesize that strain specific antimicrobial effects might be accentuated upon photoirradiation.

In this study, we identified the photoirradiation-dependent antimicrobial activity of berberine and two semisynthetic analogs against three strains of bacteria through two separate assays. We determined that berberine and 8-methylberberine had photoirradiation-dependent inhibitory activity at concentrations above 10 mM, and dihydroberberine had no antimicrobial activity.

RESULTS

We performed the Kirby Bauer assay and the infused Mueller Hinton (MH) agar assay to understand the photosensitizing ability of berberine and two semisynthetic analogs, and their effect of photoirradiation on their antimicrobial properties.

Dihydroberberine was synthesized through a borohydride reduction to berberine in which the iminium ion of berberine is reduced to an enamine (**Figure 1a**). A racemic mix of 8-methyl-7,8-dihydroberberine was synthesized through a Grignard addition with methyl magnesium bromide to berberine chloride (**Figure 1b**). The addition of substituents to carbon 8 results in the formation of a stereocenter. Berberine chloride was commercially purchased and not purified further.

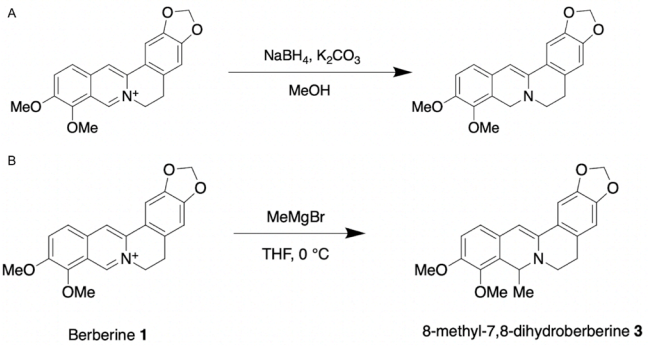

Figure 1: Reaction schematics for our synthesis of berberine analogs. (a) Synthesis of dihydroberberine 2 with NaBH4, K2CO3, and MeOH at room temperature (b) Synthesis of 8-methyl-7,8-dihydroberberine 3 with MeMgBr and THF at 0°. C.

The wavelength of light chosen for photoirradiation was based on the maximum wavelength of absorbance for all three compounds (**Figure 2**). The maximum wavelength of absorbance for the two analogs experience a blueshift in comparison to berberine.

Radii of inhibition (ROI) from the Kirby Bauer assay (**Figure 3**) are shown below. Berberine and synthesized analogs had no inhibition against *N. sicca* at all concentrations, consistent with our previously reported results. No inhibition was observed for concentrations under 10 mM for all compounds screened. ROI against *B. cereus* (**Figure 3a**), demonstrate that berberine and 8-methyl-7,8-dihydroberberine inhibit bacterial growth at high concentrations without photoirradiation, with the 100 and 50 mM concentrations having ROI that are similar and statistically insignificant (2-tail unpaired t-test; berberine *p*-value 1.00, 8-methyl-7,8-dihydroberberine *p*-value 0.109). No inhibition against *S. epidermidis* was shown at any concentration with any of the berberine analogs in the absence of photoirradiation (**Figure 3b**).

Radii of inhibition upon photoirradiation indicate that photoirradiation has a positive effect on the antimicrobial inhibitory activity of berberine analogs (**Figure 4**). A photoirradiated control demonstrated no inhibition against the growth of *B. cereus* and *S. epidermidis*, however photoirradiation with compound solutions resulted in positive

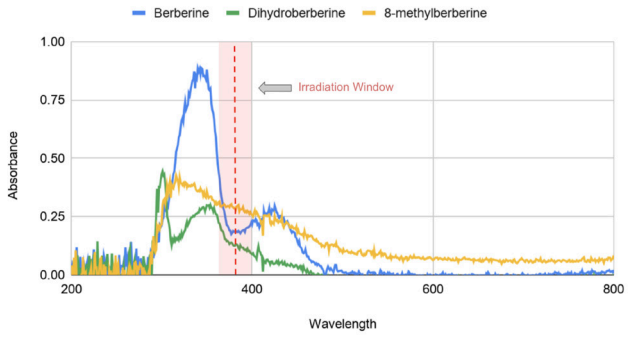

Figure 2: UV-Vis spectra of berberine, dihydroberberine, and 8-methyl-7,8-dihydroberberine. The irradiation window represents all wavelengths of light that the bacteria were exposed to.

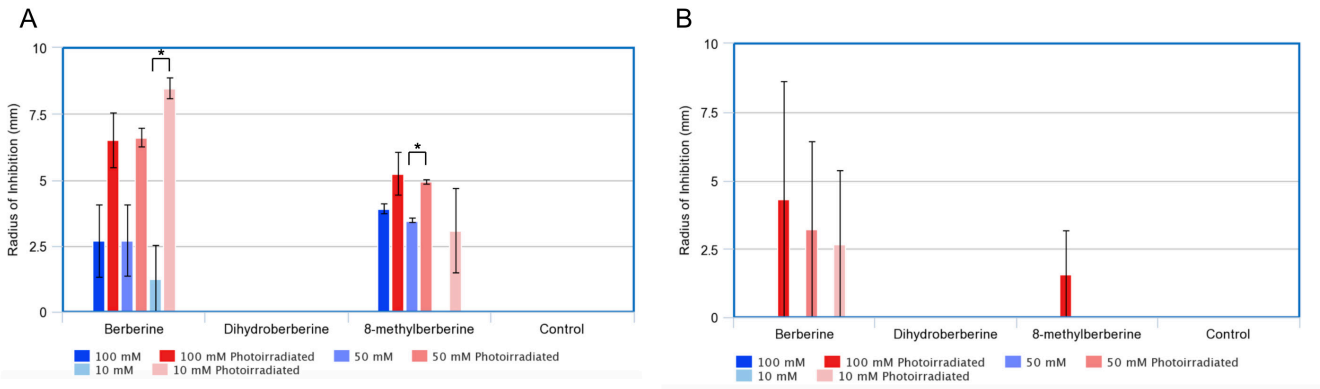

Figure 3: Radii of inhibition against *B. cereus* and *S. epidermidis* (a) The radii of inhibition against *B. cereus* at three concentrations with both photoirradated and non photoirradiated results represented. One statistically significant relationship is observed for 8-methylberberine at a 50 mM concentration (2-tail unpaired t-test 0.0002) (b) Radii of inhibition against *S. epidermidis* at three concentrations. One statistically significant relationship is observed for berberine at a 10 mM concentration (2-tail unpaired t-test 0.02). The * represented statistical significance between the two data points. Results shown are the mean of 3 technical replicates and standard error is reported.

ROI. An increase in the ROI upon photoirradiation can be observed with berberine and 8-methyl-7,8-dihydroberberine at all concentrations higher than 1 mM against both *B. cereus* and *S. epidermidis* (**Figure 3**). Dihydroberberine had no inhibitory effects against bacterial growth upon photoirradiation. The previous maximum inhibitory effects of berberine against *B. cereus* remain consistent, with the 100 mM and 50 mM resulting in statistically insignificant differences in ROI (2-tail unpaired t-test, *p*-value 0.94). At the 10 mM concentration, there is a significant difference between the inhibitory effects of berberine upon photoirradiation (2-tail unpaired t-test, *p*-value 0.02). The inhibitory effects of 8-methyl-7,8-dihydroberberine against *B. cereus* are also improved upon photoirradiation, with a statistically significant difference at the 50 mM concentration (2-tail unpaired t-test, *p*-value 0.0002) and antimicrobial activity at the 10 mM concentration, whereas there was no inhibition at the 10 mM concentration with no photoirradiation.

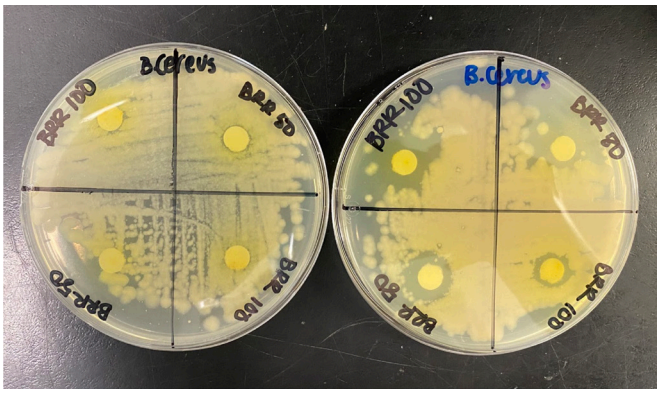

Figure 4: Bacteria growth after incubation without photoirradiation (left) and with photoirradiation (right). The compound solution shown here is berberine at 100 mM and 50 mM concentrations. The increased inhibition of bacterial growth can be seen in their respective radii of inhibition. Petri dishes shown are representative of the whole experiment. Concentrations from left to right, of berberine solutions starting with the top row: 100 mM, 50 mM, 100 mM photoirradiated, 50 mM photoirradiated, 50 mM, 100 mM, 50 mM photoirradiated, 100 mM photoirradiated.

The effects of photoirradiation on the antimicrobial effects of berberine and its analogs is consistent against *S. epidermidis* . There was no inhibition against *S. epidermidis* without photoirradiation at all concentrations and a photoirradiated control also demonstrated no inhibition, but upon photoirradiation with compound solutions, berberine demonstrated antimicrobial effects at 100, 50, and 10 mM concentrations and 8-methyl-7,8-dihydroberberine had antimicrobial effects at 100 mM.

Bacterial growth from the infused Mueller Hinton agar assay was quantified by cell density. In this study, dihydroberberine demonstrated inhibitory effects against *N. sicca* upon photoirradiation (**Figure 5**). *N. sicca* colonies covered 30.7% of the petri dish after being subjected to photoirradiation for thirty minutes, compared to the lawn of bacteria (full coverage) that grew without photoirradiation. Results for other strains of bacteria and compounds were inconclusive.

From this study, we found that the antimicrobial activity of berberine and related analogs are positively affected by photoirradiation, and the inhibitory activity remains strain specific when photoirradiated.

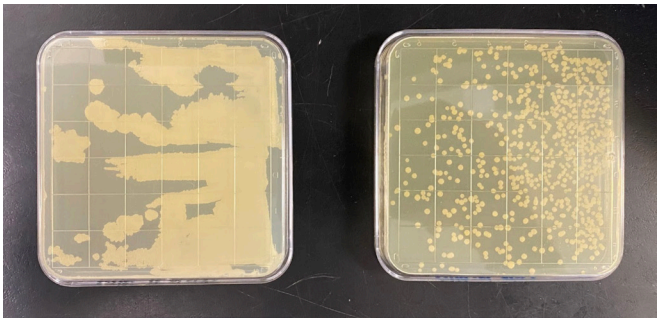

Figure 5: Petri dishes from the infused Mueller Hinton agar assay with dihyroberberine against *N. sicca*. The un- photoirradiated petri dish (left), has bacterial growth in a lawn, while the photoirradiated petri dish (right) has distinct bacteria colonies.

DISCUSSION

In this study, we report the photoirradiation-dependent antimicrobial activity of berberine and two semisynthetic berberine analogs, 8-methyl-7,8-dihydroberberine and dihydroberberine. We found that photoirradiation results in superior antimicrobial activity at all concentrations of berberine and 8-methyl-7,8-dihydroberberine in the Kirby Bauer assay, and that the antimicrobial activity remains strain specific.

In the Kirby Bauer assay, berberine and 8-methyl-7,8-dihydroberberine inhibit bacterial growth with insignificantly different radii of inhibition at concentrations of 100 mM and 50 mM both without and with photoirradiation. We believe that this is a result of the maximum inhibitory effects of berberine against *B. cereus* being within the 10 and 50 mM concentrations. It was also determined that berberine and 8-methyl-7,8-dihydroberberine have comparable inhibitory activity, however berberine is commercially available while the synthesis of 8-methyl-7,8-dihydroberberine is done in an ice bath. Further research into the viability of 8-methyl-7,8-dihydroberberine as an antibacterial agent is needed in order to determine if the compound presents significant benefits over berberine such as reduced side effects.

Differences between this study and our previously reported study, including the minimum concentrations of the berberine solutions necessary to induce inhibitory activity on *B. cereus* and the lack of inhibitory activity on *S. epidermidis* without photoirradiation, can be attributed to the modification in the composition of our Mueller Hinton agar. It has been previously reported that differences in agar composition can result in significant differences in bacterial growth rates and colony density (26).

The results of the Kirby Bauer assay and the infused agar assay suggest that the mode of administration of the compound affects its antimicrobial activity. Dihydroberberine demonstrated no inhibition in the Kirby Bauer assay, which is a disc diffusion assay, while it exhibited inhibition of bacterial growth in the infused agar assay. We believe that this may be attributed to dihydroberberine having a poor ability to diffuse, while other compounds studied were able to diffuse better, resulting in inhibition in the Kirby Bauer assay.

A limitation to the use of our synthesized berberine analogs is the possibility of cytotoxic side effects due to the blueshift in the maximum wavelength of absorption compared to berberine. DNA, aromatic amino acids, and other molecular entities have absorbances in the ultraviolet range, with DNA's absorbance around 260 nm (27). The generation of a highly reactive singlet oxygen species within DNA may also result in non-specific cytotoxicity within the human body, posing an implication to the development of berberine and its analogs as a therapeutic agent. These factors may be impactable to the design and synthesis of future berberine analogs.

Our synthesized analog, 8-methyl-7,8-dihydroberberine, had antimicrobial activity that was comparable to that of berberine. Further studies on the structure-activity relationship of the length of the alkyl chain on carbon 8 of berberine and dihydroberberine and the antimicrobial activity and strain specificity, along with analogs with substituents on different carbon positions, would be instrumental to understanding the structure relationship activity of berberine analogs and antimicrobial activity. Such structures are synthetically accessible with alternate Grignard reagents. Additionally, future optimizations to the method of delivery of berberine analogs would be instrumental to gaining insight on the effects of photoirradiation to the antimicrobial activity of berberine and the effects of diffusion versus infusion. This could guide the design of future analogs of berberine and the possible identification of novel antibacterial agents.

MATERIALS AND METHODS

Chemical Synthesis

Berberine chloride (MaxSun, >97.0%) was used for the synthesis without further purification. Synthesis of dihydroberberine was conducted according to previously reported protocols (28). Dihydroberberine is an analog of berberine that also provides access to other analogs and reactions such as stork enamine reactions and 13-alkylberberine (29,30).

Synthesis of 7,8-dihydroberberine

We added berberine chloride 1 (1.000 g, 2.690 mmol, 1.0 eq.), sodium borohydride (Fisher, >98%; 0.112 g, 2.959 mmol, 1.1 eq.), and potassium carbonate (1.100 g, 7.959 mmol, 3.0 eq.) in MeOH (30 mL) to a vacuum dried 50 mL round bottom flask charged with a teflon stir bar. The reaction mixture was stirred at room temperature for one hour and monitored by thin layer chromatography (TLC) (10% MeOH in DCM). Upon disappearance of the starting material by TLC, the reaction mixture was filtered with a Buchner funnel. The resulting material was recrystallized in ethanol to give dihydroberberine as yellow crystals (0.799 g, 2.36 mmol, 75.4% yield)

Synthesis of 8-methyl-7,8-dihydroberberine

We added 0.2 g (0.538 mmol, 1.0 eq) of berberine chloride in tetrahydrofuran (THF) to a vacuum dried 25 mL round bottom flask cooled in an ice bath and charged with teflon stir bar. A 3M solution of MeMgBr (STREM Chemicals Inc.; 1.793 mL, 5.379 mmol, 10 eq.) in THF was added dropwise through a syringe. The reaction mixture stirred for 15 minutes in the ice bath and monitored by thin layer chromatography (25% hexane in ethyl acetate). Upon disappearance of the starting material by TLC, the reaction mixture was quenched with water, and extracted with brine and ethyl acetate. The organic layer was collected and dried over anhydrous magnesium sulfate and concentrated in vacuo to give 8-methyl-7,8-dihydroberberine (0.126 g, 0.359 mmol, 66.7% yield).

Characterization

All compounds were characterized by ^{1}H nuclear magnetic resonance (NMR) spectroscopy (Nanalysis,

NMReady, 60 MHz), Fourier-transform infrared spectroscopy (Thermo Nicolet iS5, iD5 ATR assembly) and UV-visible spectroscopy (BioRad Smartspec 3000).

Dihydroberberine Characterization

(60 MHz, $CDCl_3$): δ 5.82-7.02 (m, 5H), 5.84 (s, 2H), 4.18 (d, J = 13.4 Hz, 2H), 3.80 (s, 6H), 2.59-3.65 (m, 4H); FTIR (ATR, cm^{1}): 2930.24, 2833.66, 2249.37, 1607.91, 1494.35, 1484.76, 1457.74, 1427.17, 1388.49, 1333.92, 1277.43, 1246.80, 1221.93, 1163.74, 1131.16, 1083.90, 1039.00, 990.70, 938.65, 908.41, 860.13, 799.16, 772.73, 730.86, 647.90; UV (iPrOH) λ_{max}: 301, 354

8-methyl-7,8-dihydroberberine Characterization

(60 MHz, $CDCl_3$): δ 5.75-7.14 (5H, m), 4.69 (1H, m), 3.74 (3H, s), 3.68 (3H, s), 2.67 (2H, m), 2.02 (2H, m), 1.38 (3H, d, J = 6.9 Hz); FTIR (ATR, cm^{-1}): 2931.25, 2359.69, 1681.92, 1597.43, 1482.63, 1416.18, 1343.49, 1266.07, 1229.80, 1167.99, 1096.48, 1037.44, 932.42, 847.36, 810.53, 738.87, 612.23; UV (H_2O) λ_{max}: 316

Bacteria Cultures

Live bacteria cultures of *Bacillus cereus*, Escherichia coli, *Neisseria sicca*, and *Staphylococcus epidermidis* were acquired from Carolina Biological. Overnight cultures were grown in falcon tubes with 10 mL LB media (1% tryptone, 1% NaCl, 0.5% yeast extract, 97.5% water) at 37°C for 12-14 hours.

Compound Solutions

Solutions of berberine, dihydroberberine, and 8-methyl-7,8-dihydroberberine were made at 6 different concentrations (100 mM, 50 mM, 10 mM, 1 mM, 0.1 mM, 0.01 mM). Commercial berberine chloride was used without further purification. Compounds were dissolved in solutions of 10% DMSO in deionized water. A solution of 10% DMSO in deionized water served as our control. Solutions were sonicated to help with dissolution. The appropriate dilutions were performed, and the appropriate amounts of DMSO were added to maintain a 10% DMSO solution.

Kirby Bauer Assay

Bacteria from the overnight cultures were inoculated on Petri dishes plated with modified Mueller Hinton Agar. Filter paper discs saturated with the compound solution were used to administer the compound solutions. The bacteria were incubated overnight at 37°C, and radii of inhibition measurements were taken in mm with an electric caliper. All plating was done in a sterile laminar flow hood. Triplicates with technical replicates were completed, and the results were averaged.

Infused Agar Assay

We added 1% of the 100 mM compound solutions to the modified Mueller Hinton agar, resulting in a 0.1 mM concentration of the compounds in the agar. Petri dishes were plated with the infused Mueller Hinton agar and bacteria were inoculated. The petri dishes were incubated overnight at 37°C. Results were quantified by bacteria density, which was measured by colonies per cm^2. The average size of a colony was found. All plating was done in a sterile laminar flow hood.

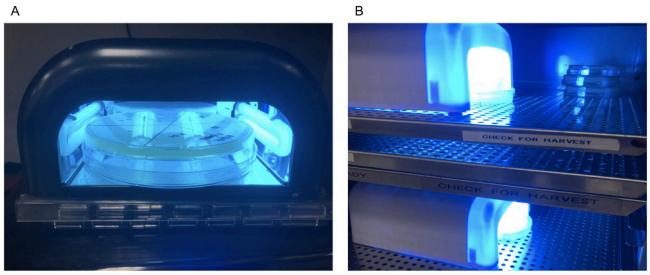

Figure 6: Experiment setup for the photoirradiation of the petri dishes. (a) Petri dishes placed inside the nail curing lamps. Each petri dish was photoirradiation for 30 minutes. (b) Nail curing lamps placed inside the incubator, at 37° C.

Photoirradation

Petri dishes were photoirradiated at 380 nm for thirty minutes while incubated at 37°C. After initial photoirradiation, all petri dishes were incubated overnight at the same temperature. A nail curing lamp set up inside of the incubator was used as the light source (**Figure 6**). The wavelength of emitted light was determined by a spectrometer (Ocean Optics).

Statistical Analysis

Radius of inhibition measurements were acquired in millimeters using an electronic caliper. The ROI from all three experiments were averaged and standard error was calculated. Statistical significance of the differences between the observed radii of inhibition was determined at the 95% confidence level using independent, 2-tailed t-testing (31).

Received: June 15, 2020
Accepted: October 31, 2020
Published: November 17, 2020

REFERENCES

1. Kim, Lindsay, *et al*. "Biological and Epidemiological Features of Antibiotic-Resistant Streptococcus Pneumoniae in Pre- and Post-Conjugate Vaccine Eras: a United States Perspective." *Clinical Microbiology Reviews*, vol. 29, no. 3, 2016, pp. 525–552., doi:10.1128/cmr.00058-15.
2. Stermitz, F. R., *et al*. "Synergy in a Medicinal Plant: Antimicrobial Action of Berberine Potentiated by 5-Methoxyhydnocarpin, a Multidrug Pump Inhibitor." *Proceedings of the National Academy of Sciences,* vol. 97, no. 4, Apr. 2000, pp. 1433–1437., doi:10.1073/pnas.030540597.
3. Wang, Haoran, *et al*. "Metformin and Berberine, Two

Versatile Drugs in Treatment of Common Metabolic Diseases." *Oncotarget*, vol. 9, no. 11, Nov. 2017, doi:10.18632/oncotarget.20807.

4. Xu, Jianhao, *et al*. "Anticancer Effect of Berberine Based on Experimental Animal Models of Various Cancers: a Systematic Review and Meta-Analysis." *BMC Cancer,* vol. 19, no. 1, 2019, doi:10.1186/s12885-019-5791-1.
5. Tillhon, Micol, *et al*. "Berberine: New Perspectives for Old Remedies." *Biochemical Pharmacology*, vol. 84, no. 10, 2012, pp. 1260–1267., doi:10.1016/j.bcp.2012.07.018.
6. Krey, A. K., and F. E. Hahn. "Berberine: Complex with DNA." *Science*, vol. 166, no. 3906, July 1969, pp. 755–757., doi:10.1126/science.166.3906.755.
7. Hirakawa, Kazutaka, *et al*. "Dynamics of Singlet Oxygen Generation by DNA-Binding Photosensitizers." *The Journal of Physical Chemistry B*, vol. 116, no. 9, 2012, pp. 3037–3044., doi:10.1021/jp300142e.
8. Hirakawa, Kazutaka, *et al*. "The Mechanism of Guanine Specific Photooxidation in the Presence of Berberine and Palmatine: Activation of Photosensitized Singlet Oxygen Generation through DNA-Binding Interaction." *Chemical Research in Toxicology*, vol. 18, no. 10, 2005, pp. 1545–1552., doi:10.1021/tx0501740.
9. Callaghan, Susan, and Mathias O. Senge. "The Good, the Bad, and the Ugly – Controlling Singlet Oxygen through Design of Photosensitizers and Delivery Systems for Photodynamic Therapy." *Photochemical & Photobiological Sciences*, vol. 17, no. 11, 2018, pp. 1490–1514., doi:10.1039/c8pp00008e.
10. Ragàs, Xavier, *et al*. "Singlet Oxygen in Antimicrobial Photodynamic Therapy: Photosensitizer-Dependent Production and Decay in E. Coli." *Molecules*, vol. 18, no. 3, 2013, pp. 2712–2725., doi:10.3390/molecules18032712.
11. Lopes, Tairine Zara, *et al*. "Berberine Associated Photodynamic Therapy Promotes Autophagy and Apoptosis via ROS Generation in Renal Carcinoma Cells." *Biomedicine & Pharmacotherapy*, vol. 125, 2020, p. 110038., doi:10.1016/j.biopha.2020.110038.
12. Sun, Stephanie, *et al*. "Comparative screening of dose-dependent and strain-specific antimicrobial efficacy of berberine against a representative library of broad spectrum antibiotics" *Journal of Emerging Investigators*, accepted manuscript.
13. Park, Ki Duk, *et al*. "Synthesis and Antifungal Activity of a Novel Series of 13-(4-Isopropylbenzyl)Berberine Derivatives." *Bioorganic & Medicinal Chemistry Letters*, vol. 20, no. 22, 2010, pp. 6551–6554., doi:10.1016/j.bmcl.2010.09.045.
14. Iwasa, Kinuko, *et al*. "Antimicrobial Activity of Some 13-Alkyl Substituted Protoberberinium Salts." *Planta Medica*, vol. 63, no. 03, 1997, pp. 196–198., doi:10.1055/s-2006-957651.
15. Kim, Sung Han, *et al*. "Antimicrobial Activity of 9-O-Acyl- and 9-O-Alkylberberrubine Derivatives." *Planta Medica*, vol. 68, no. 3, 2002, pp. 277–281., doi:10.1055/s-2002-23128.
16. Wang, Yanxiang, *et al*. "Synthesis and Biological Evaluation of 8-Substituted Berberine Derivatives as Novel Anti-Mycobacterial Agents." *Acta Pharmaceutica Sinica B*, vol. 2, no. 6, 2012, pp. 581–587., doi:10.1016/j.apsb.2012.10.008.
17. Iwasa, Kinuko, *et al*. "Antimicrobial Activity of 8-Alkyl- and 8-Phenyl-Substituted Berberines and Their 12-Bromo Derivatives." *Journal of Natural Products*, vol. 61, no. 9, 1998, pp. 1150–1153., doi:10.1021/np980044+.
18. Rodrigues, Catarina A. B., *et al*. "Synthesizing a Berberine Derivative and Evaluating Antimicrobial Activity To Reinforce with Students the Potential Significance of Small Chemical Structure Changes for Biological Systems." *Journal of Chemical Education*, vol. 95, no. 3, 2018, pp. 492–495., doi:10.1021/acs.jchemed.7b00458.
19. Hessle, Christina C., *et al*. "Gram-Positive and Gram-Negative Bacteria Elicit Different Patterns of pro-Inflammatory Cytokines in Human Monocytes." *Cytokine*, vol. 30, no. 6, 2005, pp. 311–318., doi:10.1016/j.cyto.2004.05.008.
20. Bottone, E. J. "*Bacillus cereus*, a Volatile Human Pathogen." *Clinical Microbiology Reviews*, vol. 23, no. 2, Jan. 2010, pp. 382–398., doi:10.1128/cmr.00073-09.
21. Duport, Catherine, *et al*. "Adaptation in *Bacillus cereus*: From Stress to Disease." *Frontiers in Microbiology*, vol. 7, Apr. 2016, doi:10.3389/fmicb.2016.01550.
22. Entesari-Tatafi, Damoon, *et al*. "Iatrogenic Meningitis Caused By *Neisseria sicca*/Subflava After Intrathecal Contrast Injection, Australia." *Emerging Infectious Diseases*, vol. 20, no. 6, 2014, pp. 1023–1025., doi:10.3201/eid2006.131117.
23. Liu, Guangyu, *et al*. "Non-Pathogenic Neisseria: Members of an Abundant, Multi-Habitat, Diverse Genus." *Microbiology*, vol. 161, no. 7, Jan. 2015, pp. 1297–1312., doi:10.1099/mic.0.000086.
24. Ogara, James P., and Hilary Humphreys. "*Staphylococcus epidermidis* Biofilms: Importance and Implications." *Journal of Medical Microbiology*, vol. 50, no. 7, Jan. 2001, pp. 582–587., doi:10.1099/0022-1317-50-7-582.
25. Vuong, Cuong, and Michael Otto. "*Staphylococcus epidermidis* Infections." *Microbes and Infection*, vol. 4, no. 4, 2002, pp. 481–489., doi:10.1016/s1286-4579(02)01563-0.
26. Stecchini, Mara Lucia, *et al*. "Influence of Agar Content on the Growth Parameters of *Bacillus cereus*." *International Journal of Food Microbiology*, vol. 64, no. 1-2, 2001, pp. 81–88., doi:10.1016/s0168-1605(00)00436-0.
27. Schmid, Franz-Xaver. "Biological Macromolecules: UV-Visible Spectrophotometry." *Encyclopedia of Life Sciences*, 2001, doi:10.1038/npg.els.0003142.
28. Nechepurenko, I. V., *et al*. "Berberine: Chemistry and Biological Activity." *Chemistry for Sustainable Development* , vol. 18, 2010, pp. 1–23.
29. Zhang, Lei, *et al*. "Synthesis and Cytotoxicity Evaluation

of 13-n-Alkyl Berberine and Palmatine Analogues as Anticancer Agents." *Molecules*, vol. 17, no. 10, 2012, pp. 11294–11302., doi:10.3390/molecules171011294.
30. Kotani, Kenta, *et al*. "13-(2-Methylbenzyl) Berberine Is a More Potent Inhibitor of MexXY-Dependent Aminoglycoside Resistance than Berberine." *Antibiotics*, vol. 8, no. 4, 2019, p. 212., doi:10.3390/antibiotics8040212.
31. McDonald, John H. *Handbook of Biological Statistics*. Sparky House Publishing, 2009.

JOURNAL OF
EMERGING INVESTIGATORS

Article

Estimation of Reproduction Number of Influenza in Greece using SIR Model

Cleo M. Skarpeti[1] and Dr. Michael G. Skarpetis[2]
[1]Hellenic-American Educational Foundation, Athens, Greece
[2]National and Kapodistrian University of Athens, General Department, Athens, Greece

SUMMARY

Infectious disease models are regularly used by epidemiologists to predict the course of diseases. However, the accuracy of such models remains hotly debated. In this study, we developed an algorithm to estimate the contact rate and the average infectious period of influenza using a Susceptible, Infected, and Recovered (SIR) epidemic model. The parameters in this model were estimated using data on infected Greek individuals collected from the National Public Health Organization. The data interval investigated spans 13 weeks of 2019 and the first 8 weeks of 2020. After estimating the nonlinear SIR epidemic model's parameter values, we computed the theoretical influenza reproduction number and simulated the evolution of the three SIR variables over time. We hypothesized that the reproduction number would be greater than one, which means that influenza is not like other simple diseases but is an epidemic. Our model labeled influenza as an epidemic with a basic reproduction value greater than one.

INTRODUCTION

In the 1960s, timely eradication of infectious diseases was a seemingly achievable goal. Nevertheless, contagious diseases are still a severe problem since they can lead to long-term suffering and mortality, worldwide but especially in developing countries which have a lack of resources, access to sanitation facilities, and healthcare education. As a result, pandemics or epidemics remain neglected or inadequately tackled in developing countries, which has detrimental repercussions to the population such as increased death rate. Underdeveloped countries are less likely than developed countries to combat diseases by deploying effective vaccinations to decrease transmission (1). Although Greece is not a developing country the healthcare system should be improved, because it lacks resources due to the financial crisis of 2010 (2).

Through viral evolution and microbe adaption to new circumstances and environments, diseases consistently emerge and reemerge. In particular, the influenza virus is a pathogen that evolves perpetually, usually appearing as a new variant every year. The influenza virus can adapt, change and evolve genetically, which is why it is found in various species. Viruses evolve by some basic mechanisms such as RNA reassortment or genetic shift and genetic drift. In reassortment, two genetically different influenza viruses infect the same cell in a human organism and their gene segments swap and transfer genetic information (3). Mixing this information can create one hybrid virus. In genetic drift, mutational differences can develop in the genes of the virus through changes in its surface proteins. Genetic shift happens rarely. However, the difference is that the virus that originally infected animals now can infect human beings as well. A virus that undergoes drift and shift is probably the only case that can cause a global influenza pandemic associated with harmful implications (3). According to the World Health Organization, the average number of annual influenza cases is approximately 1 billion, and 3–5 million of which are severe with a death toll of 500,000 (4). Apart from the high mortality rate, influenza also provokes financial damages worldwide. Indicatively, the total financial loss of annual influenza epidemics in the United States is approximately $87.1 billion (5).

Though influenza outbreaks consistently occur every year, it is not known when the disease will emerge, the way it will spread among populations, how many deaths will occur, and which part of the population should be vaccinated. The answers to these questions can be approached by making use of experimental tools, such as mathematical models that enable us to test theories by simplifying reality.

To control the spread of a disease, we need to make general predictions and forecasts to prevent it from becoming an epidemic that will infect a substantial number of individuals within a community, population, or region in a short period of time. The Susceptible (S), Infected (I), and Recovered (R) (SIR) epidemic model first presented by Kermack and McKendrik in 1927 divides the population into three basic compartments (S, I, R) and studies the evolution of these quantities in time via nonlinear differential equations (6). Susceptible represents the part of the population which is at risk of becoming infected. Infected denotes the members of the population who are infectious and might transfer the disease to susceptible individuals. Finally, recovered is representative of the part of the population that was previously infected but recovered and has immunity to the disease. The SIR mathematical model indicates changes in the population of each of these three basic compartments based on two parameters, the contact rate and the average infectious period. The contact rate denotes the average number of contacts with susceptible individuals that might infect them.

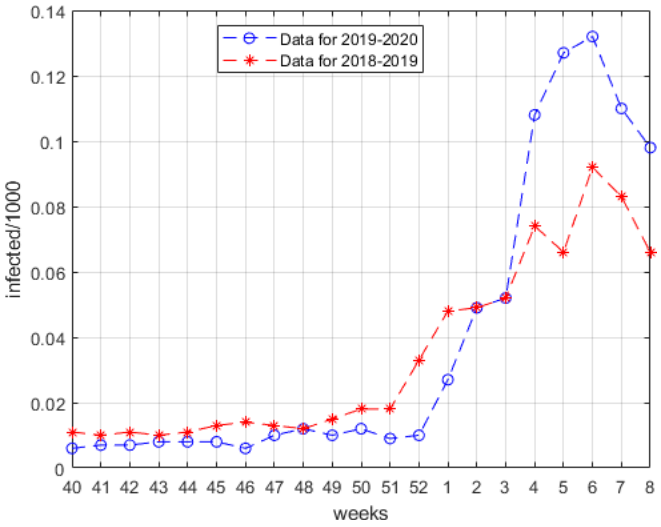

Figure 1. Number of cases of influenza infections per 1000 visits per week. Data taken from the National Public Health Organization regarding influenza infections per 1000 visits per week in Greece during the 2018-2019 (red line) and 2019-2020 (blue line) influenza season. Weeks represent week number in 2019 (40-52) and 2020 (1-8).

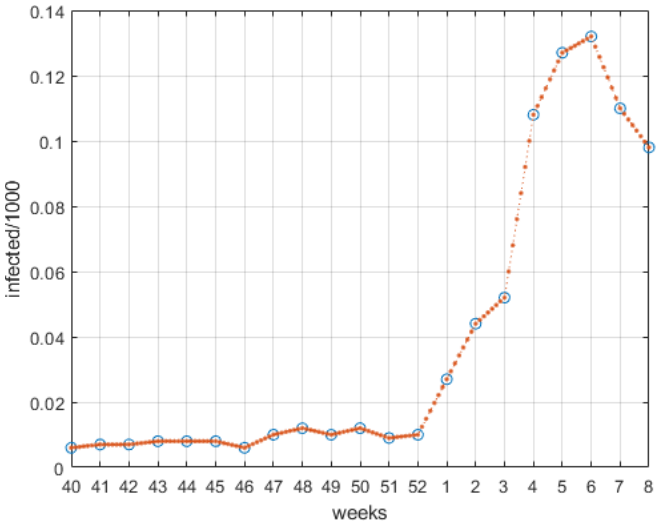

Figure 2. Number of cases of influenza infections per 1000 visits per day. Weekly case numbers underwent interpolation in MATLAB to generate visits per day.

The average infectious period denotes the time period during which an infected individual is likely to transmit the disease to a susceptible one.

The aforementioned SIR nonlinear dynamics that model the spread of influenza in Greece are presented with the following differential equations (6,7):

$$\frac{dS(t)}{dt} = -\beta S(t)I(t) \qquad (1)$$

$$\frac{dI(t)}{dt} = \beta S(t)I(t) - \gamma I(t) \qquad (2)$$

$$\frac{dR(t)}{dt} = \gamma I(t) \qquad (3)$$

where S(t), I(t), and R(t) denote the susceptible, infected, and recovered individuals in a population infected from influenza $S(t) + I(t) + R(t) = N$ where N the total number of the individuals that belong to this population). The parameter β>0 denotes the contact rate and 1/γ denotes the average infectious period.

The basic reproduction number, R_0, is the predicted number of susceptible individuals that an infected one can infect. A value of R_0 greater than 1 is indicative of the persistence of the infection in the examined population, above its baseline, whereas a value of R_0 less than 1 is indicative of the eventual eradication of the disease. In an outbreak, it is of utmost importance to apply strategies and methods to control this number and limit it. Mitigation strategies include household isolation, school and store closures, vaccination, etc. (8). This is the most famous model in epidemiology and is used by many researchers (7-16).

In this study, we developed an algorithm in order to estimate the main parameters of an SIR epidemic model, which are the contact rate and the average infectious period. First, we collected data on infected Greek individuals from the National Public Health Organization during the last 13 weeks of 2019 and the first 8 weeks of 2020 (17). The data is enriched via the interpolation function in MATLAB in order to be suitable for identification. Using the combined collected data, the parameter values are estimated and identified using grey box modelling methods (18). Finally, we presented the time evolution of the SIR model variables using simulation results.

The aim of this procedure is to answer the following question: Is influenza considered to be an epidemic in Greece in the specific time period 2019–2020 based on its reproduction number, and how does this time period compare to the same time period in 2018-2019? Using limited data from infected individuals, we determined that influenza is an epidemic in Greece, since the computed reproduction number, based on the parameter predictions, was indeed greater than 1 and the predicted infected individuals during the last week under investigation was greater than zero.

RESULTS

Data Collection and Estimation For 2019–2020

We used the data of the last 13 weeks of 2019 and the first 8 weeks of 2020 collected from National Public Health Organization (13) to visualize the number of cases of influenza infections per 1000 visits per week (**Figure 1**). We also applied the 1-D interpolation function in MATLAB, in order to enrich the data from weeks to days to create necessary data for the identification algorithm (18) (**Figure 2**).

Applying data after interpolation and using the proposed procedure (see Methods), the parameters of the epidemic model were identified using grey box modelling methods (18). Using the nonlinear SIR model equations 1–3, the differential equation-based model structure is specified. The unknown model parameters (contact rate and average infectious period) were estimated via nonlinear least squares

minimization techniques. Finally, the Euler numerical method was applied to solve these differential equations. The fit to estimation data was 84.53% and the final prediction error was 4.79567 x 10^{-5} (**Figure 3**). These values are quite satisfactory considering the form of the initial data. These estimation results were independent from the initial values of the predicted parameters.

The predicted parameter values of the SIR model are:

β=0.2044, γ=0.1113

Using the aforementioned parameters and replacing them in equations 1–3, we present the evolution of the three variables in time (S, I, & R) (**Figure 4**). The evolution of the influenza infection in Greece considering the average infectious period as nearly 1/0.1113 ~ 9 days, which means that an infected individual can transmit the virus for 9 days. The contact rate is β=0.2044 which means that an average infected individual has the potential to infect 0.2044 susceptible per day or equivalently 1 susceptible per 5 days since 1/0.2044 ~ 5 .

Since there was an increase in the number of infected people as well as the recovered ones, there was an eventual decrease in the number of susceptible individuals. We noticed that the blue line (S) did not hit zero and the green line (R) never reached 1, which meant that not every single individual in this particular population had been infected so far. Furthermore, due to the fact that the reproduction number R_0 = β/γ=1.8360>1, the disease can be characterized as an epidemic that eventually invades the population (19). It is worth mentioning that since influenza turned out to be an epidemic, the number of infected individuals is always greater than zero. The predicted infected individuals during the last week under investigation is 0.7447 .

Using 2018 data (last 13 weeks of 2018 and the first 8 weeks of 2019) of infected individuals collected from the national public health organization (**Figure 1**), we estimated the parameter values of the SIR model as follows: β=0.1254 and γ=0.0791, which was used to compute the basic reproduction number, R_0 = β/γ=1.585>1. Since this reproduction number is lower than the estimated reproduction number of 2019-2020, we conclude that the influenza outbreak was more severe in 2019-2020.

DISCUSSION

In this paper, the data from only one of the three basic involved variables (i.e. infected individuals) was used to estimate the value of the parameters β and γ of the SIR model and compute the basic reproduction number. The results concern the outbreak of influenza in 2019–2020. The initial hypothesis, that influenza is an epidemic in Greece, is validated since the basic reproduction number is greater than 1. Influenza in Greece is characterized by a rapid spread, with approximately 13.2% of the population examined during the 6th week of 2020 becoming infected (17). The model can be further validated when more data becomes available. This will support that the forecasted evolution is the same as the real one.

We considered several limitations of the SIR model used. The model assumes that everyone has the same probability of being in contact with infected individuals, which does not represent society since not all civilians come in contact with the same number of people. Moreover, the model considers the total population to be constant. As a result, births and deaths do not affect the outcome. Another limitation is that infected individuals are considered to have an equal transmission rate regardless of official diagnosis or quarantine status. Furthermore, more complex versions of the SIR model exist that consider tunable inputs, such as vaccination, educational campaigns, and immunity. Such variables affect the results and are closer to a real social

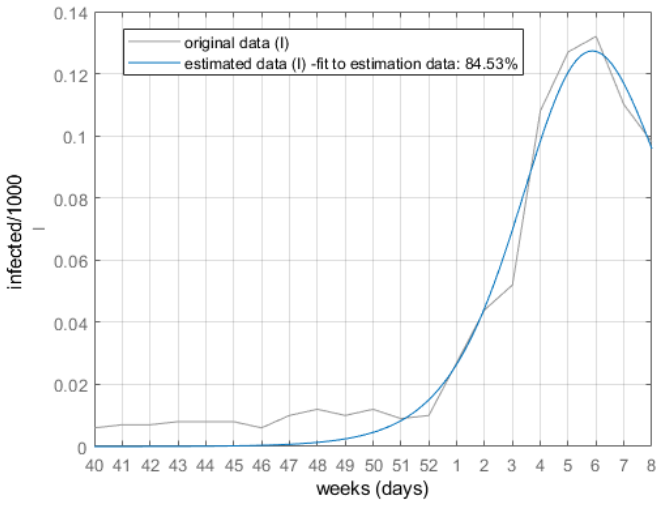

Figure 3. Predicted response of infected individuals. Comparison of original data (grey line) and estimated data (blue line). The fit to estimation data was 84.53% and the final prediction error was 4.79567 x 10^{-5}.

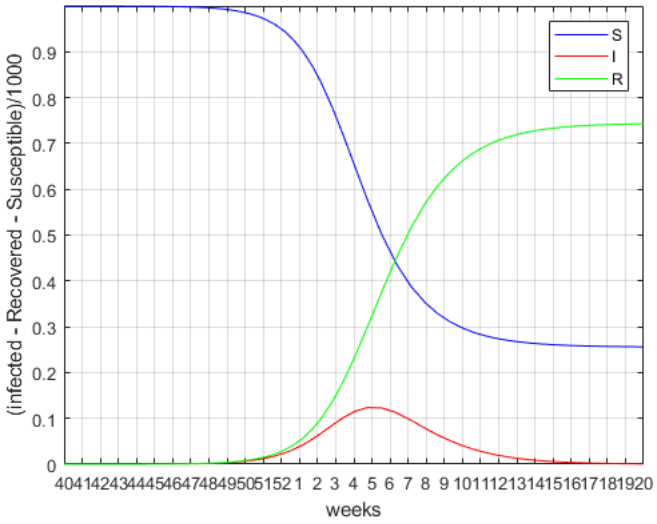

Figure 4. Simulation of SIR predicted epidemic dynamics. Model of the 2019-2020 influenza season in Greece. Weeks represent week number in 2019 (40-52) and 2020 (1-20). S, susceptible (blue); I, infected (red); R, recovered (green).

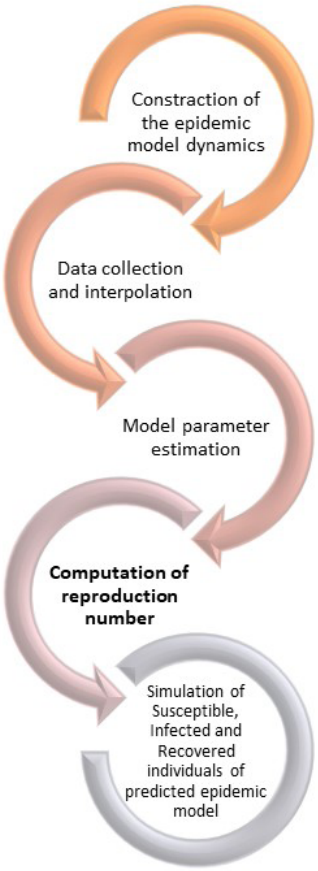

Figure 5. Flow chart for the computation of reproduction number for 2019-2020 influenza in Greece.

structure. These complex models can propose the most optimal solution to limit the repercussions of an epidemic or even pandemic. Nevertheless, the SIR model is quite useful and acceptable despite these limitations since it is accurate enough to enable the researchers to easily approximate infectious disease evolution. Using this particular model, with only a few measurements of infected individuals, general predictions about the outbreak can be made enabling experts to take action fast to limit the implications as soon as possible.

According to the results of the estimated basic reproduction numbers of influenza in 2018–2019 and 2019–2020, we understand that influenza outbreak in 2019–2020 was more severe than the outbreak in 2018–2019 (7.4% of the examined population during the 6th week of 2019 was infected). According to the estimated reproduction numbers, we observed that in 2019-2020 the predicted number of susceptible individuals that an infected one can infect is 1.836, as opposed to 2018-2019 which was 1.585. This comparison highlights that the influenza virus in 2019–2020 was transmitted more rapidly and ending up infecting a quite large number of individuals, as opposed to the previous year. Further research into the reasons why these differences exist year to year could lead to development of better strategies to mitigate and prevent further epidemics, such as influenza, in the future.

MATERIALS & METHODS

In order to compute the reproduction number of influenza, data that represent the estimated number of cases of influenza infections per 1000 visits per week, was collected from the National Public Health Organization. According to the National Public Health Organization, the number of cases per 1000 visits was estimated by weighting the country's permanent population by geographical department and urbanity (17). This information comes from the network of private doctors, the network of doctors Health Centers and the network of doctors of Health Units. The data was enriched by the interpolation function in MATLAB so as to concern influenza infections per 1000 visits per day. From the interpolated dataset, the nonlinear model with unknown parameters was identified and the unknown model parameters (namely contact rate and average infectious period) were estimated using the nonlinear SIR model and suitable functions in MATLAB. The identification was accomplished using grey box modelling methods and nonlinear least squares minimization techniques. Finally, the differential equations were solved using the Euler numerical method.

Based on these estimations, the basic reproduction number was computed. After the parameter estimation, simulation was performed. The outbreak of influenza for this specific time period was visualized by showing the evolution of the three basic variables of the model in time. The aforementioned procedure is illustrated in **Figure 5**. The proposed methodology was accomplished using a Matlab code. Full code can be provided upon request.

ACKNOWLEDGEMENTS

I wish to acknowledge the help provided by the members of the Robotics and Automation Laboratory of National and Kapodistrian University of Athens for their helpful comments regarding the MATLAB code, as well as my biology teacher Ioannis Grivas for his motivation.

This scientific paper was written within the framework of Middle Years Programme (MYP) of the Hellenic American Educational Foundation (HAEF), as a 10th Grade Personal Project.

REFERENCES

1. Peabody, John W., and Mario M. Taguiwalo. “Improving the Quality of Care in Developing Countries: Disease Control Priorities in Developing Countries.” Oxford University Press, 2006.
2. Economou C, Kaitelidou D, Karanikolos M, Maresso A. “Greece: Health System Review.” Health Syst Transit., vol. 19, no. 5, 2017.
3. Balgopal, Meena M. and Bondy, Cindi. “Antigenic Shift and Drift” Science teacher (Normal, Ill.), Jan. 2011, doi: 10.1038/283524b0
4. Clayville, Lisa R. “Influenza update: a review of currently available vaccines.” P & T : a peer-reviewed journal for

formulary management, vol. 36, no. 10, 2011.
5. Mao, Liang, et al. "Annual Economic Impacts of Seasonal Influenza on US Counties: Spatial Heterogeneity and Patterns." International Journal of Health Geographics, vol. 11, no. 1, 2012, doi:10.1186/1476-072x-11-16.
6. Kermack, WO and McKendrick, AG. "A contribution to the mathematical theory of epidemic." Proceeding of the Royal Society of London, Mathematical and Physical Sciences, vol. 115, 1927.
7. Merler, S, Ajelli, M, Pugliese, A, and Ferguson, NM. "Determinants of the spatiotemporal dynamics of the 2009 H1N1 pandemic in Europe: implications for real-time modelling." PLoS Comput Biol, 2011.
8. Biggerstaff, Matthew, et al. "Estimates of the Reproduction Number for Seasonal, Pandemic, and Zoonotic Influenza: a Systematic Review of the Literature." BMC Infectious Diseases, vol. 14, no. 1, 2014, doi:10.1186/1471-2334-14-480.
9. Liu, Lei. "The spread model of H1N1 influenza." Journal of Gansu Sciences, vol. 22, 2010.
10. Anderson, RM. ed. "Population Dynamics of Infectious Diseases." Chapman and Hall, London, 1982.
11. Hethcote, Herbert W. "The Mathematics of Infectious Diseases." SIAM Review, vol. 42, no. 4, 2000.
12. Brauer, F and Castillo-Chávez, C. "Mathematical Models in Population Biology and Epidemiology." Springer, 2012.
13. Bailey, NTJ. "The Mathematical Theory of Infectious Diseases." Grin, London, 1975.
14. Li, Gui-Hua, and Yong-Xin, Zhang. "Dynamic Behaviors of a Modified SIR Model in Epidemic Diseases Using Nonlinear Incidence and Recovery Rates." Plos One, vol. 12, no. 4, 2017.
15. Zhang, Xiang, HE, Yilin, Yang, Haiyu. "A retrospective evaluation of protective effect of seasonal influenza vaccine and influenza A(H1N1) vaccine." Chinese Journal Disease Control Prevention, vol. 16, 2012.
16. Allen, LJS. "Some discrete-time SI, SIR, and SIS epidemic models." Mathematical Biosciences, Elsevier, vol. 124, Issue 1, 1994.
17. National Public Health Organization, Weekly Report Epidemiological Surveillance of Influenza Week 8/2020 (17–23 February 2020)
18. Bohlin, Torsten P. "Practical Grey-box Process Identification: Theory and Applications." Springer Science & Business Media, 2006.
19. Chaturvedi, Ojaswita. "MATLAB - A Successful Tool for Epidemic Modelling Simulation." International Journal for Research in Applied Science and Engineering Technology, vol. 5, no. 8, 2017.

Article submitted: March 26, 2020
Article accepted: August 26, 2020
Article published: November 18, 2020

JOURNAL OF
EMERGING INVESTIGATORS

Article

The impact of effective density and compressive strength on the structure of crumpled paper balls

Hayley Chu, Rodolfo Fieller
Yew Chung International School of Shanghai Century Park, Shanghai, China

SUMMARY

Crumpling is the process whereby a sheet of paper undergoes deformation to yield a three-dimensional structure comprising a random network of ridges and facets with variable density. A regular sheet of paper can be easily teared and is very flimsy, yet when a sheet of paper is crumpled into a ball, the crumpled paper becomes much sturdier and has a large compressive strength, which is a material's maximum compressive load divided by its cross-sectional area. Scientists have extensively studied this phenomenon due to its peculiar structure; however, the physics behind paper crumpling is not yet completely understood. In this study, we investigated the structure of crumpled paper in two ways. In the first part, we explored the effective density of crumpled paper balls and hypothesized the diameter cubed of a paper ball crumpled from a square paper sheet is directly proportional to the side length squared of the paper sheet. In the second part, we studied the relationship between the number of times an A4 piece of paper is crumpled and its compressive strength. We hypothesized that the more times a paper sheet is crumpled, the greater its compressive strength. Our results supported both of our hypotheses: The first experiment demonstrated there is a directly proportional relationship between the diameter cubed of the ball and the side length squared of the sheet. We discovered in the second experiment that there was a relatively strong linear relationship between the number of times a paper sheet is crumpled and its compressive strength.

INTRODUCTION

When one crushes a sheet of paper and throws it into the bin, perhaps out of frustration, they may not realize the strange phenomenon that results from this seemingly mundane action. Crumpling is the process whereby a sheet of paper undergoes deformation to yield a three-dimensional structure comprising a random network of ridges and facets with variable density (1). A regular sheet of paper can be easily torn and is very flimsy, yet when a sheet of paper is crumpled into a ball, the crumpled paper becomes much sturdier and has a large compressive strength, which is a material's maximum compressive load divided by its cross-sectional area. A crumpled paper ball is estimated to contain around 75-90% air and cannot easily be compacted further (2).

The phenomenon whereby a sheet of paper becomes much stronger after being crumpled has been studied extensively by scientists due to its peculiar structure. Some have used methods ranging from "kvetching" (3), which refers to crushing material in a cylindrical container, to X-ray microtomography, an imaging technique that assembles three-dimensional images from thousands of two-dimensional, cross-section snapshots (4). However, the physics behind paper crumpling is not yet completely understood by scientists. Thus, this study aims to explore why crumpled paper has such a complicated and strong structure.

Bansal, Chowdhry, and Gyaneshwaran (5) studied the relationship between the side length of square sheets of paper that were crumpled into paper balls and the diameter of the crumpled balls, thereby calculating the effective density of the crumpled paper balls. Our first investigation attempted to replicate their experiment.

We have yet to come across a paper investigating the relationship between the number of times a piece of paper is crumpled and its compressive strength. We investigated this relationship by first crumpling an A4 sheet of paper a different number of times then applying compression force by hand to see how much compressive load is needed to cause significant deformation due to crushing.

Crumpled sheets are made of four main structures, which include the bend, the fold, the developable cone (d-cone) and the stretching ridge (**Figure 1**). Bending occurs when the two ends of a sheet of paper are placed on top of another so there is a bend in the middle. When force is applied to the bend, the paper will be folded, creating a fold. When stretching is

The four main structures of crumpled sheets

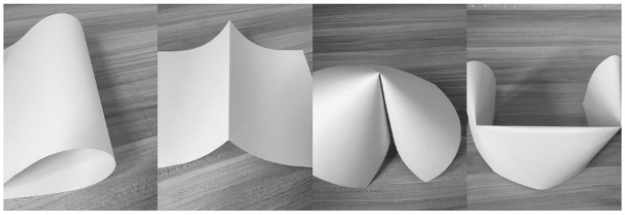

Figure 1. From left to right: the bend, the fold, the d-cone and the stretching ridge.

concentrated at one point and the rest of the sheet is bending in a cone-like shape, the vertex of the sheet is called a d-cone (6). When two d-cones are created in a sheet, stretching will occur between the d-cones and form a stretching ridge. Croll *et al*. discovered through laser scanning confocal microscopy of hand-crumpled paper that energy stored in a ridge is thought to be stored mostly along the ridge peak, seen from the two corners of the stretching ridge at the rightmost frame from **Figure 1** (2). They also concluded that, in the stretched ridges, the d-cones are fixed. While compression attempts to push them together, the d-cones cannot move and only bending occurs in the structure before the ridge buckles. This shows that the ridges deliver energy into the available soft modes (bending), which progressively stiffen until the ridge structure collapses. Stretching ridges have a high buckling strength, which measures how much force a material can withstand before buckling (2). Therefore, bending in the stretching ridge is responsible for the strength of both elastic and plastic crumples. Thus, we hypothesized that the more times a paper sheet is crumpled, the greater its compressive strength.

The first experiment showed the effective density remained almost constant and there is a directly proportional relationship between the diameter cubed of the ball and the side length squared of the sheet. We discovered in the second experiment that there was a relatively strong linear relationship between the number of times a paper sheet is crumpled and its compressive strength.

RESULTS

In order to investigate the relationship between the side length of a square paper sheet and the diameter of the crumpled paper ball for the first experiment, paper sheets of varying side lengths were crumpled into balls, the diameters were measured for each ball. This was repeated twice for each side length for a total of three trials (**Table 1**). For example, the diameter of the paper ball from the sheet of 5 cm side length was measured to be 1.05 cm in Trial 1 and the diameter cubed was 1.16 cm^3.

The standard dimensions of A4 paper are 21 cm x 29.7 cm x 0.01 cm, and the standard mass is 4.50 g. Thus, the measured density for an A4 sheet of paper is:

$$\rho_p = \frac{mass}{volume} = \frac{4.5\ g}{21\ cm \times 29.7\ cm \times 0.01\ cm} = 0.72\ g/cm^3 \quad (6)$$

The effective density for the paper with a side length of 5 cm was calculated to be:

$$\rho_e = \frac{6\rho_p l^2 t}{\pi d^3} = 0.30 \pm 0.03\ g/cm^3 \quad (7)$$

The average effective density for the paper of all side lengths (on the very right column) for all three trials was then calculated to be 0.24±0.03 g/cm^3. This value is significant as it remains mostly constant for all side lengths and determines the diameter cubed of each crumpled paper ball for each side length squared of the square sheet.

The margin of error for side length shown in **Table 1** was derived from the systematic error from the ruler, which was half of the measuring unit. As the measuring unit was 0.1 cm, the margin of error was ±0.05 cm. The margin of error for the side length squared was calculated by multiplying the margin of error of the side lengths by two to give ±0.01 cm^2. The margin of error for the diameter was derived from the systematic error from the Vernier caliper, with the measuring unit of 0.01 cm, thus giving the margin of error of ±0.005 cm. For the diameter cubed, the margin of error was the margin of error of the diameter multipled by three, which was ±0.015 cm^3.

For the first experiment, we used a one-way ANOVA to test the statistical significance of the diameter and effective density values and found the p-value is equal to 0.0001. Thus, the ANOVA test result supports our alternate hypothesis that the diameter cubed of the crumpled paper ball is directly proportional to the side length squared of the paper sheet.

Since the effective density remains almost constant, the hypothesis that the diameter cubed of the crumpled paper ball is directly proportional to the side length squared of the

Table 1. Raw quantitative data for the effective density experiment, including the average diameter³ and effective density values.

Side length (cm) ΔL = ±0.05 cm	Side length² (cm^2) ΔL^2 = ±0.1 cm^2	Avg. Diameter (cm) ΔD = ±0.005 cm	Avg. Diameter³ (cm^3) ΔD^3 = ±0.015 cm^3	Avg. Effective density (g/cm^3)
5	25	1.05	1.16	0.2971
8	64	1.42	2.84	0.3097
10	100	1.73	5.21	0.2642
12	144	2.02	8.20	0.2416
15	225	2.35	12.98	0.2385
17	289	2.80	21.95	0.1811
20	400	3.20	32.77	0.1679

paper sheet is supported.

In order to investigate the relationship between the number of times a sheet of paper was crumpled and the crumpled ball's compressive strength in the second experiment, we placed the crumpled A4 paper on the force platform and compressed it until it became crushed, and the reading on the datalogger was equal to the compressive load value.

The data was processed by first calculating the area of the A4 paper, which is 210 mm × 297 mm = 62370 mm^2. This measurement was kept constant because the crumples formed irregular shapes from which a diameter could not be determined, and thus the cross-sectional area could not be calculated. The compressive strength was found by dividing each compressive load by the area, which for the paper crumpled 2 times was:

$$Compressive\ strength = \frac{compressive\ load}{surface\ area} = \frac{36.77\ N}{62370\ m^2} = 0.00058955\ MPa = 589.55\ N/m^2 \quad (8)$$

The same process was repeated for the different crumple numbers and an additional two replicates to give three total trials (**Table 2**). The margin of error for compressive load shown in **Table 2** was derived from the systematic error from the force platform, which was half of the measuring unit. As the measuring unit was 0.01 N, the margin of error was ±0.005 N.

For the second experiment, we also used a one-way ANOVA test to test the statistical significance of the compressive load values and found the p-value is equal to 2.33E-10, significantly below the significance threshold. Thus, the ANOVA test result provided evidence disproving the null hypothesis that there is no different in a paper sheet's compressive strength when the number of times the paper is crumpled is varied. It supported the alternate hypothesis that the more times a paper sheet is crumpled, the greater its compressive strength.

Since the greater the number of times the paper was crumpled indicated a greater compressive load and compressive strength, the hypothesis that there is a directly proportional relationship was supported.

Table 2. Raw quantitative data for the compressive strength experiment, including the average compressive load and compressive strength values.

No. of times crumpled	Average Compressive load (N) ΔF = ±0.005 N	Average Compressive strength (Pa) ΔCS = ±0.005 Pa
2	36.77	589.55
3	50.84	815.19
4	99.36	1593.07
5	126.67	2030.94
6	142.52	2285.07
7	196.12	3144.46
8	266.62	4274.76
9	290.73	4661.32

DISCUSSION

Our results from the first experiment demonstrate that the effective density of the crumpled paper balls is three times less than the measured density of the paper sheet. This supports the idea that crumpled paper is mostly made up of air (2). While the diameter cubed of the paper ball varies with the side length squared of the paper sheet (**Figure 2**), the effective density decreases somewhat as the side length increases. A reason for this could be that the larger the piece of paper, the harder it is to crumple and ensure that the maximum force is being applied by hand. This would result in a larger than proportional crumpled ball and a larger volume and therefore a lower effective density.

Rearranging equation (2) from the Materials and methods section and using the slope of the trendline (which is the average thickness of the paper), the thickness can be calculated by:

$$t = \frac{\rho_e \pi d^3}{6\rho_p l^2} = \frac{\rho_e}{\rho_p} \times \frac{\Delta d^3}{\Delta l^2} \times \frac{\pi}{6} = \frac{1}{3} \times 0.0849 \times \frac{\pi}{6} = 0.015 \pm 0.030\ cm \quad (9)$$

This is quite close to the standard thickness of A4 paper, 0.01 cm, thus supporting the hypothesis as it means that equations (1) and (2) hold true, demonstrating the relationship between side length squared and diameter cubed. One reason the calculated value for thickness is a little larger than the standard thickness could be due to the fact that the 0.3097 g/cm^3 value for the average effective density when the side length is 8 cm is an outlier. Since the diameter cubed is inversely proportional to the effective density, the value for the diameter cubed at this side length may have been smaller in actuality, making the trendline slope larger due to an artificially high value. However, a Thompson-Tau test revealed that there are no outliers in this experiment, though the 289 cm^2 and 400 cm^2 values of 0.1811 g/cm^3 and 0.1679 g/cm^3 respectively are close to being outliers. If this experiment were repeated, we could measure whether the

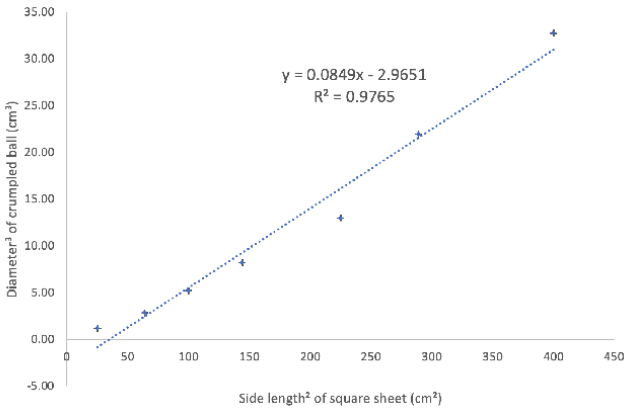

Figure 2. The graph of diameter^3 against side length^2. Statistical analysis performed by one-way ANOVA, p = 0.0001. As the errors were negligible, the error bars were not plotted.

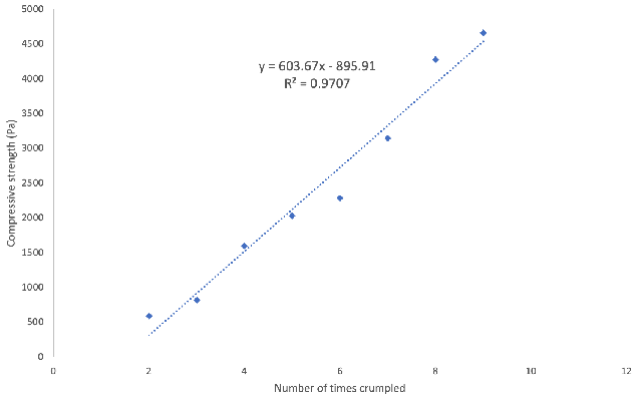

Figure 3. The graph of compressive strength against the number of times crumpled. Statistical analysis performed by one-way ANOVA, p = 2.32973E-10. As the errors were negligible, the error bars were not plotted.

Vernier calliper is applying any unwanted force to the paper ball during diameter measurements. Moreover, more side lengths could be tested to ensure that the relationship holds for large sized crumpled paper balls. Another reason for this outlier could be that the crumpling process was conducted entirely by hand, meaning that it was very hard to keep the compacting force constant for all the paper balls. For example, it may have been much easier to crumple a smaller piece of paper than a large one, as a larger one would trap more air in its crumpled form. This would mean the crumpled paper ball made from the 5 cm paper sheet was artificially denser than the ball made from the 20 cm paper sheet due to disparities in force application. To integrate our investigations of effective density and compressive strength, we could compare compressive strength for paper sheets of different side lengths to determine whether a higher or lower density of a paper ball leads to a higher compressive strength value.

In the second experiment, there is a relatively strong linear relationship between the number of times the paper was crumpled and its compressive strength (**Figure 3**). By the time the paper was folded eight times, it was almost completely crumpled into a uniform ball, so the increase in compressive strength between the paper folded eight times and the paper folded nine times was not as significant. Nonetheless, the differences in compressive strength between the paper folded four, five and six times are of similar magnitude. This positive correlation also supports the hypothesis that the more crumples there are in a piece of paper, the greater its compressive strength. Our results have interesting implications, as this means that there is a difference in structural strength between a partially crumpled piece of paper and a completely crumpled paper ball. The more crumples the paper has, the harder it is to compress due to the fact that it contains a large amount of air (2).

As mentioned in the Results section, the cross-sectional area of the partially crumpled paper balls could not be calculated because the crumples formed irregular shapes. The surface area measurement for the uncrumpled paper sheet was used instead. This is a significant limitation, as we assumed in this experiment that the area remained constant when it may not necessarily be the case. Unless a new way of crumpling paper into perfect spheres is discovered, there is no easy solution to minimise the error in the area calculations.

Since a mechanical compressor was not used in this experiment, the air remained trapped inside the paper structure and prevented the paper from becoming deformed easily. If we had used a mechanical compressor, we could expect the force applied to be constant regardless of crumple number. Another reason for fully crumpled paper's unusual compressive strength is the stacks or folds in the paper created from the crumpling process providing strength to the structure in all angles. As these multiple folded layers come together, they act as structural pillars. Since they are aligned in many different, random directions and are isotropically arranged (7), they strengthen the crumpled ball in every direction. Thus, no matter which angle one presses down on the crumpled ball, he or she is pressing down against these columns, which resist being crushed in all directions. In future experiments, we could study how the compressive strength may depend on the shape of the paper balls since different shapes, especially when the paper is only partially crumpled, trap different amounts of air, which could affect how resistant it is to compression.

In automobiles, crumple zones are areas, usually in the front or back, that are designed to deform in a collision to ensure passenger safety (8). The aim of crumple zones is to absorb as much kinetic energy as possible by reducing the initial force of the crash and redistributing the force before it reaches the vehicle's occupants. Newton's second law, $F = ma$, shows that the greater the acceleration, the greater the force. Thus, as crumple zones absorb energy to decrease acceleration by adding time to the crash, the impact experienced by the occupant will decrease. Many may believe that the stronger the materials used to make cars, the safer the vehicle. However, this isn't true as the force from a collision would immediately be felt by the occupant. Less stiff plastics and polymer fibres are often used to manufacture crumple zones as these result in the maximum crushing, ensuring the occupant is protected in the car (9). This again shows that the lower the flexural rigidity of a material, the more likely it is to become crumpled, and in this case, ensure automobile safety. Thus, a potential future area of study would be to examine whether the crumpling properties of plastics and polymer fibres are similar to those of paper and if there could be applications of how they crumple on how to best design crumple zones to maximise safety in the case of a crash.

MATERIALS AND METHODS

In the first experiment, identical sheets of A4 paper were cut into square pieces with different side lengths (10).

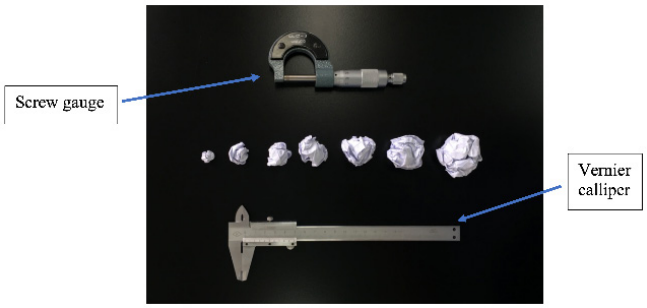

Figure 4. The different sized crumpled paper balls and apparatus set-up. The Vernier caliper and screw gauge were used to measure the diameter of the crumpled paper balls.

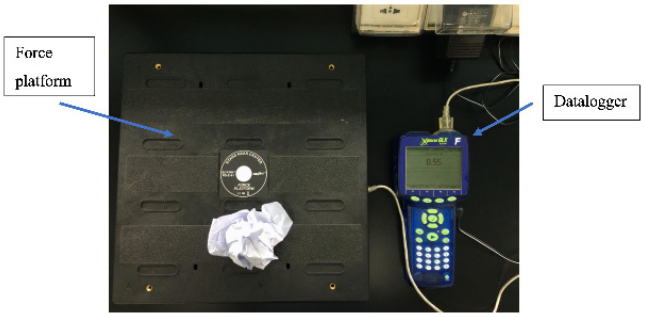

Figure 5. The paper ball on the PASCO PASPORT Force Platform and apparatus set-up, including the Xplorer GLX datalogger which was used to record the data from the force platform.

The sheets were then crumpled by hand to form the shape of a ball. These were crumpled once completely, with the maximum amount of force that could be applied by hand. We used a Vernier calliper and a screw gauge to measure the diameter of the paper balls (**Figure 4**). The variables for the first experiment are: (independent) the side length squared of the paper sheets, (dependent) the diameter cubed of the crumpled paper balls, (controlled) the compression force applied by hand and the material of the paper.

We began by equating the mass of a paper sheet to the mass of the crumpled paper balls:

$$\rho_p l^2 t = \rho_e \frac{4\pi r^3}{3} \text{ or } \rho_p l^2 t = \rho_e \frac{\pi d^3}{6} \quad (1)$$

where ρ_p is the measured density of the paper sheet, l is the side length of the square sheet of paper, t is the thickness of the paper, ρ_e is the effective density of the paper ball and d is the diameter of the paper ball. Rearranging, we have:

$$d^3 = \frac{\rho_p 6 t l^2}{\rho_e \pi} \quad (2)$$

Since $d^3 \propto l^2$, we hypothesized that the diameter cubed of the crumpled paper ball is directly proportional to the side length squared of the paper sheet. On the other hand, the null hypothesis is that there is no difference in diameter cubed of the paper ball when the side length squared of the paper sheet is varied.

In the second experiment, one crumple was defined as one squeeze of the paper with two hands. Since it was hard to get definite crumpling with just one crumple (the paper tended to fold itself rather than crumple), the smallest value for the number of times crumpled was two, and the greatest value was nine. By nine crumples, the paper was completely crumpled into a ball. We first crumpled the A4 paper two times then placed it on the PASCO PASPORT Force Platform, which was connected to the Xplorer GLX datalogger (**Figure 5**). The crumpled paper structure was compressed until it deformed (i.e., it became crushed). The data output was compressive load. This process was repeated for the number of paper crumples from three to nine crumples two times to give three trials. The variables for the second experiment are: (independent) the number of times the A4 paper is crumpled by hand, (dependent) the compressive strength of the crumpled paper balls, (controlled) the type and size of the A4 paper and the force applied per crumple.

The one-way ANOVA tests were conducted using the StatPlus computer application for both experiments, and the significant threshold we used was $p < 0.05$. The equations used were:

$$F = \frac{MST}{MSE} \quad (3)$$

$$MST = \frac{\sum_{i=1}^{k} \left(\frac{T_i^2}{n_i}\right) - \frac{G^2}{n}}{k-1} \quad (4)$$

$$MSE = \frac{\sum_{i=1}^{k} \sum_{i=1}^{k} Y_{ij}^2 - \sum_{i=1}^{k} \left(\frac{T_i^2}{n_i}\right)}{n-k} \quad (5)$$

where F is the variance ratio for the test, MST is the mean square due to treatments between groups, MSE is the mean square due to error within groups, Y_{ij} is an observation, T_i is a group total, G is the grand total of all observations, n_i is the number in group i and n is the total number of observations.

Received: June 16, 2020
Accepted: November 16, 2020
Published: December 2, 2020

REFERENCES

1. Hanaor, D., *et al*. "Mechanical properties in crumple-formed paper derived materials subjected to compression." *Heliyon*, vol. 3, no. 6, June 2017, doi:10.1016/j/heliyon.2017.e00329.
2. Croll, Andrew B., *et al*. "The compressive strength of crumpled matter." *Nature Communications*, vol. 10, 3 Apr. 2019, doi:10.1038/s41467-019-09546-7.
3. Roberts, Siobhan. "How scientists are using crumpled paper to better understand DNA." *Independent*, 12

Dec. 2018, www.independent.co.uk/news/science/dna-physics-crumpling-paper-science-solar-sail-satellite-how-what-history-a8666526.
4. Keim, Brandon. "The cutting-edge physics of a crumpled paper ball." *Wired*, 22 Aug. 2011, www.wired.com/2011/08/crumpled-paper-physics.
5. Bansal, Tarush, *et al*. "Effective density of crumpled paper balls." *Journal of Basic and Applied Engineering Research*, vol. 5, no. 2, 2018, pp. 123-125.
6. Cambou, Anne D. *On the crumpling of thin sheets.* Diss. UMass Amherst, 2014. Web. 13 June 2020.
7. Cambou, Anne D., and Narayanan Menon. "Three-dimensional structure of a sheet crumpled into a ball." *Proceedings of the National Academy of Sciences of the United States of America*, vol. 108, no. 36, 6 Sept. 2011, pp. 14741-14745, doi:10.1073/pnas.1019192108.
8. Grabianowski, Ed. "How Crumple Zones Work." HowStuffWorks, 11 Aug. 2008, auto.howstuffworks.com/car-driving-safety/safety-regulatory-devices/crumple-zone.htm.
9. *Crumple Zone Physics - How Plastics in Cars Can Save Lives*. Automotive Plastics, 29 Aug. 2019, www.automotiveplastics.com/blog/physics-in-the-crumple-zone-demonstrate-how-less-stiff-materials-like-plastic-can-help-prevent-injury-and-save-lives/.
10. Tallinen, T., *et al*. "The effect of plasticity in crumpling of thin sheets." *Nature Materials*, vol. 8, Jan. 2009, pp. 25–29, doi:10.1038/nmat2343.

JOURNAL OF
EMERGING INVESTIGATORS

Article

The Impact of the Covid-19 Pandemic on Mental Health of Teens

Afaf Saqib Qureshi[1], Shamaila Fraz[2], Kiran Saqib[3]
[1]Roots Ivy International School, Islamabad, Pakistan
[2]McMaster University, Ontario, Canada
[3]University of Waterloo, Ontario, Canada

SUMMARY

The stress, fear, and uncertainty created by the COVID-19 pandemic can wear anyone down, but teens may have an especially tough time coping emotionally. In this study, we aim to highlight the impact of this pandemic on the mental health of teens, who account for almost 50% of the population in Pakistan. We conducted a descriptive cross-sectional study in Islamabad, Pakistan. Due to the COVID-19 lockdown in Pakistan, we collected data through a validated online questionnaire from the students at private schools enrolled only in Cambridge Assessment International Examination (CAIE) system. The study included a total of 289 students, comprised of 116 males and 173 females within the age range of 13–19 years. Our study showed that the prevalence of signs of mental illness was quite high amongst teenagers, with slightly higher prevalence in female respondents. These signs included feeling socially disconnected, frequent mood swings, constant worry, self-dissatisfaction, change in eating habits, and change in sleep cycle. Since there is evidence that significant burden of mental illnesses originates at a young age, we assert that close attention to mental health of young people in quarantine is warranted to avoid any long-term consequences.

INTRODUCTION

COVID-19, the novel coronavirus disease that was first detected in China in November 2019, has now spread to 206 countries. As of July 26, 2020, 16.1 million cases have been reported worldwide, with 650,148 confirmed fatalities (1). Public health emergencies, like the COVID-19 pandemic, take a toll both on physical and mental health. The restrictive measures during the COVID-19 pandemic undoubtedly have affected the social and mental health of individuals from across the board (2). A pandemic is not just a medical phenomenon; it affects individuals and society and causes mental stress and anxiety (3).

Stress, defined as emotional tension or mental strain, is all too common a feeling for most of us. Too much stress can produce both physical and emotional symptoms. The fear and uncertainty created by the COVID-19 pandemic can stress anyone down, but teens may have an especially tough time coping emotionally. Although the number of teenagers affected by COVID-19 is small, and most of the affected teens show only mild symptoms (4), the disease and the containment measures are likely to negatively impact their mental health and well-being (5).

As articulated by psychologist Erik Erikson, 'Identity vs Role Confusion' is the fifth of eight stages of psychosocial development that takes place between the ages of twelve and nineteen (6). An important event during this stage is developing social relationships. Teenagers and college students have amplified energy, novelty, motivation, curiosity, and enthusiasm that make them hard to isolate at home. The hormonal changes that come with puberty collude with adolescent social dynamics to make them highly attuned to social status, peer group, and relationships. Teens may feel frustrated, nervous, disconnected, nostalgic, and bored because of social distancing during this pandemic.

Feeling depressed, hopeless, anxious, or angry, having moods swings, loss of interest, a change in behavior, loss of appetite or overeating, a difficult time falling or staying asleep, or starting to sleep all the time during the COVID-19 pandemic may be signs which indicate that teens need more support during this difficult time (7). Moreover, exposure to mass media coverage of crisis events and unverified information circulating on social media may aggravate the mental distress. For teens, the coronavirus pandemic adds new pressure to their world (8). It is not only the fear and anxiety about the coronavirus disease but also unprecedented school closures, disrupted routines, separation from relatives and friends, worries regarding current world events, and adjusting to new ways of learning and working is hard (9). With schools closed for indefinite periods, exams cancelled or postponed, proposed grading system and executive orders calling for people to stay home, many students have found themselves struggling with mental health in ways they previously have not.

Throughout the world, the public is being informed about the physical effects of severe acute respiratory syndrome coronavirus 2 (SARS-CoV-2) infection and guidelines are provided regularly on how to prevent exposure to the coronavirus and to manage symptoms of COVID-19 if they appear. However, the effects of this pandemic on one's mental health have not been studied at length and are still unknown. Since most of the efforts are focused on understanding the epidemiology, clinical features, transmission patterns, and management of the COVID-19 outbreak, there has been very little concern expressed over the effects on one's mental health and on strategies to prevent stigmatization.

Data from the COVID-19 studies in Italy, Spain, and

Demographic Characteristics	Mean (SD) Or N (%)
Age	16.9 (1.61)
Gender	
Females	173 (59.8%)
Males	116 (40.2%)
Grades (O or A level)	
O level	100 (34%)
A level	189 (66%)
Family Structure	
Nuclear	202 (69.8%)
Joint	87 (30.1%)

Table 1. Demographic information of study participants. Data presented as mean (SD) or N (% of total).

China suggest significant emotional and behavioral changes during quarantine in children and adolescents (10). A review published in *The Lancet* mentioned that the separation from loved ones, loss of freedom, boredom, and uncertainty can cause a deterioration in an individual's mental health status (11). According to the American Psychological Association, a lack of social connection heightens health risks, creating an effect similar to smoking 15 cigarettes a day or having an alcohol use disorder (12).

Ignoring the immediate and long-term psychological effects of the COVID-19 pandemic would be disastrous, especially for children and young people, who account for almost 50% of population in Pakistan (13). The students had to acquaint themselves with a new approach to online classes and cancellation of multiple examinations, including Cambridge Assessment International Examination (CAIE). COVID-19 has not only affected their learning process but has also narrowed down their social interaction, forcing them to interact only through social media apps. This study aims to highlight the impact of this pandemic and associated lifestyle changes on teens mental health in Pakistan.

RESULTS

A total of 301 students consented to be part of this study and 289 participants who fulfilled the inclusion criteria were recruited. Total sample of 289 participants comprising 59.8% females and 40.2% males with mean age of 16.9 ± 1.61. Basic demographic characteristics of the study population were collected (**Table 1**).

Prevalence of signs of depression and anxiety

It was observed in our study that the prevalence of signs of mental illness was quite high amongst teenager with slightly higher prevalence in female respondents compared to males (**Table 2 & Figure 1)**. These signs include feeling socially disconnected, frequent mood swings, constant worry, self-dissatisfaction, change in eating habits, and change in sleep cycle. We noted that most commonly repeated sign was a change in eating habits with 255 (88.2%) participants reporting either loss of appetite or

Study variable	% Responses of study population (n)			
Gender	**Males = 40.2% (116)**		**Females = 59.8% (173)**	
	Yes	**No**	**Yes**	**No**
Little to no interest in doing activities/things	83.6% (97)	16.3% (19)	82.6% (143)	17.3% (30)
Feeling down, depressed/hopeless	72.4% (84)	27.5% (32)	83.2% (144)	16.7% (29)
Feeling disconnected	56.0% (65)	48.57% (51)	59.5% (103)	40.4% (70)
Frequent mood swings	80.1% (93)	19.8% (23)	85.5% (148)	14.4% (25)
Constant worry or feeling mentally overburdened	47.4% (55)	52.5% (61)	58.3% (101)	41.6% (72)
Feeling of self-dissatisfaction/self-depreciation	40.5% (47)	59.4% (69)	65.3% (113)	34.6% (60)
Change in sleep cycle	60.3% (70)	39.6% (46)	73.4% (127)	26.5% (46)
Change in eating habits	87.0% (101)	12.9% (15)	89.0% (154)	10.9% (19)
Feeling disturbed due to current issues on social media	47.4% (55)	52.5% (61)	61.2% (106)	38.7% (67)
Feasibility of online classes	15.5% (18)	84.4% (98)	21.3% (37)	78.6% (136)
Feeling disadvantaged by the grade policy for CAIE	67.2% (78)	32.7% (38)	59.5% (103)	40.4% (70)

Table 2. Gender-based distribution of key study variables and signs of mental illness. Data is expressed as percentages (n).

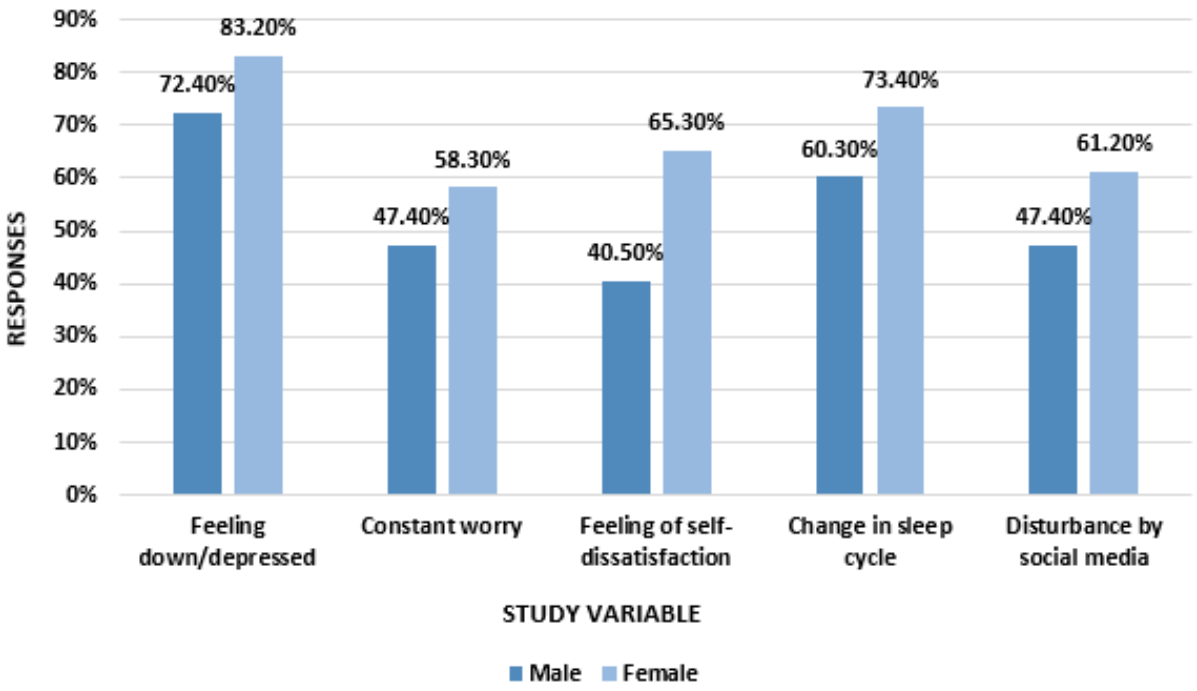

Figure 1. Gender-based distribution of signs of mental illness in study population

overeating. A total of 168 participants (58.1%) reported a feeling of disconnect, 241 (83.3%) reported mood swings, 158 (54.6%) were occupied by constant worry, 161 (55.7%) had a feeling of self-dissatisfaction, while 197 (68.1%) reported change in sleep cycle (insomnia, disturbed sleep or oversleeping) (**Figure 2**).

Out of the total sample, 240 participants, including 83.6% (97) males and 82.6% (143) females, reported "little or no interest in doing things," while 228 subjects, including 72.4% (84) males and 83.2% (144) females, reported "feeling down, hopeless or depressed" over the past two weeks (**Table 2**). Both of these responses are early warning signs of depression, according to Patient Health Questionnaire (PHQ-2 & PHQ-9) (15). Overall, 67 (28%) participants reported trouble falling asleep, 26 (11%) mild insomnia, 70 (29%) oversleeping, while 77 (32%) reported no change in sleep cycle (**Figure 3**).

Several other variables including disturbance due to news on social media, feeling disadvantaged by predicted grade policy by CAIE system, and feasibility of online classes were also recorded. 47.4% of (55) males and 61.2% (106) of females reported that they were disturbed by the news on social media. 84.4% (98) of males and 78.6% (136) of females expressed their dissatisfaction over the feasibility of online classes. A total of 67.2% (78) of males and 59.5% (103) of females expressed their concern over the predicted grade policy announced by CAIE.

DISCUSSION

The COVID-19 outbreak has been unexpected in most countries and has resulted in an increase in known risk factors for mental health problems. Mitigation strategies such as quarantine, although necessary to contain viral spread, have a negative psychological impact, such as causing post-traumatic stress symptoms, emotional disturbance, depression, and insomnia (14). Teen aged individuals are especially sensitive to the negative impacts of the uncertainty, lockdown, physical distancing, inactivity, increased access to food, and false information online caused by the COVID-19 pandemic.

A commonly used screening tool for depression, the PHQ-2, lists feelings of "little or no interest" and "down or depressed" as preliminary signs of depression (15). Notably, our study found that more than 80% of participants experienced these feelings. The purpose of the PHQ-2 is not to establish a final diagnosis or to monitor depression severity but rather to screen for depression as a "first step" approach. Teen depression is associated with subsequent adult depression and other psychiatric illnesses. Depressed teens are more likely to have significant coexisting emotional and behavioral problems, such as anxiety, post traumatic stress disorder (PTSD), hyperactivity, drug use, and aggressive behavior (16). In some studies, teens reporting probable depression showed diminished productivity and lower educational attainment, compared with nondepressed peers (16).

The prevalence of signs of mental illness was also found to be quite high in our study. This result complies with other studies showing that being female, a younger age, or a student put individuals at higher risk for increased anxiety and depression symptoms (17). Pakistan, like many other countries, has emphasized the practice of social

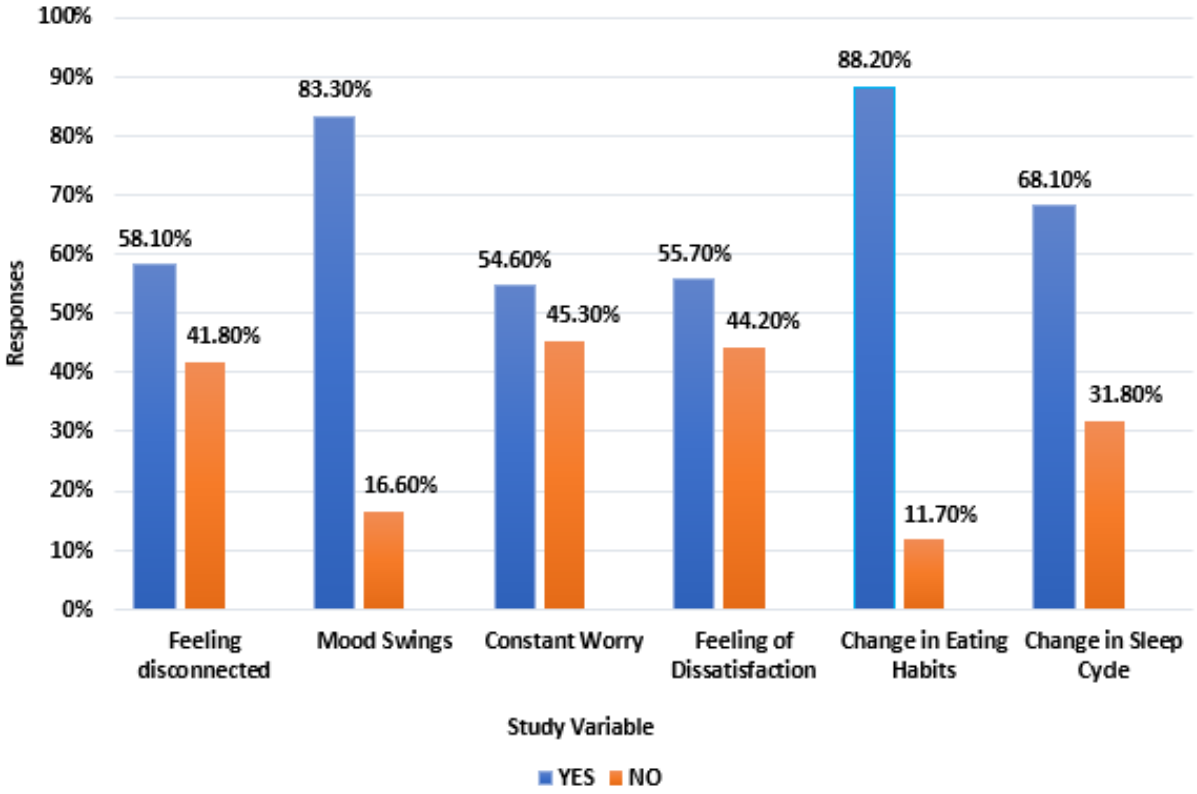

Figure 2. Signs of mental illness in study population

distancing in order to combat the spread of COVID-19. Educational institutions have been closed and exams have been postponed. The rise in the number of infected cases and deaths, the disruption of daily routines, the home confinement, fear of infection, social distancing from peers and friends, and lack of access to educational resources have created a feeling of uncertainty and anxiety among children and adolescents (13). The situation is further deteriorated by the news and online information available on social media, and the uncertainty about exams and grading policies in CAIE. It is suggested by some studies that repeated media exposure to public health crises, including infectious diseases, can cause heightened psychological distress (18,19).

Studies found elevated levels of anxiety, distress, and depression among quarantined individuals (20). There is evidence that children and young individuals subjected to quarantine in pandemic disasters have a higher likelihood of developing acute stress disorder, adjustment disorder, and grief, and reported four times higher scores of PTSD compared to those who were not quarantined (21). None of the studies on children looked at duration of quarantine and its association with psychological impact, but literature suggests higher PTSD symptoms in those quarantined for longer duration, specifically for more than ten days (22). Given the fact that Short-lived infectious outbreaks like SARS in 2002 were associated with a high prevalence of PTSD. Therefore, it is likely that young populations will experience long lasting distress and trauma due to the larger scale and prolonged nature of the COVID-19 pandemic.

The COVID-19 pandemic has forced the whole world to question whether we are prepared for such pandemics. Even developed nations, despite having enough resources to tackle such pandemic situations, may have to think manifolds but especially when it comes to preparing for the physical and emotional security of young adults and teens (23). As there is evidence that significant burden of mental illnesses originate at a young age, and adult life productivity is also deeply rooted in early years, close attention to the mental health of young people in quarantine is warranted to avoid any long-term consequences (24).

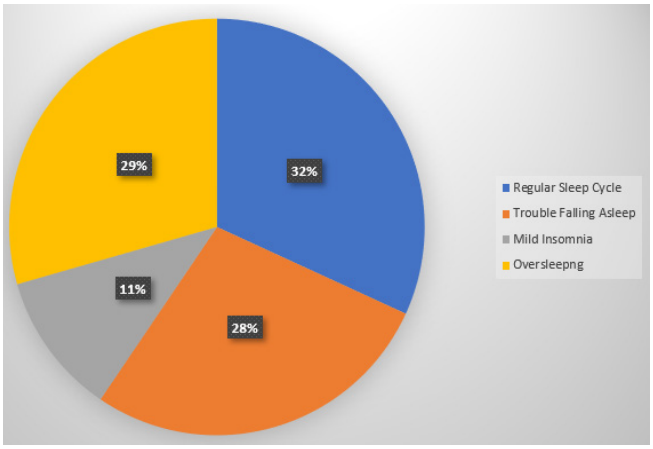

Figure 3. Changes in sleep cycle within study population.

To overcome this, measures at the individual and societal levels are required. The present situation requires raising awareness in public, which can be helpful to deal with this calamity (25). Many questions remain about how to mitigate the mental health effects of the COVID-19 pandemic. Community monitoring and mental health screening could be implemented in selected groups, or digital health could be used to switch from individual-based approaches to population-wide screening (26).A more immediate alternative would be to integrate psychiatric screening into primary care, using validated instruments, such as the Patient Health Questionnaire depression scale (PHQ-9) and the Generalized Anxiety Disorder scale (GAD-7), to identify initial symptoms of depression and anxiety and to enable early, targeted intervention.

Researchers specializing in psychology, psychiatry, behavioral and social science, and digital health, as well as healthcare providers, policymakers, and other stakeholders, must work together toward innovative and practical technologies to address the mental-health needs under the current pandemic condition. As the crisis caused by the COVID-19 pandemic shifts from acute to protracted, we must pay attention to the potentially devastating effects on population-wide mental health and emotional and social well-being. There will be no easy solution, but high-quality research, coupled with recent innovations in digital health, could enable health services to offer proactive and tailored mental health care for those in need (27). Public awareness campaigns focusing on the maintenance of mental health in the prevailing situation are urgently needed.

To the best of our knowledge, this is the first study to evaluate the depression and anxiety of teens in Pakistan during the COVID-19 pandemic. There is a remarkable dearth of data on the impact of the pandemic on the mental health of young individuals. The present study was a large internet-based cohort study with certain limitations as no previous data on mental health of participants was available. Therefore, it was difficult to predict whether these symptoms were present prior to the pandemic or developed as a result of mitigation strategies and changes in lifestyle due to COVID-19. Moreover, as inferential statistical tests were not conducted due to certain data limitations, the results cannot be generalized to all individuals as most of the sample was aged 13–19, and participants were enrolled in CAIE system only. We elected to conduct an anonymous survey to ensure maximum disclosure by study participants. This approach prevented us from conducting follow up studies with the same sample or to track individuals at a high risk for anxiety and depression.

METHODS

A descriptive cross-sectional study was conducted in Islamabad, Pakistan. Due to COVID-19 lockdown in the country, data was collected through a validated online questionnaire from the students at private schools enrolled only in CAIE (Cambridge Assessment International Examination) system. All participants were informed about the objectives of the study and were recruited after informed consent, which was prompted before the questionnaire. The questionnaire comprised of items adopted from Patient Health Questionnaires (PHQ-2 & PHQ-9), which are screening tools for depression based on DSM-IV criteria (15). All participants who gave informed consent were enrolled. Initially, five questionnaires were administered to ensure validity and few minor changes in text were done for better understanding of the context.

The questionnaire was posted online through Facebook and Instagram accounts. Nonprobability convenience sampling method was used. Only students aged 13–19 years and enrolled in O and A levels (International General Certificate of Education) were included. Data was collected over a period of one month from the 20th of May to the 20th of June, 2020. A total of 289 students comprising116 males and 173 females within the age range from 13–19 years were included in the study. We elected to conduct an anonymous survey to ensure maximum disclosure by study participants. This approach prevented us from conducting follow up studies with the same sample or to track individuals at a high risk for anxiety and depression. The confidentiality of all information was ensured. To calculate percentages, means and standard deviation STATA 12 was used.

ACKNOWLEDGEMENTS

I would like to thank Kulsoom Nawab and Salma Nadeem for their support of this research. Thank you for introducing me to the basic research, for your continuous support and guidance in my project and for keeping me motivated throughout the writing and editing of this article.

REFERENCES

1. Worldometer."Coronavirus Cases." *Worldometer*, 2020, pp. 1–22, doi:10.1101/2020.01.23.20018549V2
2. Sanchez Nicolas, Elena. "WHO Warning on Lockdown Mental Health." *EU Observer*, 2020, https://euobserver.com/coronavirus/147903.
3. Javed, Bilal, *et al*. "The Coronavirus (COVID-19) Pandemic's Impact on Mental Health." *The International Journal of Health Planning and Management*, NLM (Medline), June 2020, doi:10.1002/hpm.3008.
4. Qiu, Haiyan, *et al*. "Clinical and Epidemiological Features of 36 Children with Coronavirus Disease 2019 (COVID-19) in Zhejiang, China: An Observational Cohort Study." *The Lancet Infectious Diseases*, vol. 20, no. 6, June 2020, pp. 689–96, doi:10.10 16/S1473-3099(20)30198-5.
5. Dalton, Louise, *et al*. *Protecting the Psychological Health of Children through Effective Communication about COVID-19*. 2020, doi:10.1016/S2352-4642(20)30041-9.
6. Davis, D, Clifton, A. "Erikson's Stages." *Psychological Theory:Erikson*, http://ww3.haverford.edu/psychology/

ddavis/p109g/erikson.stages.html. Accessed 26 July 2020.
7. *Mental Health During COVID-19: Signs Your Teen May Need More Support - HealthyChildren.Org*. https://www.healthychildren.org/English/health-issues/conditions/COVID-19/Pages/Signs-your-Teen-May-Need-More-Support.aspx. Accessed 24 July 2020.
8. *Is COVID-19 Affecting Your Teen's Mental Health? – Health Essentials from Cleveland Clinic*. https://health.clevelandclinic.org/is-covid-19-affecting-your-teens-mental-health/. Accessed 24 July 2020.
9. *COVID-19 and Youth Mental Health | Voices of Youth*. https://www.voicesofyouth.org/campaign/covid-19-and-youth-mental-health. Accessed 24 July 2020.
10. Orgiles, Mireia, *et al*. "Immediate Psychological Effects of COVID-19 Quarantine in Youth from Italy and Spain." *SSRN Electronic Journal*, Apr. 2020, doi:10.2139/ssrn.3588552.
11. Yao, Hao, *et al*. "Patients with Mental Health Disorders in the COVID-19 Epidemic." *The Lancet Psychiatry*, vol. 7, no. 4, 1 Apr. 2020, p. e21, doi:10.1016/S2215-0366(20)30090-0.
12. *"Uncertainty and Loss": The Impact of COVID-19 on Student Mental Health - The State News*. https://statenews.com/article/2020/04/uncertainty-and-loss-the-impact-of-covid-19-on-student-mental-health?ct=content_open&cv=cbox_latest. Accessed 27 July 2020.
13. Imran, Nazish, Muhammad Zeshan, *et al*. "Mental Health Considerations for Children & Adolescents in COVID-19 Pandemic." *Pakistan Journal of Medical Sciences*, vol. 36, no. COVID19-S4, Pakistan Journal of Medical Sciences, May 2020, doi:10.12669/pjms.36.covid19-s4.2759.
14. Adhanom Ghebreyesus, Tedros. "Addressing Mental Health Needs: An Integral Part of COVID-19 Response." *World Psychiatry*, vol. 19, no. 2, 1 June 2020, pp. 129–30, doi:10.1002/wps.20768.
15. *Patient Health Questionnaire-2 (PHQ-2) - Mental Disorders Screening - National HIV Curriculum*. https://www.hiv.uw.edu/page/mental-health-screening/phq-2. Accessed 16 Aug. 2020.
16. Jaycox, Lisa H., *et al*. "Impact of Teen Depression on Academic, Social, and Physical Functioning." *Pediatrics*, vol. 124, no. 4, , Oct. 2009, pp. e596–605, doi:10.1542/peds.2008-3348.
17. Solomou, Ioulia, and Fofi Constantinidou. "Prevalence and Predictors of Anxiety and Depression Symptoms during the COVID-19 Pandemic and Compliance with Precautionary Measures: Age and Sex Matter." *International Journal of Environmental Research and Public Health*, vol. 17, no. 14, July 2020, pp. 1–19, doi:10.3390/ijerph17144924.
18. Yao, Hao. "The More Exposure to Media Information about COVID-19, the More Distressed You Will Feel." *Brain, Behavior, and Immunity*, vol. 87, 1 July 2020, pp. 167–69, doi:10.1016/j.bbi.2020.05.031.
19. Garfin, Dana Rose, *et al*. "The Novel Coronavirus (COVID-2019) Outbreak: Amplification Public Health Consequences by Media Exposure." *Health Psychology*, vol. 39, no. 5, 1 May 2020, pp. 355–57, doi:10.1037/hea0000875.
20. Brooks, Samantha K., *et al*. "The Psychological Impact of Quarantine and How to Reduce It: Rapid Review of the Evidence." *The Lancet*, vol. 395, no. 10227, 14 Mar. 2020, pp. 912–20, doi:10.1016/S0140-6736(20)30460-8.
21. Sprang, Ginny, and Miriam Silman. "Posttraumatic Stress Disorder in Parents and Youth after Health-Related Disasters." *Disaster Medicine and Public Health Preparedness*, vol. 7, no. 1, Feb. 2013, pp. 105–10, doi:10.1017/dmp.2013.22.
22. Hawryluck, Laura, *et al*. "SARS Control and Psychological Effects of Quarantine, Toronto, Canada." *Emerging Infectious Diseases*, vol. 10, no. 7, Centers for Disease Control and Prevention (CDC), 2004, pp. 1206–12, doi:10.3201/eid1007.030703.
23. Saxena, Rakhi, and Shailendra K. Saxena. "Preparing Children for Pandemics." *Coronavirus Disease 2019 (COVID-19)*, Nature Publishing Group, 2020, pp. 187–98, doi:10.1007/978-981-15-4814-7_15.
24. Kessler, Ronald C., et al. "Age of Onset of Mental Disorders: A Review of Recent Literature." *Current Opinion in Psychiatry*, vol. 20, no. 4, July 2007, pp. 359–64, doi:10.1097/YCO.0b013e32816ebc8c.
25. Imran, Nazish, Irum Aamer, *et al*. "Psychological Burden of Quarantine in Children and Adolescents: A Rapid Systematic Review and Proposed Solutions." *Pakistan Journal of Medical Sciences*, vol. 36, no. 5, July 2020, pp. 1106–16, doi:10.12669/pjms.36.5.3088.
26. "Keep Mental Health in Mind." *Nature Medicine*, vol. 26, no. 5, Nature Research, 1 May 2020, p.631, doi:10.1038/s41591-020-0914-4.
27. Holmes, Emily A., *et al*. "Multidisciplinary Research Priorities for the COVID-19 Pandemic: A Call for Action for Mental Health Science." *The Lancet Psychiatry*, vol. 7, no. 6, 1 June 2020, doi:10.1016/S2215-0366(20)30168-1.

JOURNAL OF
EMERGING INVESTIGATORS

Article

The effect of floating plant on water purification: Comparison of the water purification capability of Water Hyacinth, Duckweed, and Azolla

Jiwoo Park[1], Jonathan Richard[1]
[1]American School of Bombay, Mumbai, India

SUMMARY

Water pollution is a critical issue for human health, aquatic plant and animal biodiversity. While there are several different approaches to resolve this issue, our research investigates one possible solution of using aquatic plants as a natural treatment system. To identify the optimal plant for treating polluted water in India, we selected water from the Mithi river and three types of floating plants: water hyacinth (*Eichhornia crassipes*), duckweed (*Lemna perpusilla*), and azolla (*Azolla pinnata*). We used a total of six measurements (dissolved oxygen, conductivity, turbidity, pH, color of water, and the number of colonies grown on the culture media) taken for seven days to compare the effect of each floating plant on the change in water quality. We hypothesized that duckweed would be the best plant to purify water in India since its effect on reducing turbidity or biochemical oxygen demand (BOD) was found in past research.

Our results show that all three floating plants are effective at purifying the water. Further, duckweed significantly reduced the turbidity and number of bacteria in the water, suggesting it may be the most optimal water purifier among those three. Based on the results from this experiment, we recommend floating plants as one alternative to resolving water pollution in India, which would effectively purify water as well as require less cost for construction and maintenance.

INTRODUCTION

Water, one of the fundamental constituents of the Earth covering three-quarters of its surface area, exists in the form of wetland. According to National Oceanic and Atmospheric Administration (NOAA), a wetland is classified as a land saturated with water and divided into five general types: estuarine (estuary), palustrine (marsh), riverine (river), marine (ocean), and lacustrine (lake). Wetland has significance in providing habitat for birds and fish, preventing erosion of soil, and maintaining water quality and rate of water flow (1, 2). However, studies suggest that these wetlands are becoming polluted due to the rapid industrialization, improper waste disposal, and the growing population (3). Many wetlands have a high concentration of nitrogen, phosphorus and organic pollutants, which exceeds wetland's self-purification capability, resulting in severe eutrophication–an excessive growth of algae or plants caused by a surfeit of nutrients in water (4,5). Some of the wetlands have algal blooms due to the overgrowth of blue-green algae, and those areas show a depletion or lack of dissolved oxygen (DO). Thus, countermeasures are required to resolve eutrophication, which threatens the ecosystem.

In India, clean water access is vital not only for economic purposes such as industrial use and irrigation, but also for various cultural and religious ceremonies, and sometimes for community bathing and washing (6). However, because contaminants from domestic sewage, large industries, or agricultural run-off flow into the water without filtration, water quality often does not meet the criteria for biochemical oxygen demand (BOD), total coliform numbers (TC), fecal coliform numbers (FC), dissolved oxygen (DO), and ions (7).

To solve the water pollution issue, scientists have conducted research on physical (8) and chemical treatments (9). However, due to the economic and technical constraints of these treatments, a new method for water purification is being explored: natural treatment (10). Particularly, the effect of aquatic plants on water purification has been consistently researched since 1980 (11), and recent studies investigate the application of aquatic plants such as creating an artificial wetland or island to purify water (12). Researchers have shown that aquatic plants significantly reduce nitrate, phosphate, and toxic metals (13). Unlike other physical and chemical treatments, the use of aquatic plants does not cause additional damage, such as destruction of the ecosystem, and involves less cost for construction and maintenance (14). However, it has limitations because it is a seasonal treatment, and not much research has been done for different types of water. Although some researchers investigate the effect of aquatic plants on purifying water, they use similar types of plants that have been researched previously.

Aquatic plants are divided into two categories: hydrophytes attached to the substrate and free-floating hydrophytes, depending on how they grow and live (15). Hydrophyte refers to plants living in water. It can prevent erosion, stabilize the soil of wetland, absorb nutritive salts or harmful substances, and prevent excess growth of phytoplankton (16). Hydrophyte can be subdivided into three types: emergent hydrophytes, submerged hydrophytes and floating hydrophytes. Unlike emergent plants such as lotus, or submerged plants such as coontail, that need soil to fix their roots in the bottom of the water, floating plants require no soil and are easier to grow in a controlled environment.Therefore, our study compared the water purification effectiveness of three types of floating plants: water hyacinth (*Eichhornia crassipes*), duckweed (*Lemna perpusilla*), and azolla (*Azolla pinnata*). We

Use of water	Class	Criteria
Propagation of wildlife, fisheries	D	– pH: 6.5 to 8.5 – DO ≧ 4 mg/L – Free ammonia ≦ 1.2 mg/L

Table 1a. Water quality criteria for various uses of water suggested by the Central Pollution Control Board.

Measurement	Dissolved Oxygen	Conductivity	Turbidity	pH	Number of colonies
Low	Less preferred	NA	Preferred	NA	Preferred
High	Preferred	NA	Less preferred	NA	Less preferred
Permissible limit	>2 mg/L	150-500 µS/cm	Not specifically determined	6.5-8.5	< 2000 cfu/100mL

Table 1b. The criteria to evaluate water quality in this experiment.

determined their ability to purify water by taking several types of measurements to evaluate water quality. These floating plants were chosen because they are common floating plants inhabiting India and research suggests water hyacinth, azolla, and duckweed have an effect on quality (17,18,19). While that research provided deep analysis of each of the plants, there are no comparisons of those plants in India. Therefore, the comparison between the three different types of floating plant will be the key to this research.

In this research, we measured the pH, turbidity, conductivity, dissolved oxygen, color, and bacteria growth in the culture medium of the water samples in order to identify an optimal floating plant to solve the water pollution problem in India.

The conductivity of water is affected by the amount of ionic nutrients such as sodium, chloride, or sulfate dissolved in water. High conductivity, which indicates more solute salts and ions, can lead to poor plant growth and toxicity, whereas low conductivity results in slow-growing plants (20). Fresh streams ideally have a conductivity between 150 to 500 µS/cm. The pH determines the solubility and biological availability of chemical constituents such as metals and nutrients (21). Majority of aquatic creatures have a narrow pH tolerance range of 6.5-9, and excessively high or low pH is harmful to the animals and plants living in the water. The level of DO is the number of oxygen (O_2) molecules per million total molecules in a sample. It is affected by a physical condition such as temperature and pollutants and higher DO level is preferred for fish growth and activity. Turbidity is the amount of light scattered by particles in water. It is used to determine the water clarity and to estimate the amount of dissolved colored material and suspended solids in water. High turbidity levels may disrupt the natural movements, cause illness, or expose fish to potential pathogens or toxins, as well as reduce the aquatic plant's accessibility of light. Lastly, the number of bacteria living in water also determines water quality since the water with an excessive number of bacteria is considered impaired. Among two ways of culturing bacteria, culturing them in liquid or in a medium, we chose to use culture medium since it is easy to observe the group of fungi or bacteria in a form of colony despite their slow growth. Some research suggests that for water to be considered clean, the number of fecal coliforms should be less than 2,000 cfu and that of *E. coli* be less than 1,260 cfu in 100mL water sample (22). This is because fecal coliform bacteria may present in water as a result of disposal of human waste or overflow of domestic sewage, indicating the contamination of water. The presence of fecal coliform bacteria further indicates that there may be a harmful pathogen that can cause waterborne pathogenic diseases such as typhoid fever (23).

Indian governmental report suggests different criteria for evaluating water quality based on the usage of water: drinking, outdoor bathing, propagation of wildlife, and irrigation/ industrial cooling. In this research, data was compared to the criteria for class D as the goal of the research was to have water that propagates wildlife and fisheries (24) (**Table 1a**). Based on the criteria used by Indian government, this research has set up new permissible limits to compare water purification capability of plants (**Table 1b**).

Prior to the experiment, we hypothesized that duckweed would be the best plant to purify water in India since past research suggested that duckweed was effective in decreasing turbidity by removing total suspended solids (TSS) and in reducing BOD (25).

RESULTS

Floating plants moderately change the conductivity, pH, and DO, but drastically reduce the turbidity of the water

To determine how three different types of floating plant play a role in improving water quality, four different groups, including a control group, were used. Here, each of three experiment groups—water hyacinth, duckweed, and azolla—had one type of floating plant in the water. The control group, on the other hand, had nothing inside the water to observe any possible change in water quality without any involvement of plants. In order to reduce the error, there were four set-ups

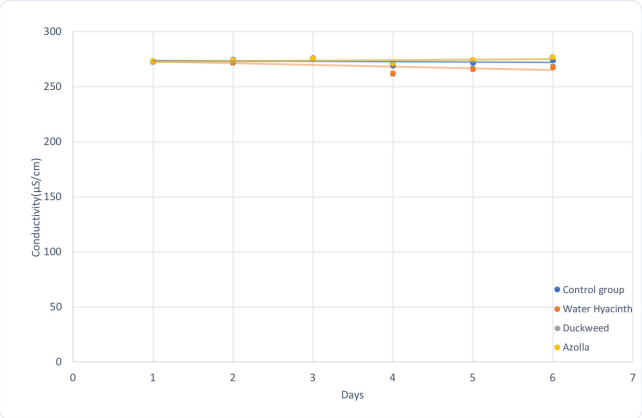

Figure 1. Effect of floating plants on conductivity. The change in conductivity of control group, water hyacinth, duckweed and azolla for 6 days; linear trendline; data represent the average; error bars represent standard deviation

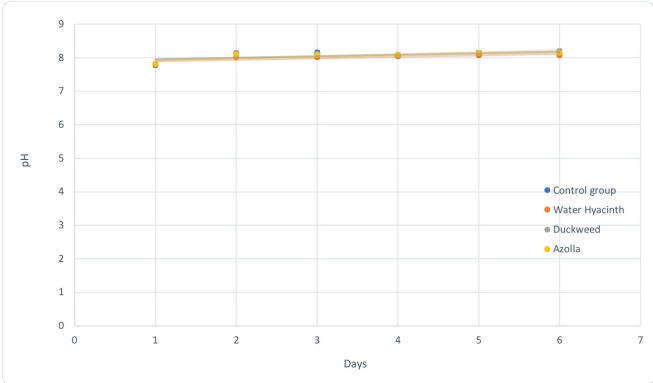

Figure 2. Effect of floating plants on pH. The change in pH of control group, water hyacinth, duckweed and azolla for 6 days; linear trendline; data represent the average; error bars represent standard deviation

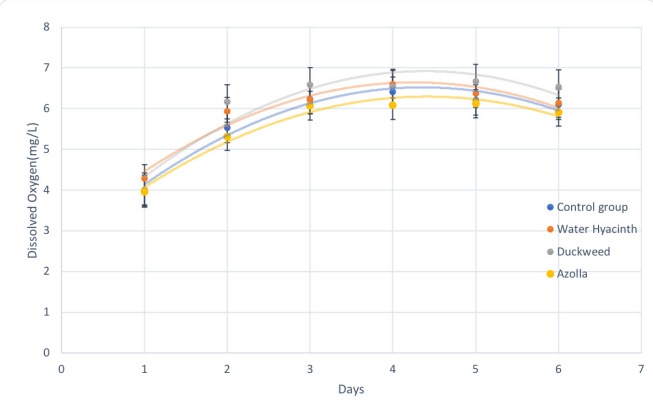

Figure 3. Effect of floating plants on increasing dissolved oxygen level. The change in dissolved oxygen of control group, water hyacinth, duckweed and azolla for 6 days; polynomial trendline; data represent the average; error bars represent standard deviation.

per group, and every measurement was taken five times per set-up. Then, the results were averaged within its group and plotted graphically.

First, the conductivity of all the groups showed a constant increase, except from day 3 to day 4 (**Figure 1**). The trend of both the control and experimental groups were similar, indicating that floating plants did not have a significant impact on conductivity. The increase in conductivity was not sharp and the conductivity of all groups was in the permissible level of 150-500 µS/cm from day 1 to day 6.

For pH testing, all groups showed an increase between day 1 and day 2, then remained constant from day 2 to day 6 (**Figure 2**). All the groups were in the permissible limit of pH 6.5 to 8.5. The slopes of duckweed, azolla and water hyacinth were similar to the control group, which indicated that these plants did not affect the pH of water.

For dissolved oxygen level, the overall trend of the graph indicated that dissolved oxygen of water increased until day 4, then started to decrease (**Figure 3**). Although dissolved oxygen started to decrease, all the measurements were in the permissible range, exceeding 2 mg/L. By comparing the polynomial trendline for each group in the graph, it can be said that the most effective plants to increase dissolved oxygen was Duckweed > Control group > Azolla > Water hyacinth. In this sense, the experiment suggested that plants were not effective in terms of increasing DO since only duckweed ranked higher than the control group. However, a drastic increase of DO for all four groups from day 1 to day 2 indicated that between day 1 and day 2, water might have been in the stage of going towards equilibrium. Thus, when considering the trend from day 2 to day 6, the control group and water hyacinth group showed steeper decrease in DO from day 4 to day 6 than the duckweed group and azolla group. This indicated that duckweed and azolla were more effective than water hyacinth in impeding the decrease in DO. Thus, the order of the groups which showed effectiveness in increasing or maintaining dissolved oxygen level was Duckweed > Azolla > Control group > Water Hyacinth.

Lastly, for turbidity, all groups showed a decrease in turbidity over time (**Figure 4**). This might also be due to the precipitation of floating matter as time went on since the turbidity of the control group also decreased as the time proceeded. Comparing the trendlines of the experimental groups to that of the control group, all three plants—water hyacinth, duckweed, and azolla—were effective at decreasing the turbidity level since they had a steeper slope, which indicated that turbidity was decreasing faster. The measurement of turbidity for each group from day 1 to day 6 showed that the order of the most effective group for reducing turbidity was Water Hyacinth > Duckweed > Azolla > Control group.

Floating plants led to an improvement in the transparency of water

In addition to quantitative measurement from an apparatus, qualitative data were also taken when evaluating the water quality of experiment groups. To determine the effectiveness of floating plants, the clearness and the color of the water were taken into account since if the water had a green color,

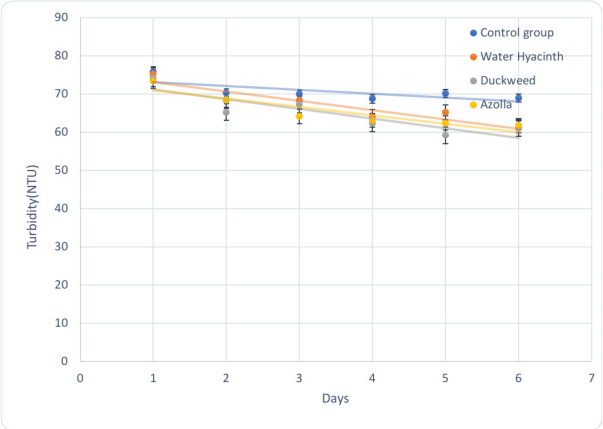

Figure 4. Effect of floating plants on decreasing turbidity. The change in turbidity of control group, water hyacinth, duckweed and azolla for 6 days; linear trendline; data represent the average; error bars represent standard deviation.

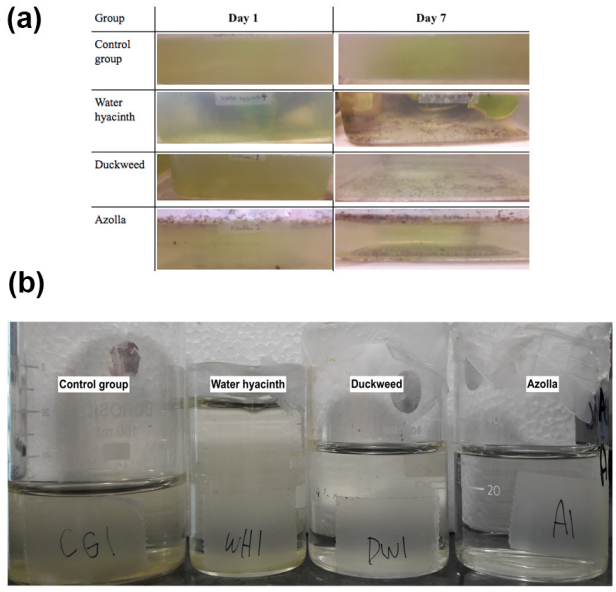

Figure 5. Change in color of water over 7 days. (**a**) Representative images of the color and transparency of water on day 1 and day 7; plants weren't removed from the water to identify possible contaminants attached to plant's roots or subsided on the bottom of containers. (**b**) Representative images of the color and transparency of water samples that were collected on day 7; water samples were taken from the setup to only observe contaminants dissolved in water.

it was assumed that the algae and other chemicals were included in the water and thus, water was contaminated.

The color of water was compared in two ways. First, the color was compared when there were plants in the water (**Figure 5a**). The color of water was observed when the plants were not displaced from water to observe density of color without any outside movement. After seven days from the start of the experiment, the water of all experimental groups turned almost transparent, whereas the water color of the control group did not change. The order of most purified water was therefore water with duckweed > water hyacinth > azolla > control group. This order corresponded to the order of turbidity, indicating that the results were consistent. The color of water was also compared through taking the water sample on the last day (**Figure 5b**). Although all samples were more transparent than the color observed when plants remained in water, the extent of its clarity varied. The observation showed that the order of the most purified water was the water with duckweed > water hyacinth > azolla > control group, which corresponded with the order with the color of the water with plants (**Figure 5a**).

Floating plants drastically reduced the number of colonies that grew on culture medium

On day 7, the sample of water was taken from each set up to measure the number of bacteria inhabiting in the water. We cultured water samples from day 1 and day 7 on culture media to compare the water quality before and after exposure to the floating plants. Then, we counted the number of colonies grown from each sample as a measurement of water quality. We considered that if there was a decrease in the number of colonies grown on culture medium, plants would have reduced the bacterial growth in water.

As expected, the number of colonies varied across the culture media of the water samples from different groups (**Figure 6a**). The control group had the highest density of colonies, while the duckweed and azolla groups had the lowest density. The samples grew five different types of colonies, which indicated the existence of different types of bacteria inhabiting the water. To count the number of colonies for each type of bacteria, the colonies were categorized into five different types depending on their color, size, and morphology (**Figure 6b**). Type 1 was the orange colony, type 2 was the white colony with a solid border line, type 3 was the small and white colony, type 4 was the white colony with the inside filled, and type 5 was the red colony. Then, the average number of colonies was counted. In summary, the water hyacinth had reduced the number of type 3 bacteria, duckweed reduced type 2 and 4, and azolla reduced type 3 and 4 (F**igure 6c**). All groups did not satisfy the permissible limit of fecal coliform numbers (FC) for drinking water: 20 cfu/mL. However, compared with the number of colonies that grew in the water before the experiment, all the experimental groups showed reduction in the number of bacteria. Thus, we concluded that the order of the most effective at reducing bacteria growth was azolla > duckweed > water hyacinth > control group.

DISCUSSION

The six measurements in this experiment—conductivity, pH, turbidity, dissolved oxygen, color, and the number of bacteria colonies—showed that water hyacinth, azolla and duckweed did not always have an effect on water quality. For instance, there were subtle differences between experimental groups and the control group for conductivity, pH, and dissolved oxygen. On the other hand, turbidity and

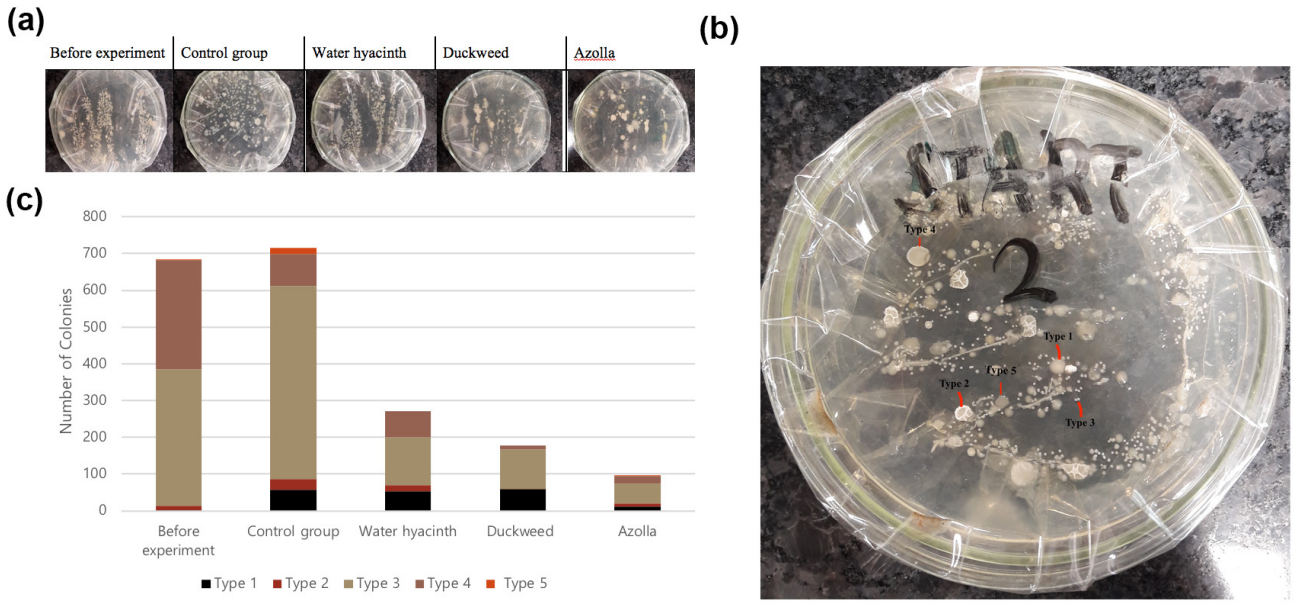

Figure 6. Colonies grown on culture media. (**a**) Representative images of bacteria grew on agar badges with water samples from day 7; The photo was taken 24 hours after the culture media were kept in 31°C incubator; "Before experiment" refers to the water sample from day 1. (**b**) Representative image of different types of bacteria grew on agar plate with water sample taken on day 7; bacteria were differentiated based on its physical feature (**c**) The average number of different types of colonies found on agar badges with water samples from day 7; The number was counted 48 hours after the culture media were kept in 31°C incubator; Before experiment refers to the water sample from day 1.

the number of bacteria in water changed drastically when the plants were added into the water; experimental groups were more effective at water purification compared to the control group since they had a larger decrease in turbidity and less bacteria growing on the culture media.

To determine the most effective group for purifying water, we ranked the groups based on their results from each measurement over the six-day experiment. The results from the experiment supported my hypothesis that the duckweed would be the most effective plants to purify water compared to water hyacinth or azolla. The water from the duckweed group showed the highest effectiveness of purification for most of the results; had the measurements of conductivity (276.9 μS/cm ± 0.95%) and pH (8.20 ± 3.13%) in the acceptable range set up before the experiment, had greatest increase in DO level (4.00 mg/L→ 6.53 mg/L ± 10.%) and the second greatest decrease in turbidity (74.16 NTU→61.06 NTU ± 0.36%) on average with almost colorless water on day 7, and had the second-lowest FC (178 cfu/mL) grown on culture media.

The results from each of the measurements showed correlation, which added to the reliability of the data. For example, turbidity had a close relationship with the color of water since turbidity measures the amount of suspended particles in water, which we can visually observe from the transparency of water. Similarly, in this experiment, the order of water purification was almost the same for the turbidity measurement and the color observation. However, there were also some limitations to the data. First, for pH, DO, and turbidity measurements, there was a rapid change between day 1 and day 2 across all four groups, compared to the change after day 3. The pH increased 0.30 on average from day 1 to day 2, then changed by 0.10 per day afterward. Similarly, dissolved oxygen increased by 1.68 mg/L on average between day 1 and day 2, while it changed by less than 0.54 mg/L per day afterward. Less change in pH and DO level after day 2 indicates that water was in the process of reaching equilibrium—such as solids settling out or adapting to the atmosphere of the lab—from day 1 to day 2. To reduce the error coming from this changing variable, the day 1 measurement was excluded from the analysis in order to identify the trend of equilibrium post-collection. Another limitation is that there was a sign of systematic error in the conductivity data. In its graph, the measurements for both the control group and the experimental group dropped between day 3 and day 4. This drop may be due to incorrect calibration of the measuring tool. Thus, the order was determined by comparing each group to the trend of the control group measurement, which reduces the accuracy of conductivity data. Further, since conductivity measurements for all groups—whether it shows increasing or decreasing trend—were in the permissible range, we decided not to include the order of conductivity when identifying the optimal floating plants for water purification. Another possible error could have been caused by the temperature at which the bacteria were grown on the culture media. In the experiment, the temperature of the incubator was set to 31°C, which may have suppressed the growth of bacteria that have different optimal growth temperatures. This error could be improved through multiple trials with different temperatures, which would allow the researcher to observe the pattern of bacteria growth.

	Conductivity	pH	Turbidity	Dissolved oxygen *trend from day 3 was considered	Number of Colony	Color	Total
Control Group	Acceptable range (273.8µS/cm)	Acceptable range (pH 8.15)	4 (-6.39NTU)	3 (+2.10 mg/L)	4 (715cfu)	4	15
Water hyacinth	Acceptable range (267.8µS/cm)	Acceptable range (pH 8.07)	1 (-14.25NTU)	4 (+1.85 mg/L)	3 (271cfu)	2	10
Duck- weed	Acceptable range (276.9µS/cm)	Acceptable range (pH 8.20)	2 (-13.10NTU)	1 (+2.53 mg/L)	2 (178cfu)	1	6
Azolla	Acceptable range (276.8µS/cm)	Acceptable range (pH 8.14)	3 (-11.67NTU)	2 (+1.96 mg/L)	1 (97cfu)	3	9

Table 2. Compilation of results from various measurements.

Furthermore, dissolved oxygen measurements for water hyacinth had inevitable limitations due to the inability to set up the same environment as an actual pond or river. Cornwell's research suggests that water hyacinth needs a water level of 0.7-1.8 meters to perform photosynthesis effectively (26). Acknowledging that plants need enough space and carbon dioxide to perform photosynthesis effectively, if the experiment is conducted in open-space where it meets those needs, it is possible that an experiment group could perform better on increasing DO. In addition, the absence of water flow may have affected the measurements of dissolved oxygen.

However, despite the limitations this research contains, we expect that the application of a natural treatment system using floating plants will bring a positive impact on water quality, providing better habitat for aquatic life as well as increasing the usefulness of the water. For instance, duckweed can be added to a pond in which wildlife cannot propagate due to contamination from wastewater. This can reduce the peril of wastewater with less cost than physical or chemical treatments. The government can even adopt constructed wetlands, where microorganisms and aquatic plants act as a filter as water slowly enters the wetland; nutrient and pollutant in water naturally breaks down and is taken up by plants and bacteria. This way, the wastewater from agricultural run off or human, industrial waste can be treated with low cost and energy consumption, protecting the environment (27). However, there are some limitations of using duckweed. Duckweed has a high rate of reproduction, however, excess quantity of duckweed can contaminate water quality when it covers the water surface and blocks the sunlight needed for microorganisms that decompose contaminants. In fact, some countries had to undergo disposal of duckweed in sewage systems as duckweed propagated more than they expected (28). Hence, future studies could focus on the relationship between the number of duckweed covering water surface and water purification level.

MATERIALS AND METHODS

Water sample collection

Water samples from the Mithi river were collected in five 20 L plastic bottles. Collected water was directly used in the experiment without any other disinfection or treatment in order to predict the effect of floating plants on water in reality. The water samples were then distributed equally to 16 plastic bowls for 16 set-ups (four set-ups per group).

Group set up

The experiment included one control group and three experimental groups. The control group did not contain any floating plants, but only a water sample. The experimental groups—water hyacinth, duckweed, and azolla—each contained a type of floating plant covering approximately 80% of the surface area of the water. Each group had 4 set-ups to reduce the random error; hence, a total of 16 samples (four groups with four set-ups) were used in this experiment. Observations only happened for seven days due to our inability to replicate the environment of the real river; after seven days, plants started to function less due to space restraints and the water started to be more contaminated due to the absence of its flow. The set-ups were placed indoors, right next to the window, to prevent excess evaporation of water from strong sunlight and high temperatures, which may affect the dissolved oxygen level and turbidity of water. The average ambient temperature of the setting was 29.0°C and the intensity of sunlight was 5.4 kWh m-2 day-1.

Data collection of conductivity, pH, dissolved oxygen, and turbidity

Four types of measurements—pH, turbidity, conductivity, and dissolved oxygen—happened every day. For each test, measurements were taken five times per set-up. pH was measured with pH meter (± 0.01), turbidity was measured with a turbidity meter (±0.01 NTU), conductivity was measured with electrical conductivity meter (± 0.1µS/cm), and dissolved oxygen was measured with dissolved oxygen meter (± 0.1 mg/L). In addition, photos were taken for each set-up every day for the comparison of the water color.

Data collection of the colony forming units

After seven days, water samples were collected for each test subject in order to be used for culture medium. On the agar plate, 1.00 ± 0.01 mL of each sample was sprayed using a pipette. Then, the agar plates were put in an incubator at 31.0 ± 0.1 °C according to the literature for the optimal temperature to grow most of the types of *E. coli* (29). Observation of agar plates happened every 12 hours, and the final number of

colonies was counted after 48 hours. This was due to the fact that the number of bacteria surviving on the agar plate started to diminish after 48 hours.

Determine the ranking of water plants that were most effective in water purification

The order of effective water plants to purify water was determined in consideration of six testings (**Table 2**). First, we identified whether pH and conductivity was within acceptable range set up before the experiment. Then we created a table with numbers. which are the rankings of different experimental groups in each of the testnings: Turbidity, DO, FC, and color of water. Then, we summed all the numbers for each group to find the group with the lowest sum of numbers–a group that ranked relatively high in all four testings.

Received: July 15, 2020
Accepted: October 22, 2020
Published: November 21, 2020

REFERENCES

1. Ghosh, D. and S. Sen. "Ecological history of Calcutta's wetland conservation." *Environmental conservation*, no.14, 1996, pp. 219-226
2. Cox, R. and J. Cullington. "Wetland Ways: Interim Guidelines for Wetland Protection and Conservation in British Columbia." **Environmental Stewardship Division**, 2009.
3. Cohen, A.S., Bills, R., Cocquyt, C.Z. and Caljon, A. "The Impact of Sediment Pollution on Biodiversity in Lake Tanganyika." *Conservation Biology*, no. 7, 1993, pp. 667-677.
4. Kim H., Lee H., Seo D., *et al.* "A Study on the Improvement of Treatment Efficiency for Nitrogen and Phosphorus by Improved Sewage Treatment Process in Constructed Wetland by Natural Purification Method." *Journal of Agricultural Chemistry and Environment*, vol. 27, no.1, 2008, pp.27-35.
5. Schindler, D. W. "Recent advances in the understanding and management of eutrophication." *Limnology and Oceanography*, no. 51, 2006, pp. 356-363.
6. Bhardwaj R.M. "Water quality monitoring in India-Achievements and constraints." *International Work Session on Water Statistic*, 2005.
7. Cohen, A.S., Bills, R., Cocquyt, C.Z. and Caljon, A. "The Impact of Sediment Pollution on Biodiversity in Lake Tanganyika." *Conservation Biology*, no. 7, 1993, pp. 667-677.
8. C. de Latour and H. Kolm. "Magnetic separation in water pollution control - II." *IEEE Transactions on Magnetics*, vol.11, no. 5, 1975, pp. 1570-1572
9. Im K., "Remediation of Soil and Purification of Ground Water Enhanced by Surfactants." *Journal of Industrial and Engineering Chemistry*, vol. 5, no. 6, 2002, pp. 7-15.
10. Choi D., Kang H., Lee M. "Feasibility of Aquatic Plants(Eichhornia crassipes and Water dropwort) for Nutrients Removal." *Environmental Engineering Research*, vol. 32, no. 2, 2010, pp.141-148.
11. Lee K., Kim M., Pyon J., Lee J. "Studies on Removal of Water Pollutants by Aquatic Plants - 2. Removal of Water Polluted Nutrients and Heavy Metals by Water Hyacinth." *Weed Biology and Management*, vol.5, no.2, 1985, pp. 149-154.
12. Yoon Y., Lim. H., Kim W., Jung J., Park J. "Development and Application of Multi-Functional Floating Wetland Island for Improving Water Quality." *Ecology and resilient infrastructure*, vol.3, no.4, 2016, pp. 221- 230
13. "Aquatic plants may help remove contaminants from lakes." *ScienceDaily*, South Dakota State University, 16 Nov. 2017,www.sciencedaily.com/releases/2017/11/171116183907.htm. Accessed 13 June 2020.
15. Sculthorpe C.D. "Biology of Aquatic Vascular Plants." Science, *St. Martin's Press*, vol. 160, no.3824, 12 Apr. 1967, pp.179.
16. Kim C., Ko J., Lee J., Hwang J., Park S., Kang H. "Screening of Nutrient Removal Hydrophyte and Distribution Properties of Vegetation in Tributaries of the West Nakdong River." *Korean Journal of Environmental Agriculture*, vol.25, no.2, 2006, pp. 147-56.
17. Gideon, O., Louw, W., and Dan, P. "Waste Water Recycling by Duckweed for Protein Production and Effluent Renovation." *Water Science Technology*, vol.17, no.4-5, 1985, pp. 803-817.
18. Isao, A. Hisao, N. "Uptake of Nitrogen and Phosphate, and Water purification by Water Hyacinth Eichhornia Crassipes(Mart.) Solms." *Water Science Technology*, vol.28, no.7, 1993, pp.47-53.
19. Zhao, M., Duan, J.R., Van Hille R.P. "Removal and recovery of zinc from solution and electroplating effluent using Azolla filiculoides." *Water Research*, vol.33, no.6, 1999, pp.1516-1522
20. "Grace, "Understanding Water Quality, Water EC, and PH." *AEssense*, 2016, http://cdn2.hubspot.net/hubfs/2679989/AEssense Corporation Nov 2016/PDF/Understanding-Water-Quality-pH.pdf. Accessed 20 May 2020.
21. Michaud, Joy P. A. "Citizens Guide to Understanding and Monitoring Lakes and Streams." *Olympia*, WA: Puget Sound Water Quality Authority, 1991.
22. "Bacteria: Sources, Types, Impact on Water Quality." *Minnesota pollution control agency*, 2008, https://www.pca.state.mn.us/sites/default/files/wq-iw3-20.pdf. Accessed 28 May 2020.
23. Oram, B. "Fecal Coliform Bacteria in Water." *Water Research Center*, https://www.water-research.net/index.php/fecal-coliform-bacteria-in-water. Accessed 2 June 2020.
24. Cohen, A.S., Bills, R., Cocquyt, C.Z. and Caljon, A. "The Impact of Sediment Pollution on Biodiversity in Lake Tanganyika." *Conservation Biology*, no.7, 1993, pp.667-677.
25. Barnes, Wilson. "The Design and Operation of Small Sewage Works." *Cambridge University Press*, 1976, pp. 200
26. Cornwell, D. A., Zolt Jr., J., Patrinely, C. D., Furman, T. and Kim, J. I. "Nutrient removal by water hyacinth." *Water*

Pollution Control Federation, 1977, pp.49, 57-65.
27. Dimuro, J. L., Guertin, F. M., Helling, R. K., Perkins, J. L., Romer, S. "A Financial and Environmental Analysis of Constructed Wetlands for Industrial Wastewater Treatment." *Journal of Industrial Ecology*, vol.18, no.5, 2014, pp.631-640.
28. Bonomo, L., Pastorelli, G., & Zambon, N. "Advantages and limitations of duckweed-based wastewater treatment systems." *Water Science and technology*, vol.35, no.5, 1997, pp.239-246.
29. Raghubeer E.V., Matches J.R. "Temperature Range for Growth of Escherichia coli Serotype 0157:H7 and Selected Coliforms in E. coli Medium." *Journal of Clinical Microbiology*, vol.28, no.4, 1990, pp.803-805

JOURNAL OF
EMERGING INVESTIGATORS

Article

A study to determine the anti-cancer and pro-apoptotic properties of *Amaranthus spinosus* Linn. Extract, AS20

Ishir Sharma[1], Pooja Kasture[2], Ankita Umrao[2], Jyothsna Rao[2], Gururaj Rao[2]
[1] The International School Bangalore, NAFL Valley, Whitefield – Sarjapur Road, Bangalore, KA, India, 562125
[2] iCREST-International Stem Cell Services Limited, 9/1, Mission Road, Bangalore

SUMMARY

Complementary approaches to cancer treatment seek methods that integrate into existing therapies such as chemotherapy and radiotherapy. The most common form of complementary medicine is the usage of external antioxidants, including Ayurvedic herbal extracts, which assist in the mitigation of the side effects of cancer treatment on healthy cells. Herbal extracts are usually evaluated only for their antioxidant properties for complementary use in cancer treatment. Ayurvedic products are rarely evaluated for their anti-cancer properties. In this paper, we hypothesized that AS20, a crude extract of the whole *Amaranthus spinosus* (AS) plant, would induce higher cell death to the HeLa cancer cell line compared to other extracts of individual parts of the plant. Significantly lower IC50 values were found for both 24 hours (11.56 µg/ml) and 48 hours (1.77 µg/ml) exposure compared to any of the other individual extracts of the plant part for the given exposure duration. Also, apoptosis was observed in HeLa cells treated by the IC50 concentration of AS20 using fluorescent stains such as Hoechst dye, DAPI and dual staining (Acridine Orange and Propidium Iodide). It is thus concluded that AS20 formulation exhibited cytotoxic activity on HeLa cancer cell lines and their action mechanism is via apoptosis.

INTRODUCTION

Complementary and alternative approaches to cancer treatment are premised upon relieving the symptoms of cancer treatment (1). A common complementary therapy is the usage of antioxidants (2), which assists in the mitigation of the side effects of chemotherapeutic drugs and radiotherapy on healthy cells. Hence, by complementing natural antioxidants with external herbal products, we would theoretically be able to prevent oxidative cell damage to healthy body cells, while retaining the anti-carcinogenic properties of the mainstream drug. Ayurvedic treatment is not considered a mainstream method. However, if the complement herbal product was to possess anti-cancer properties of its own which added on to those of the mainstream drug, it might be possible to reduce the dosage of the mainstream drug, still maintain the anti-cancer potential, and have the added benefit of the antioxidant properties to eliminate the side effects.

Secondary metabolites (alkaloids, saponins, flavonoids, polyphenols, tannins etc.) are organic compounds produced primarily by plants as waste products of their metabolism. These compounds are known for their medicinal properties (3). A large variety of alkaloids, for instance, have been shown to display compelling anti-carcinogenic activity and anti-cancer drugs have been created from alkaloids (4). Saponins are known for their cytotoxicity against cancer cells (5) as well as the inhibition of carcinoma growth (6). Saponins prevent the proliferation of cancer cells due to their ability to interfere with DNA replication (7). Polyphenolic compounds, including flavonoids and tannins, have been shown to possess anti-cancer activities in addition to their high antioxidant potencies (8). These metabolites are thus known to possess anticancer properties.

The *Amaranthus spinosus* (AS) Linn. plant is a medicinal plant which is found in abundance in India and around the world. This plant has been used extensively in Ayurveda (9), the traditional folk medicine of India, to treat diabetes, jaundice (10) and various other ailments. In our earlier studies (11), solvent extractions (water, ethanol, methanol, chloroform and acetone) were prepared for each part of the AS plant. We phytochemically screened the various parts of the AS plant. The phytochemical quantitative tests were conducted for total alkaloid, saponin, flavonoid, polyphenol and tannin contents. Subsequently, a crude herbal formulation, AS20 was prepared and assessed for its free-radical scavenging properties. AS20 is a crude herbal formulation consisting of the methanol extract of the leaves and the acetone extract of the inflorescence of the AS plant. This formulation was created based on maximum total alkaloid, saponin/tannin, polyphenol and flavonoid content of the entire plant since these metabolites were known to possess both antioxidant and anti-cancer properties. Some studies also suggest anti-carcinogenic properties of AS leaves in both in vivo and in vitro analyses (12). Hence, our AS20 formulation was a promising formulation to display anticancer properties.

HeLa is named so after Henrietta Lacks, a lady who died of cervical cancer in 1951 (13). Ever since the distribution of her cells, this cell line has been commonly used to evaluate the effects of various anticancer drugs (14). HeLa cells have been used to investigate the phytocomponents (plant-based components) and the apoptotic mechanism of the anti-cancer activity of the ethanolic extract of mango peel (15). Apoptosis is a mode of programmed cell death (16) that does not result in harm to surrounding cells. An alternate form of cell death, necrosis, is induced by chemotherapeutic drugs (17). Necrotic

cell death damages the body (18) and hence apoptosis is a more desirable mode of death, as it is an alternative mechanism of cell death which avoids the side effects seen in necrotic cell death. HeLa is an immortal cancerous cell line that is considered to be the single longest-living cell line (19).

Hence, the anti-cancer properties of the entire plant were of interest in this study. In this study, we evaluated the ability of the crude extract formulation of AS20 to exhibit a greater anti-cancer and pro-apoptotic properties than constituents and other extracts of individual parts of the plant. This, in addition to its potent free radical scavenging property (11) would make it potentially suitable complementary cancer drug. Apart from the ordinary HeLa cell line employed in this study, a 5-fluorouracil (5-FU) drug-resistant variety (HeLa-R) was developed (20) and employed in the study. The morphology of cells was also evaluated. To create this herbal formulation, we mixed extracts of different parts of the plant, which are the most potent in the desired phytocomponents, to create a crude extract that is a genuine representative of the potency of the entire plant. Thus, it was hypothesized that the crude extract, containing a greater content of the secondary metabolites, would display significant anti-cancer properties determined by the MTT assay. Crude Ayurvedic combinations have not been studied in this manner and this is an essential step in the field of integrative oncology.

RESULTS

Medicinal herbs and their derivative phytocompounds are being recognized as useful complementary and alternative medicinal treatments for cancer. *Amaranthus spinosus* (AS) Linn. plant is a medicinal plant which has been used extensively in Ayurveda. Recent studies also showed that Amaranthus spinosis has antioxidant and anticancer properties. This study was conducted to assess the cytotoxic activities using MTT assay and induced apoptosis of the formulation AS20 on HeLa cells as well as HeLa-R (5-FU drug resistant) cells.

Cytotoxicity of HeLa cells by AS20

MTT assay was used to measure cytotoxicity (loss of live cells). This is based on metabolic reduction of the soluble MTT salt, 3(4,5-dimethylthiazol-2-yl)-2,5-diphenyltetrazolium bromide which reflects the normal function of mitochondria dehydrogenase activity and cell viability, into purple coloured formazan product, which was measured spectrophotometrically.

The percentage viability of HeLa (drug-sensitive) and HeLa-R (5-FU drug-resistant) cells with an increase in the concentration of AS20 was determined by carrying out the MTT assay in a 96 well plate to determine the IC50 value of AS20. HeLa-R cell line was also employed to determine the anticancer effect of AS20 on cancer cells which are resistant to commercial anti-cancer drugs such as 5-FU. The IC50 obtained for 24 h and 48 h by using acetone extracted inflorescence was 47.3 and 22.31 µg/ml, respectively. Leaf extracted in methanol and water showed an IC50 at 23.48 µg/ml on its 24 h exposure and 13.19 and 6.28 µg/ml during 48 h treatment, respectively (**Figure 1 (a), (b), (c)** and **Figure 2**). The IC50 values at 48 h were significantly lower than that at 24 h (p<0.05 and p<0.001).

It was evident that the herbal formulation, AS20 on HeLa cells had a significantly (p<0,001) lower IC50 value of 11.56 µg/ml (24 hours) and 1.77 µg/ml (48 hours) than any of the

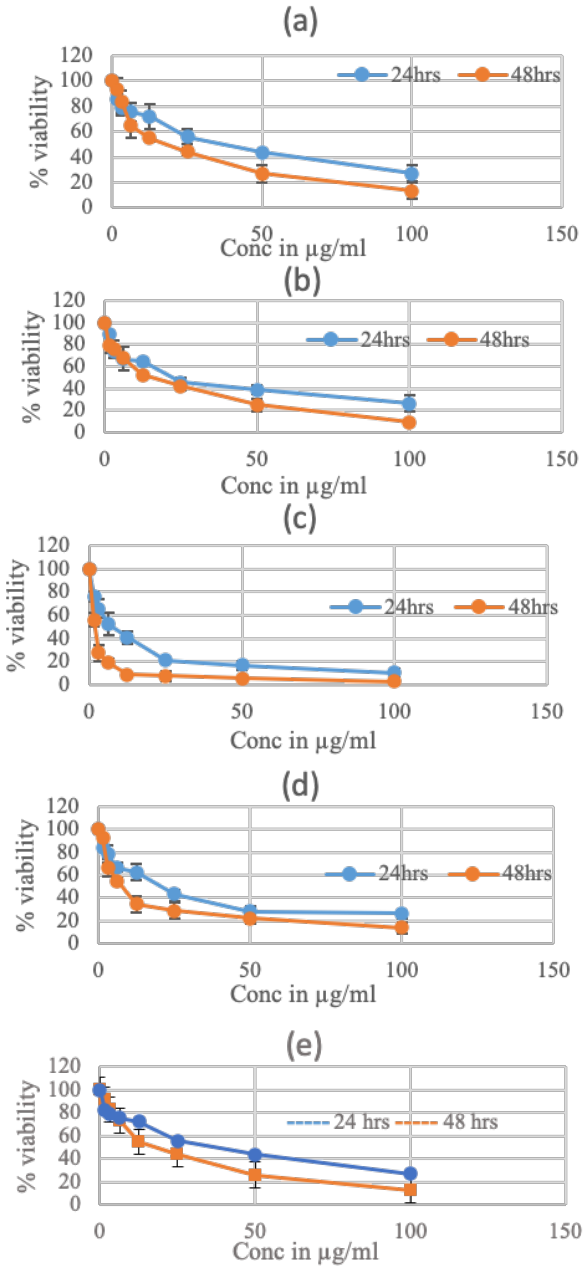

Figure 1: Graph displaying decrease of percentage viability of HeLa cells with increase in concentration of *Amaranthus spinosus*-derived extracts using MTT assay: (a) AS Inflorescence Acetone extraction, (b) AS Leaves Methanol extraction, (c) AS Leaves Water extraction, (d) AS20, and (e) AS20 on HeLa-R cells, following 24 hours and 48 hours of drug exposure. Results are expressed as percentage (%) at each concentration in µg/ml (N=3, mean±SD).

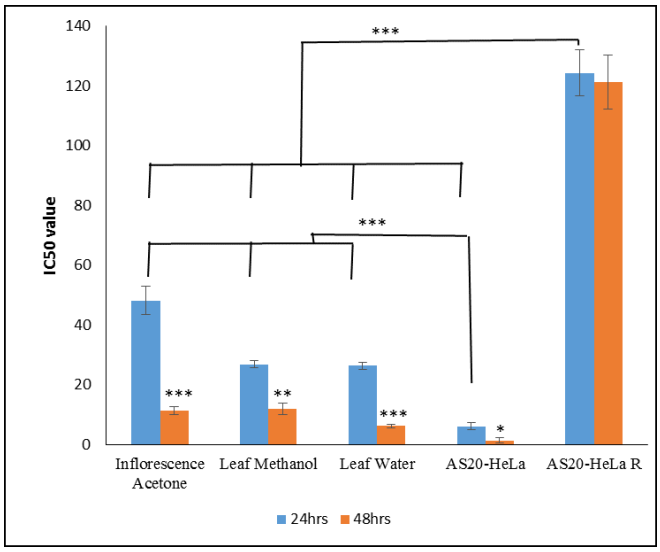

Figure 2: Bar graph showing the IC50 values for the MTT cell viability assay for the five groups tested. The concentration was expressed in µg/ml (N=3, mean±SD). HeLa cell viability decreases with increasing concentrations of *Amaranthus spinosus*-derived extracts using MTT assay. Effect of the extracts and formulation on 24 h and 48 h was compared. AS20 effect on HeLa and HeLa-R was compared with other groups. Groups were considered statistically significant if $p<0.05$ (*), $p<0.01$ (**) and $p<0.001$ (***).

other individual component groups for the given exposure duration (**Figure 1 (d)** and **Figure 2**). Similarly, for the HeLa-R cells, AS20 had IC50 values of 124.28 µg/ml at 24 hours and decreased to 99.82 µg/ml at 48 hours ($p<0.001$) (**Figure 1 (e)** and **Figure 2**).

Induced apoptosis by AS20

Subsequently, the cell and nuclear morphology were observed before and after drug action, under the fluorescent microscope using dual staining with Acridine orange and Propidium iodide (**Figure 3**), Hoechst staining and DAPI staining to determine the possible mode of cell death. Acridine orange stains live cells green, propidium iodide stains dead cells red. Hoechst's and DAPI staining fluoresces the nucleus blue when it binds to dsDNA, which is usually present in apoptotic cells (21). Thus, DAPI positive cells are a possible indicator of the apoptotic cell death. In the estimated cell counts, 0.23% and 0.33% death was obtained in the untreated control group of HeLa and HeLa-R cells, the percentage of apoptotic cells in the vehicle-treated group (dimethyl sulfoxide) of HeLa and HeLa-R cells was found to be 5.88% and 3.17%, respectively, whereas that in the treated group was 53.25% and 51.61% suggesting a notable impact of the IC50 AS20 on apoptotic death of HeLa and HeLa-R cells, respectively (**Figure 4**). The cells undergoing apoptosis, represented by the morphological changes of apoptotic nuclei were observed in AS20 treated group (**Figure 3**). The apoptotic process seems to be a bit slower in AS20 treated HeLa-R cells when compared with that in HeLa cells.

DISCUSSION

The results obtained have implications in the field of integrative oncology as AS20 is suggestive of the amplified in vitro anti-cancer and pro-apoptotic properties of the AS plant. As a result, this formulation can be further studied to work as a complementary and alternative approach to mainstream cancer therapies both to enhance the anti-cancer properties of the mainstream treatment and to alleviate its undesirable repercussions on the body.

Figures 1 and **2** support our hypothesis that AS20 possessed greater anti-cancer properties than extractions of individual parts of the plant. Specifically, the formulation displayed a far greater anti-cancer property than its different components and the positive control group (leaves water extract), since a lower concentration was required to kill 50% of the cancerous HeLa cells. Furthermore, a significant difference existed between the IC50 value for 24 hours and 48 hours, which showed the substantial impact of exposure time of AS20 on killing cancerous cells. A similar trend in the results was obtained for HeLa-R cells with the use of AS20. It showed that AS20 also has the potential to destroy cancerous cells despite their resistance to anti-cancer drugs.

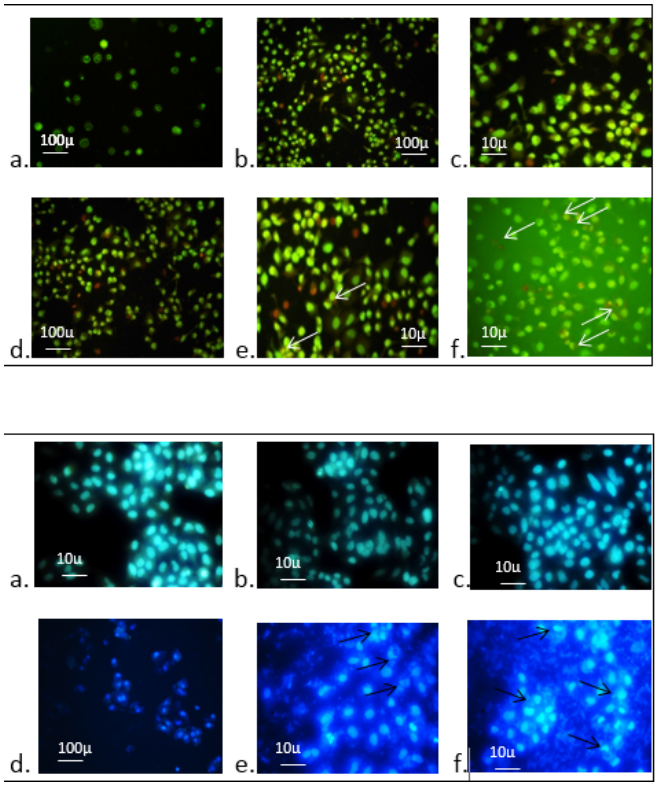

Figure 3: Apoptosis caused by AS20 on treated groups: (a) HeLa control, (b) HeLa-R control, (c) HeLa vehicle control (DMSO), (d) HeLa-R vehicle control (DMSO), (e) HeLa treated, and (f) HeLa-R treated cells were observed under fluorescent microscope using Acridine Orange and Propidium Iodide (dual) staining (20x) (top) and Hoechst and DAPI (dual) staining (20x) (bottom) with NA of 0.34. Presence of fluorescent nuclear fragmentation and blebs is indicative of apoptosis marked as white arrow in Acridine Orange and Propidium Iodide (dual) staining and as black in Hoechst and DAPI (dual) staining. Scale bar: 10µ and 100µ.

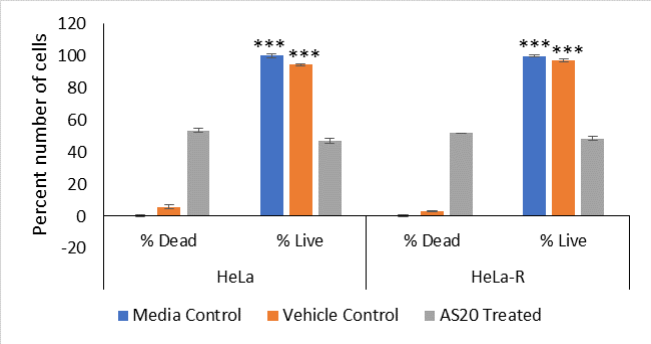

Figure 4: Bar graph showing dead and living cells obtained from fluorescent staining of HeLa and HeLa-R cells in media control, vehicle control and with the treatment of AS20 (N=3, mean±SD). The graph shows significant difference (p<0.001) between living and dead cells in media control group of both the cell types, as well, in the vehicle (DMSO) control group. There was no significance found in the groups treated with AS20.

As the IC50 of AS20 on HeLa-R cells was significantly higher, it could be used in a complementary fashion.

From the cell morphology obtained in Figure 3 and 4, it is evident that there was a higher number of DAPI positive cells in the treated HeLa than in control. In the treated group, there is evidence of both live and dead cells since the HeLa was treated with the IC50 of the drug (50% of cell death), hence suggesting the efficacy of drug action in killing cancer cells. There was an increase in apoptotic cells by 48% (Hoechst's stain) in the group treated with AS20, indicating a notable impact of the IC50 of AS20 on the apoptotic death of cancerous cells. The stained images of HeLa-R after the treatment also displayed higher DAPI positive cells.

As the experiment involved several steps, there was scope for human error. For instance, the serial dilution procedure required pipetting minimal volumes from well to well, which could have introduced errors. For the MTT assay, the incubation start time was assumed to be the same, even the addition of MTT was done sequentially. Besides, the cell counting in Hoechst's staining was carried out manually, to prevent errors.

While our results for the MTT assay on HeLa cells compared the anti-cancer property of the AS20 formulation with that of its constituents, the same was not done for the HeLa-R as it assumed to show similar characteristics. Additionally, a limitation of our study was that quantitative cell counting was done only for Hoechst's staining method as there was no difference in observation between Hoechst's and DAPI methods. Future studies could: 1) compare AS20 with its constituents for MTT assay against the HeLa R cell line 2) carry out quantitative cell counting based on morphology using DAPI as well 3) explore additional staining methods to confirm that it is indeed apoptosis that is occurring on addition of AS20. An example of a method which can be explored is the usage of an antibody for cleaved caspase-3, a more accurate apoptotic marker which is activated at the start of apoptosis (22).

Future experimentation in this field could expand on other pharmacological properties of AS20, such as antimicrobial, antifungal and anti-inflammatory. Other species in the Amaranthus genus can be assessed for their anti-carcinogenic properties in a similar manner. Furthermore, AS20 can be combined with other crude extracts and explored for enhanced anti-cancer properties. Other cancerous cell lines may also be explored, which could be an exciting future direction.

MATERIALS AND METHODS

Cell viability assay

The parameters chosen for MTT assay (4, 5-dimethyl tetrazolium-2-yl, 2, 5-diphenyl tetrazolium bromide assay) were based on the high presence of phytochemicals from previously conducted phytochemical screening (11). From the phytochemical studies, the constituent groups of AS20 were of particular interest. A positive control group (leaves water extract) which contained all the phytochemical groups was included in this evaluation (Table 1). Dimethyl sulfoxide (DMSO) was used as a vehicle control.

The MTT assay protocol was adapted from that described by Morgan D.M.L (23). 0.3 x 106 HeLa cells were cultured in a 96 well plate with Dulbecco's Modified Eagle Medium (DMEM) in 10% Fetal Bovine Serum (FBS) (100 µl, 3000-5000 cells per well). The cells were left for 24 hours of incubation for cell adhering. The samples were then treated with two-fold serial dilutions of AS inflorescence acetone, AS leaves methanol, AS leaves water and the AS20 (10% of the original stock solution was used as first concentration for all groups). Incubation was carried out for 48 hours and 24 hours of drug action. After these durations, 20 µl of MTT (3-(4, 5-dimethylthiazol-2-yl)-2, 5-diphenyltetrazolium bromide) was added and the plates were incubated for 4 hours to allow for action of MTT on the mitochondria of live cells. Subsequently, the media from each well was discarded and 100 µl DMSO was added to dissolve the purple formazan crystals. The presence of purple formazan crystal indicated the presence of live cells. The absorbance readings were taken at a wavelength of 545nm in the spectrophotometer.

Table 1: Groups considered for MTT cell viability assay. Range (+++) represented concentrations in the range 1001-2000 µg/ml.

Samples	Phytochemicals	Range
Inflorescence Acetone	Flavonoids	+++
Leaf methanol	Polyphenols Saponins Alkaloids	+++
Leaf water	Flavonoids Polyphenols Alkaloids Saponins	+++
AS20 (Combination of acetone extracted inflorescence and leaf extract in methanol)	Flavonoids Polyphenols Alkaloids Saponins	+++

Three independent sets of experiments were conducted in triplicates to increase accuracy. The following formula determined the percentage of cell viability:

$$Abs_{Sample} / Abs_{Control} \times 100$$

The formula calculated the percentage cell cytotoxicity:

$$(Abs_{Control} - Abs_{Sample}) / Abs_{Control} \times 100$$

From the absorbance readings obtained, the cell viability values were obtained for each concentration of each sample. The percentage viability graphs were plotted against the concentration of the sample for all four groups. The IC50.tk software (24) was used to determine the IC50 value for MTT assay for each of the four groups (after both 24 and 48 hours of drug action). Similar protocol was performed to determine the IC50 value of AS20 on HeLa-R cells.

Cell Staining and Microscopy

HeLa cells were cultured in a 24 well plate with Dulbecco's Modified Eagle Medium (DMEM) in 10% Fetal Bovine Serum (FBS) (1 ml, 0.1 x 106 cells per well) and were treated with the IC50 concentration of AS20 as was carried out for the MTT assay. After 24 hours of drug action, the media was discarded and the cells were washed with Phosphate Buffer Saline (PBS), which was maintained at a pH of 7.4 using Hydrochloric acid (HCl), Sodium Hydroxide (NaOH) and litmus paper. After the addition of PBS, the well plate was incubated for 5 minutes at room temperature. After this incubation, fixative Methanol was added to the wells and incubated for a further 5 minutes. Subsequently, the cells were washed once more with ice-cold PBS. The fluorescent stains were used in the dark and were covered with aluminium foil to prevent exposure of the wells to ambient light. The respective dyes were added after fixation and the wells were observed immediately under an Olympus fluorescent microscope (25), to prevent the possibility of cell death over time.

Dual staining: Dual staining method was adapted from that used by Mascotti *et al*. (26). 5 µl of (1 mg/ml) Acridine Orange and 5 µl of (1 mg/ml) Propidium Iodide were added to the cells and the treated sample, as well as the control sample, was observed under the fluorescent microscope in a dark room at 488-493 nm (excitation), 630 nm (emission).

Hoechst's staining: Hoechst's staining method was adapted from the protocol, followed by Crowley *et al*. (27). 50 µl-100 µl (0.5 µg/ml) Hoechst's stain was added to the cells and the treated sample, as well as the control sample, was observed under the fluorescent microscope in a dark room at 350-460 nm. For the Hoechst's staining, an approximated quantitative analysis was also carried out and cells were counted under the fluorescent microscope using a manual counter.

DAPI staining: The Hoechst's staining method used was adapted for DAPI (4′,6-diamidino-2-phenylindole). 50 µl-100 µl (1000 mg/ml) DAPI stain was added to the cells and the treated sample, as well as the control sample, was viewed under the fluorescent microscope in a dark room at 359-461 nm.

The images were captured by ProgRes® Capture Pro software (28) using Olympus microscope under 20X magnification and 0.34 numerical aperture (NA). These staining protocols indicated the possibility of the apoptotic mode of cell death.

Statistical analysis

GraphPad Prism software was used to analyze the data. ANOVA was used to analyze the statistical difference between groups, which was followed by Tukey's test. All the experiments were performed three times independently in triplicates. $P<0.05$ was considered as significant, denoted by single asterisk, $p<0.01$ was denoted by double asterisk and $p<0.001$ by triple asterisk.

Received: July 2, 2020
Accepted: November 12, 2020
Published: November 24, 2020

REFERENCES

1. "Complementary Therapies". Cancer.Org.Au, 2020, https://www.cancer.org.au/cancer-information/treatment/complementary-therapies. Accessed 5 August 2020
2. "Antioxidants And Cancer Prevention". Foh.Psc.Gov, 2020, https://foh.psc.gov/NYCU/antioxidents.asp#:~:text=Antioxidants%20and%20Cancer%20Prevention&text=Antioxidants%20protect%20cells%20from%20damage,that%20is%20associated%20with%20cancer Accessed 5 August 2020
3. Wink, Michael. "Modes of Action of Herbal Medicines and Plant Secondary Metabolites." *Medicines* (Basel, Switzerland) vol. 2, no. 3, 2015, pp. 251-286. doi:10.3390/medicines2030251 Accessed 11 April 2020
4. Lu, Jin-Jian *et al*. "Alkaloids Isolated From Natural Herbs As The Anticancer Agents". *Evidence-Based Complementary And Alternative Medicine*, vol 2012, 2012, pp. 1-12. Hindawi Limited, doi:10.1155/2012/485042. Accessed 11 April 2020.
5. Zhang, Yan *et al*. "Cytotoxic Triterpene Saponins From The Leaves Of Aralia Elata". *Fitoterapia*, vol 83, no. 4, 2012, pp. 806-811. Elsevier BV, doi:10.1016/j.fitote.2012.03.015. Accessed 11 April 2020.
6. Hu, Xingjiang *et al*. "Development And Validation Of Liquid Chromatography–Tandem Mass Spectrometry Method For Quantification Of A Potential Anticancer Triterpene Saponin From Seeds Of Nigella Glandulifera In Rat Plasma: Application To A Pharmacokinetic Study". *Journal Of Chromatography B*, vol 967, 2014, pp. 156-161. Elsevier BV, doi:10.1016/j.jchromb.2014.07.030. Accessed 10 June 2020.

7. Yildirim, Isil, and Turkan Kutlu. "Anti-cancer Agents: Saponin And Tannin". *International Journal Of Biological Chemistry*, vol 9, no. 6, 2015, pp. 332-340. Science Alert, doi:10.3923/ijbc.2015.332.340. Accessed 11 April 2020.
8. Lamoral-Theys, D. *et al*. "Natural Polyphenols That Display Anticancer Properties Through Inhibition Of Kinase Activity". *Current Medicinal Chemistry*, vol 17, no. 9, 2010, pp. 812-825. Bentham Science Publishers Ltd., doi:10.2174/092986710790712183. Accessed 10 May 2020.
9. Vipin Chandra Pal *et al*. "Pharmacognostical Studies of *Amaranthus spinosus* Linn"*Pharmaceutical and Biosciences Journal* ISSN: 2582-0540 http://dx.doi.org/10.20510/ukjpb/1/i1/91112 (2013).
10. Tewari, Devesh *et al*. "Ethnopharmacological Approaches for Therapy of Jaundice: Part vitro". *Frontiers in Pharmacology* (2017). 8.
11. Ishir Sharma, Pooja Kasture, Ankita Umrao, Jyothsna Rao, Gururaj Rao., "Phytochemical analysis of *Amaranthus spinosus* Linn.: An in-vitro analysis". *Journal of Emerging Investigators*, 2020. In-Press.
12. Saravanan, R., "Evaluation of In-Vitro and In-Vivo Anticancer Activity of Leaf Extracts of *Amaranthus spinosus* Linn." Master's thesis, College of Pharmacy Madras Medical College, Chennai. (2016) ; pp. 21-22. Accessed 5 May 2020.
13. Batts, Denise Watson "Cancer cells killed Henrietta Lacks- then made her immortal". *The Virginian-Pilot*. vol. 1, 2010, pp. 12–14. Accessed 20 April 2020
14. Zhang, Jun-Xiao *et al*. "Anticancer Activity Of 23,24-Dihydrocucurbitacin B Against The Hela Human Cervical Cell Line Is Due To Apoptosis And G2/M Cell Cycle Arrest". *Experimental And Therapeutic Medicine*, 2018. Spandidos Publications, doi:10.3892/etm.2018.5710.
15. Kim, Hyeonji *et al*. "Induction of apoptosis by ethanolic extract of mango peel and comparative analysis of the chemical consists of mango peel and flesh". *Food Chemistry*. Vol. 133, no. 2, 2012, pp. 416–422. doi:10.1016/j.foodchem.2012.01.053 Accessed 14 April 2020
16. "NCI Dictionary Of Cancer Terms". National Cancer Institute, 2020, https://www.cancer.gov/publications/dictionaries/cancer-terms/def/apoptosis. Accessed 5 August 2020
17. Eastman, A. "Activation of programmed cell death by anti-cancer agents: cisplatin as a model system". Cancer Cells, vol. 2, 1990, pp. 275–280. Accessed 11 April 2020
18. Stone, Richard M, and Tinsley Randolph Harrison. *Harrison's Principles Of Internal Medicine*. Mcgraw-Hill Professional Publishing, 2001.
19. Rahbari, Raheleh *et al*. "A Novel L1 Retrotransposon Marker For Hela Cell Line Identification". *Biotechniques*, vol 46, no. 4, 2009, pp. 277-284. Future Science Ltd, doi:10.2144/000113089. Accessed 12 April 2020.
20. Maja Osmak and Damir Elijuga. "The characterization of two human cervical carcinoma HeLa sublines resistant to cisplastion" (1993) *Research in Experimental Medicine,* 193(1):389-396.
21. "Hoechst 33342 Protocol For Imaging | Thermo Fisher Scientific - UK". Thermofisher.Com, 2020, https://www.thermofisher.com/in/en/home/references/protocols/cell-and-tissue-analysis/protocols/hoechst-33342-imaging-protocol.html.
22. Caspase-3-. "Caspase-3- A Marker Of Programmed Cell Death". *Novus Biologicals*, 2020, https://www.novusbio.com/antibody-news/antibodies/caspase-3-a-marker-of-programmed-cell-death#:~:text=One%20specific%20effector%20caspase%20is,and%20other%20subst
23. Morgan, David M. L. "Tetrazolium (MTT) Assay For Cellular Viability And Activity". *Polyamine Protocols,* pp. 179-184. Humana Press, doi:10.1385/0-89603-448-8:179. Accessed 22 June 2020.
24. "Very Simple IC50 Tool Kit - Calculate, Measure, Determine IC50 Online.". Ic50.Tk, 2020, http://ic50.tk/. Accessed 4 April 2020.
25. "Olympus BX63 for Fluorescent Microscopy." *Biocompare*, www.biocompare.com/pfu/10242895/soids/872669-2254327/Microscopes_and_Cell_Imaging_Systems/Microscopes_Fluorescence?vids=100250#:~:text=A sample is illuminated with,beamsplitter), and emission filter.
26. Mascotti, K. *et al*. "HPC Viability Measurement: Trypan Blue Versus Acridine Orange And Propidium Iodide". *Transfusion*, vol 40, no. 6, 2000, pp. 693-696. Wiley, doi:10.1046/j.1537-2995.2000.40060693.x. Accessed 25 April 2020.
27. Crowley, Lisa C. *et al*. "Analyzing Cell Death By Nuclear Staining With Hoechst 33342". *Cold Spring Harbor Protocols*, vol 2016, no. 9, 2016, p. pdb.prot087205. Cold Spring Harbor Laboratory, doi:10.1101/pdb.prot087205. Accessed 22 June 2020.
28. "Image Capture Software For Progres® Microscope Cameras". Jenoptik.Com, 2020, https://www.jenoptik.com/products/cameras-and-imaging-modules/microscope-camera/software-solutions/image-software-progres-capture-pro.

Sponsorship

Editor's Circle $10,000+

ALLOY THERAPEUTICS

Patron $5,000+

NEW ENGLAND BioLabs® Inc.
enabling technologies in the life sciences

PORTFOLIOS WITH PURPOSE®

Institutional Supporters

HARVARD UNIVERSITY

HARVARD MEDICAL SCHOOL

Tufts UNIVERSITY

Charitable Contributions

We need your help to provide mentorship to young scientists everywhere.

JEI is supported by an entirely volunteer staff, and over 90% of our funds go towards providing educational experiences for students. Our costs include manuscript management fees, web hosting, creation of STEM education resources for teachers, and local outreach programs at our affiliate universities. We provide these services to students and teachers entirely free of any cost, and rely on generous benefactors to support our programs.

A donation of $30 will sponsor one student's scientific mentorship, peer review and publication, a six month scientific experience that in one student's words, 're-energized my curiosity towards science', and 'gave me confidence that I could take an idea I had and turn it into something that I could put out into the world'. **If you would like to donate to JEI, please visit https://emerginginvestigators.org/support, or contact us at questions@emerginginvestigators.org.** Thank you for supporting the next generation of scientists!

'Journal of Emerging Investigators, Inc. is a Section 501(c)(3) public charity organization (EIN: 45-2206379). Your donation to JEI is tax-deductible. '

emerginginvestigators.org